POLITECNICO DI TORINO

Master's degree in Aerospace Engineering

Conceptual design methodology and tools for human Mars landers: Mission analysis

Supervisors

Prof. Roberta FUSARO
Prof. Nicole VIOLA
Ing. Giuseppe NARDUCCI

Candidate

Matteo MARTONE

July 2024

Abstract

Key goals of NASA's Evolvable Mars Campaign (EMC) [1] include expanding the human presence on Mars by 2030 to promote scientific progress, innovation and international collaborations. This interest requires the development of new EDL technologies to carry heavy payloads and support human presence. It is essential to create multifunctional and reusable landers that include the Martian Ascent Module (MAV), minimizing its weight to meet the requirements of human missions. This thesis work aims at developing mission analysis techniques to complement the conceptual design of a human Mars lander with the capability to ascend and descend from Martian orbit. The proposed methodology deals with the sizing of the lander in its systems and subsystems, integrating it with a mission analysis to evaluate its performance. Mission analysis, particularly for Martian ascent and descent, is the main topic covered by this thesis, and is useful to verify feasibility and provides useful variables for design refinement, such as velocity gain and losses. The mission analysis is initially implemented via a subroutine in MATLAB for quick and approximate evaluation, preparatory to the development of a more complex and representative model using ASTOS software to simulate both ascent and descent. The descent study also focuses on developing a realistic aerodynamic model to investigate EDL technologies. The models are validated using a reference vehicle in the literature by comparing the results between ASTOS and MATLAB. With a difference of less than 15 percent, the design routine is considered valid. This output, which provides the velocity increment for lander sizing, implies that future developments could use the mission analysis routine concurrently with the systems and subsystems sizing routine, continuously exchanging results until convergence is reached in estimating the velocity increment. The detailed integration with the sizing part is left as a future development to create a viable methodology for lander design that can be implemented in a tool.

Table of Contents

List of Tables

List of Figures

Acronyms

CAMTOS Computer Aided Multidisciplinary Tool for Optimization of Spacecraft. 63

DAV Descent Ascent Vehicle. 3

EDL-SA Entry, Descent and Landing System Analysis. 8

F-TPS Flexible Thermal Protection System. 12

HIAD Hypersonic Inflatable Aerodynamic Decelerator. 9

HML Human Mars Lander. 38

HMO High Mars Orbit. 3

IRVE Inflatable Reentry Vehicle Experiment. 12

ISRU In-Situ Resource Utilization. 17

ISS International Space Station. 3

LMO Low Mars Orbit. 3

MTV Mars Transfer Vehicle. 3

NTR Nuclear Thermal Rocket propulsion. 3

PCPF Planet-Centered Planet-Fixed, Reference Frame. 61

SHAB Surface habitat and lander for the reference mission. 3

SIAD Supersonic Inflatable Aerodynamic Decelerator. 9

SM Service Module. 38

SPTO Single Phase to Orbit. 15

TOD True of Date, Reference Frame. 88

TPS Thermal Protection System. 11

TPTO Two Phase to Orbit. 15

Chapter 1
Introduction

1.1 Mars Landers & Missions

The first Mars missions date back to the 1960s. Since then, numerous vehicles have been launched towards the planet regularly, driven by the scientific potential it holds, such as the possibility of water and life. These missions are highly complex, with roughly half of them successfully reaching Mars. The first mission to get a vehicle near Mars was NASA's Mariner 4 [2], launched on November 28, 1964. It passed within 9844 km of Mars and captured 22 images. Significant lander missions include the Viking program and the Mars Pathfinder mission. There was a 20-year gap between these missions during which all attempts to land on Mars or insert a vehicle into orbit failed. The Viking program [3], launched in 1975, comprised Viking 1 and Viking 2, each with an orbiter and a lander. This program successfully landed both landers on Mars, providing the first images of the Martian surface. The orbiter-lander pairs had a total mass of 3519 kg, with the lander capsules weighing 1194 kg, the parachutes 118 kg, and the aeroshell heat shields 593 kg. The entry, descent, and landing sequence took around 10 minutes. The Mars Pathfinder mission was part of NASA's Discovery program [4] [5], successfully landing on Mars in 1997. The lander weighed approximately 900 kg, including propellant and the small rover Sojourner, the first wheeled vehicle used to analyze the Martian surface and rocks. This mission introduced new entry, descent, and landing technologies, including inflatable parachutes. Among the most important missions there is Mars Science Laboratory (MSL)[6]. This recent mission successfully landed the Curiosity rover on Mars, using entry, descent, and landing technologies derived from the Viking missions. The mission included a launch phase, an interplanetary transfer, and a final entry, descent, and landing phase, completed in about 7 minutes using an aeroshell for atmospheric deceleration, a parachute, and retropulsion, allowing the rover to land on its wheels. This mission delivered the largest payload to

the Martian surface, weighing about one ton. Figure 1.1 shows Viking 1, Mars Pathfinder and MSL's landers.

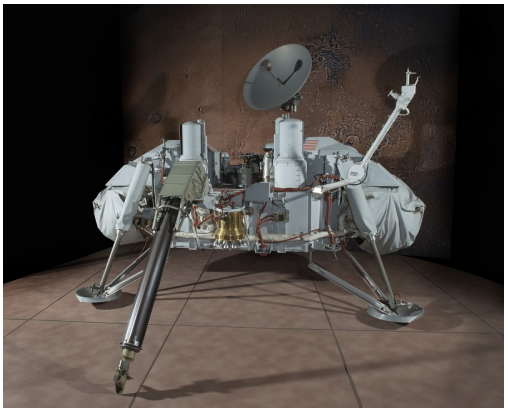

(a) Viking [3]

(b) Mars Pathfinder [4] [5]

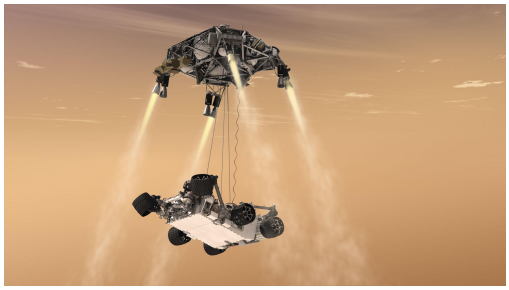

(c) MSL Curiosity Landing [6]

Figure 1.1: Successful Missions involving Mars Landing

The performance achieved by these landers in the mentioned missions shows how difficult it is to deliver even very small masses to the Martian surface, for human missions in fact 100 t of payload would be required, and half of this mass will be used for ascent alone, including ascent vehicle, power system, the habitation module and eventually rovers and other modules.

1.2 Mars Human Missions

Sending a crew of astronauts to Mars and enabling their exploration of the planet presents a highly complex engineering challenge due to the mission's inherent requirements caused by a long journey from Earth with constrained resources and

space. No definitive or proven mission architecture exists, instead, there are several reference missions that explore potential methods for human exploration of Mars. These serve as a starting point for mission studies, integrating numerous insights and data gathered from robotic missions to Mars, research conducted on the International Space Station (ISS), and lessons from the Apollo lunar missions.

These reference missions were detailed by NASA in a technical report [7]. This report outlines three initial missions for human exploration of the Martian surface, to be conducted on consecutive trajectories spaced decades apart. This phased approach is due to current technological and knowledge limitations, making it feasible to meet time and cost requirements by dividing the mission this way. Moreover, the passage of decades would allow for the acquisition of more information and the definition of clearer objectives for the mission.

These missions would follow a series of tests and trials on Earth, on the ISS, in Earth orbit, on the Moon, and on Mars via robotic missions. The proposed missions involve a crew of six astronauts per mission, with multiple landing sites on Mars being analyzed to gather a comprehensive understanding of the planet's diverse conditions. Each mission would employ a technique known as "pre-deploy" or "split mission," which involves sending necessary vehicles ahead to pre-deploy. This approach allows for greater payload mass and the use of low-energy trajectories and fits well with In-Situ Propellant Production. This technique enables the production of propellant from the Martian atmosphere, allowing the crew to arrive and find a ready supply of propellant for their return journey.

Such a reference mission involves using multiple vehicles to complete the mission, pre-assembled in Low Earth Orbit (LEO) and then sent on low-energy transfer trajectories to Mars at the opening of the launch window, two years before the crew's arrival. Specifically, the mentioned vehicles include a lander for crew ascent, which lands independently (Descent Ascent Vehicle, DAV), and a surface habitat (SHAB) designed for extended surface stays. Nuclear thermal rocket propulsion (NTR) is employed for these trips, and the vehicles are placed in high Martian orbit to await the crew. At the next launch window, a third vehicle, the Mars Transfer Vehicle (MTV), is planned to transfer the crew to Martian orbit, where they will rendezvous with the SHAB for descent and surface operations.

To initiate the Entry, Descent, & Landing (EDL) phase, both the DAV and the SHAB must detach and reach a Low Mars Orbit (LMO) circular orbit. Two options are available for this:

- Aerobraking: a maneuver that reduces apoapsis by maneuvering at periapsis against the atmosphere, thus being slowed down by it;
- Classic Hohmann Transfer: this involves two maneuvers, the first moving from High Mars Orbit (HMO) to an elliptical orbit with periapsis at the LMO circular orbit altitude, and the second to circularize.

According to the reference mission, summarized in figure 1.2, the stay on Mars would last 18 months. Initially, the crew would convert the SHAB from lander mode to habitat mode by transferring key ascent components to the DAV. This time would then be dedicated to surface exploration and scientific experiments. Upon departure, the SHAB would be placed in a dormant mode for future crews, and the DAV would be used for ascent and rendezvous with the MTV, which would return the crew to Earth.

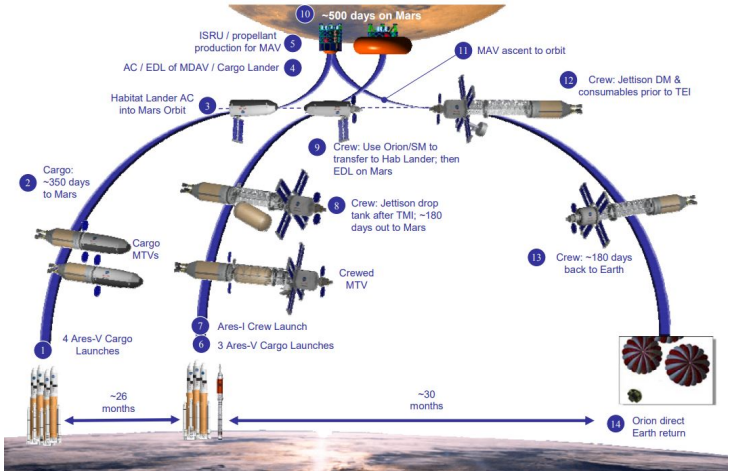

Figure 1.2: Mars Design Reference Architecture 5.0 mission sequence summary [7]

1.3 Thesis Objectives

As can be seen from this brief introduction in section 1.2, there are various spacecraft typologies, including cargo vehicles, pre-deployed crew vehicles required for the long stay on the planet, manned and un-manned landers of different sizes and purposes. Thus, starting from the reference mission, the objective of the following thesis is to lay the groundwork for the creation of a tool for the design of a Human Mars Lander. The design methodology for which it is intended to lay the foundations is composed by a design routine and a mission anlysis routine, this thesis work specifically focuses on the mission analysis routine by making use of simulation software such as ASTOS, and using codes for optimizing the input variables to the equations of motion implemented on MATLAB. The primary objective of the mission analysis routine is to output design variables for the design routine, the operation of which will not be discussed here. However, the type of design that this work proposes to achieve is intended to deviate slightly from the initial idea pre-posed by the reference mission and creating a vehicle specialized solely in descent and ascent to and from the Martian surface in a manned case,

thus not referring to the SHAB which is instead multifunctional in that it can be used as a ground habitat. This choice was made in order to meet NASA's expectations for Mars missions and space exploration concerning an Evolvable Mars Campaign (EMC) [1], which includes the development of a reusable human lander for ascent and descent, among other proposals. The objectives of the thesis can be summarized as follows:

1. Creation of a database containing information related to Martian ascent modules (MAVs) and technologies used for entry, descent & landing about total masses, dry mass, payload mass, number of passengers, types of propellant used, orbits involved, and numerous data useful for the creation of an initial statistical design methodology that is based on dividing the dry mass into percentages for each system/subsystem and especially for identifying a reference vehicle and mission similar to those whose design is of interest to conduct;

2. Creation of a model for ascent mission simulation that ensures mission feasibility by taking the design variables of the reference vehicle as input. Creation of a rapid subroutine in MATLAB that simulates all mission's phases considering 2dof, integrating the equations of motion taking as input optimizable variables, and returning lander trajectory during ascent, the evolution over time of variables such as altitude, velocity but especially the first values for ΔV, atmospheric and gravity losses, crucial input variables for lander's design;

3. Refinement of the ascent model , implementing it on ASTOS by re-modeling the phases and setting their duration and attitude over time in 3dof. This approach allows to have as output the same variables obtained on MATLAB, but guaranteeing greater accuracy at the cost of a slower simulation and optimization;

4. Modeling of the atmospheric drag coefficient in the entry, descent & landing phases at varying Mach and for different reference altitudes, preparatory to laying the groundwork for a model on ASTOS for descent similar to the one for ascent, which returns in output the ΔV and propellant mass for subsystems design.

This thesis work is being conducted in parallel with a second thesis work that will instead focus in its entirety on the design routine, concerning lander sizing in its systems/subsystems by laying the groundwork for the tool and also starting from the statistical analysis conducted in an adjunct manner, refining the first statistical methodology proposed here. A breakdown of these thesis work is shown in figure 1.3.

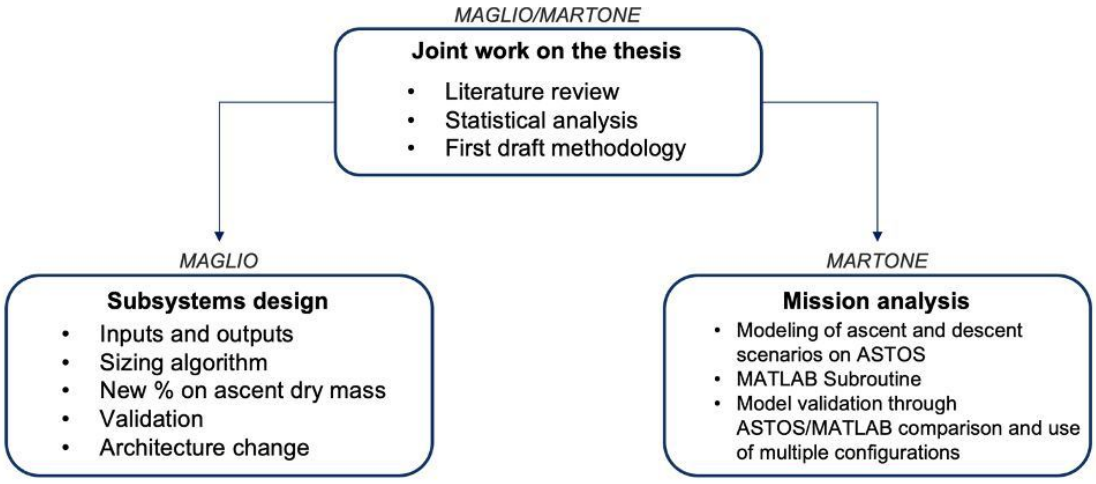

Figure 1.3: Breakdown of Thesis Work

1.4 Research outline

Within this thesis work report, **Chapter 2** will focus on the analysis of the current state of the art regarding Human Mars landers, the already mentioned reference missions will be better explored especially to identify the critical points regarding ascent and descent mission scenarios, different types of Entry, Descent and Landing Systems (EDL) and architectures will be analyzed in section 2.2, types of orbits employed in section 2.3, typical mission phases in section 2.2.1, propellant and propulsion system options in section 2.3.2 and section 2.3.3, and finally atmospheric models for Mars will be analyzed in section 2.4. In **Chapter 3** much of the information gleaned from the literature will be used in order to create a database, conducting a literature review more focused on numerical data. These data will be used and discussed, conducting a statistical analysis that captures notable configurations for Human Mars landers investigated in different scientific articles and technical reports, graphs and appropriate statistical trends of some design variables will be plotted. Then in **Chapter 4**, a reference vehicle will be chosen, and the ascent mission scenario will be modeled, creating a MATLAB subroutine and an ASTOS main design routine. Similarly, **Chapter 5** will better discuss the descent mission scenario. Lander's drag coefficient will be analyzed in section 5.1, and the ASTOS model will be created to simulate lander's mission variable temporal evolution. Last step is the evaluation of the results summarized in **Chapter 6**, where conclusions drawn from the thesis work and future insights will be discussed.

Chapter 2
Literature Review

This chapter will report all the notable information useful in understanding the different design options of the Human Mars Lander, taking up technical publications and scientific articles that conduct studies on various types of human landers, listing their merits and shortcomings. These kinds of concepts are useful in drawing guidelines for the design in broad strokes and then explore the most advantageous and feasible configurations in the mission study and design itself. Different possibilities for performing ascent and descent missions, and the different phases that make up these two mission scenarios, will then be detailed in section 2.2 and in section 2.3.

2.1 Launch Vehicle

Referring back to [7], to bring the lander into LEO orbit requires the use of a Heavy-Lift Launch Vehicle, the idea proposed in the report at the time was to use the **Ares V** launcher, which had several design options for lunar missions and could be adapted to the objectives of Martian missions. The launcher, through the shroud, influences the size, mass, and performance of the lander and EDL System architecture, as well as all other mission payloads. For Ares V shroud's size varied between 8.4 and 12 m in diameter and between 12 and 35 m in length, there was also a dual-shroud architecture with a length of 30 m and a transition cone with an outer diameter of 10 m. The main information that comes from the launch segment's choice is thus the starting value for the design of the EDL System and lander in terms of diameter and width, which then can correspond to 10 m in diameter by 30 m in length if the dual-shroud option is used. Currently, however, the candidate heavy launcher to carry the lander and generally vehicles intended for lunar and Martian missions into low Earth orbit is the **Space X's Starship system** [8] shown in figure 2.1. The latter is a two-stage super heavy

rocket, a booster stage and the "Starship", with the latter representing the actual spacecraft. It is a reusable system designed specifically for this type of mission. The fairing size is of about 9 meters into which the payload can be loaded; it is currently the launcher, and can guarantee the largest volume on the market.

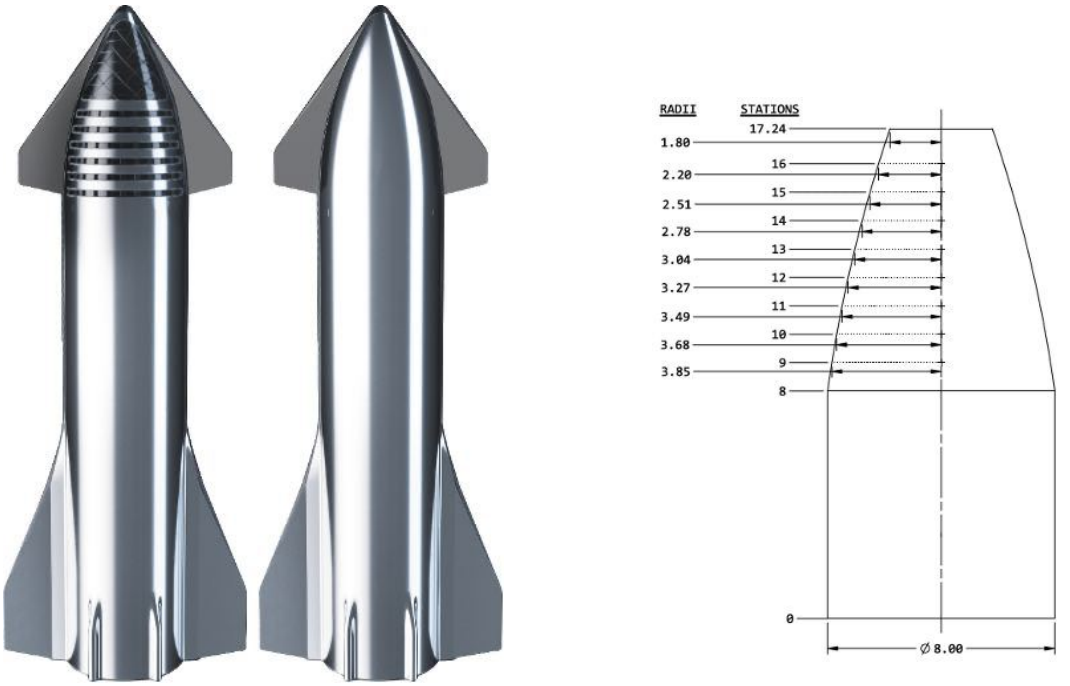

(a) Starship (b) Starship internal dimensions

Figure 2.1: Space X's Starship system [8]

2.2 Mars Entry Descent & Landing: Reference Architectures

For human exploratory missions to Mars, it emerges from NASA's report [7] that high-fidelity models and greater technological advances are needed in several areas but especially there is a shortage in terms of technology for the Entry, Descent & Landing phases. To address this deficiency, NASA has initiated an Entry Descent and Landing System Analysis (EDL-SA) involving multiple research centers and with a three-year duration. The first year focused on exploration missions targeting ground payload transport of at least 40t, the second on the transport of smaller payloads (1-3t or 3-5t), and a final year on technology development for all mission classes. The EDL-SA study established reference architectures related to exploration missions with respect to the Aerocapture and EDL phases, including

an initial architecture with a mid range L/D ratio (Rigid Mid-L/D) for the aerocapture and entry phase that then uses supersonic retro-propulsion technology for the descent and landing phases. A total of 8 architectures have been proposed including the use of inflatable aerodynamic decelerators in the hypersonic and supersonic ranges (HIAD and SIAD) jointly with supersonic or subsonic retro-propulsion technologies, one of the architectures also proposes an all-propulsive solution. All architectures and relative technology used in the various stages of aerocapture, and EDL in the hypersonic, supersonic and subsonic ranges are shown in table 2.1 and figure 2.2.

Table 2.1: Comparison of Reference Architectures Across Flight Regimes [9]

Architecture	**Aerocapture**	**Hypersonic**	**Supersonic**	**Subsonic**
Architecture 1	Rigid Mid-L/D	Rigid Mid-L/D	Propulsion	Propulsion
Architecture 2	Lifting HIAD	Lifting HIAD	Propulsion	Propulsion
Architecture 3	N/A	Propulsion	Propulsion	Propulsion
Architecture 4	Rigid Mid-L/D	Lifting HIAD	Propulsion	Propulsion
Architecture 5	Rigid Mid-L/D	Lifting HIAD	Same LHIAD	Propulsion
Architecture 6	Lifting HIAD	Lifting HIAD	Same LHIAD	Propulsion
Architecture 7	Rigid Mid-L/D	Rigid Mid-L/D	Drag SIAD	Propulsion
Architecture 8	Lifting HIAD	Lifting HIAD	LSIAD–Skirt	Propulsion

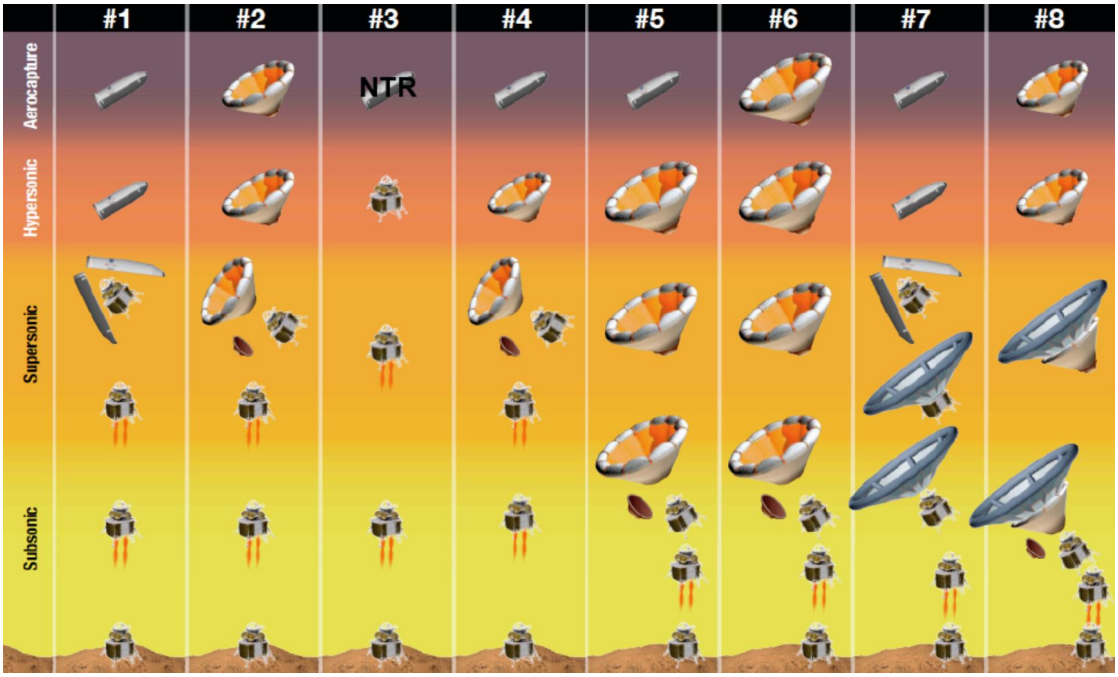

Figure 2.2: EDL-SA proposed architectures for exploration class missions [9]

An overview of the architectures proposed by EDL-SA with in-depth studies

using mass-based simulation models is higlighted in [9]. Briefly, all mass, aerodynamic, aerothermic models regarding aerocapture and Thermal Protection System and for retro-propulsion are integrated in the POST2 (Program to Optimize Simulated Trajectories) simulation that analyzes various mission phases.

2.2.1 EDL Phases

All architectures include aerocapture, EDL phases starts from an orbit of 1 Sol (33793km x 250km), the landing site is at an altitude of 0m. The aerocapture is evaluated distinctly from EDL phases. Regarding the **entry** portion of the trajectory, the modeled phases included are as follows:

- **Deorbit, decrease periapsis**: the ΔV needed from the apoapsis of the elliptical 1 Sol orbit is applied;
- **Atmospheric entry**: in the simulation the atmosphere model is activated;
- **Pull-out**: the trajectory is adjusted as a function of velocity in the simulation;
- **Heading alignment**: phase whose goal is to control the azimuth so as to be directed toward the landing site.

The **descent**, on the other hand, consists of the following phases in the simulation:

- **Separation**: the simulation determines the optimal altitude to jettison the inbound deceleration device (rigid aeroshell, HIAD, SIAD depending on architecture), previously considered as instantaneous [7], and in this context modeled more realistically;
- **Terminal descent phase** : in which the simulation tries to balance the amount of fuel saved with the need to land in the landing site with an accuracy of 50m

Finally, the **landing phase** is based on Viking missions, the vehicle must reach 1 m/s speed and maintain it for 5 seconds before touching the surface. From the EDL-SA study emerges the need to subdivide the descent phases according to flight regime, from the legacy of viking missions the landing requirement just described is established, while in the transitions from hypersonic to supersonic and supersonic to subsonic the jettison of inflatables, rigid heat shields, and possibly parachutes is enshrined.

2.2.2 Rigid Aeroshell

Architecture 1 in table 2.1 consists of a mid L/D rigid aeroshell for aerocapture and hypersonic flight in the entry phase and uses supersonic retro-propulsion for the descent and landing phases. This is a configuration with high technological maturity and reliability (high TRL) compared to configurations using drag devices, as well as heavier, complex in modeling, packaging, and separation. This type of rigid aeroshell is a slender body with a good L/D value. When a rigid aeroshell is chosen, entry vehicle's shape should be analyzed with special emphasis, in [10] a slender body with L/D of 0.68 similar to that of architecture 1 and a blunt body with L/D=0.30 are analyzed, shown in figure 2.3.

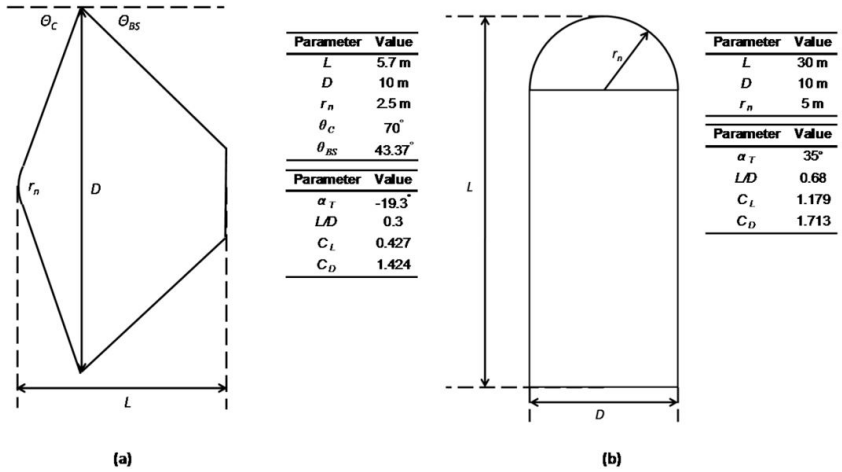

Parameter	Value
L	5.7 m
D	10 m
r_n	2.5 m
θ_C	70°
θ_{BS}	43.37°
Parameter	Value
α_T	-19.3°
L/D	0.3
C_L	0.427
C_D	1.424

Parameter	Value
L	30 m
D	10 m
r_n	5 m
Parameter	Value
α_T	35°
L/D	0.68
C_L	1.179
C_D	1.713

Figure 2.3: Rigid shell analysed options [10]

It is described how high L/D and slender bodies allow better handling of the final descent stages while blunt bodies have less exposed surface area and therefore less load for the TPS, this results in lower masses. Comparing the two options , as the mass at entry increases, the gain in mass of payload transportable to the Martian surface decreases. Blunt bodies can provide high enough L/D to decelerate entry masses through the atmosphere with adequate staging while there is a penalty in payload mass fraction of 0.3 for slender bodies. Using a direct entry into the Martian atmosphere (v=6.75 km/s) reduces payload mass fraction by 15 percent compared to an entry from orbital velocity of about 4 km/s, these results are shown in figure 2.4.

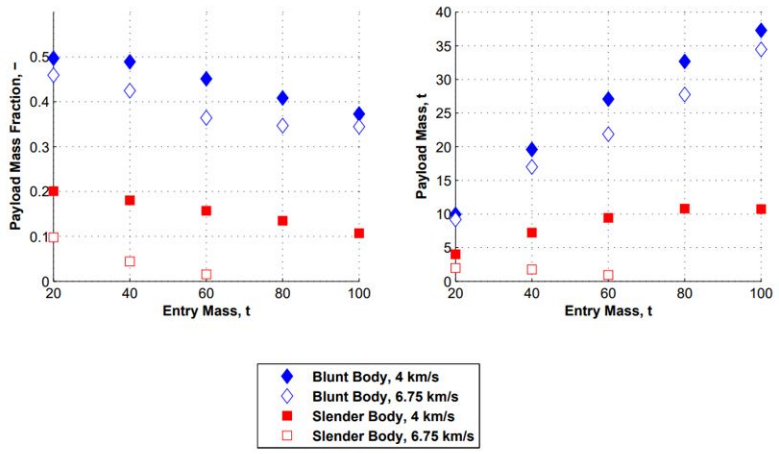

Figure 2.4: Payload mass comparison between the rigid shells [10]

It can be seen that as the entry mass increases, the payload mass increases but the same cannot be said of the payload mass fraction, this is due to the fact that higher entry masses involve flying in denser areas of the atmosphere that involve higher thermal loads and higher masses. This implies the existence of a point of optimum for the maximum payload mass.

2.2.3 Inflatable Aerodynamic Decelerator (HIAD, SIAD)

An Inflatable Aerodynamic Decelerator (IAD) is a deployable aeroshell made up of an inflatable framework that retains its form during atmospheric flight and a Flexible Thermal Protection System.(F-TPS). This type of technology is built to increase drag during EDL phases and also functions as a primary heat shield. For Martian missions, especially human missions, these types of configurations is usually selected for EDL, this is because the Martian atmosphere is non that thick to provide good deceleration, but at the same time thick enough to generate heat, when there is a need to transport high masses to the surface they are lighter than rigid aeroshells because of the lightweight and flexible materials, they are also able to reduce the ballistic coefficient and peak heating. The design of these structures is based on the stacked toroid concept, several inflatable torii increase the resistant area and act as structural support for protective thermal layers. A nitrogen tank is usually used to pressurize the torii [11]. The stacked toroids configuration stems from a series of experiments carried out on inflatables, the most important of which include the Inflatable Reentry Vehicle Experiment (IRVE I, II, III), the third experiment involved 7 toroids consisting of Kevlar tubes held together by radial straps to minimize oscillations [12]. This experiment was critical

in the development of Brown's models [13]) for analytically estimating the inflation pressure of torii and Samareh's model [14] for analytically estimating IAD's mass from input variables such as the diameter of the launch vehicle shroud. The graphic representation of inflatable systems is shown in the figures 2.5 and 2.6.

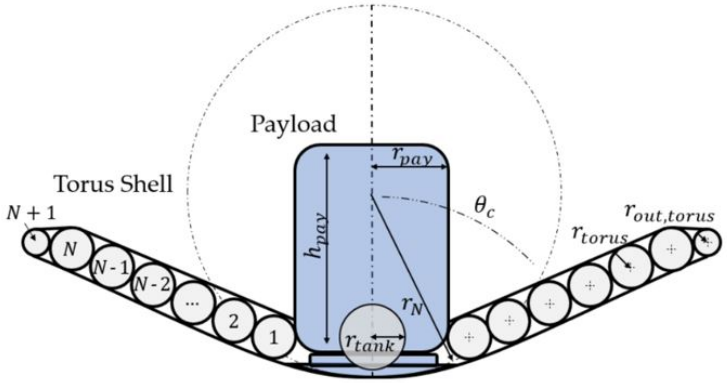

Figure 2.5: Stacked toroid parametrization [14]

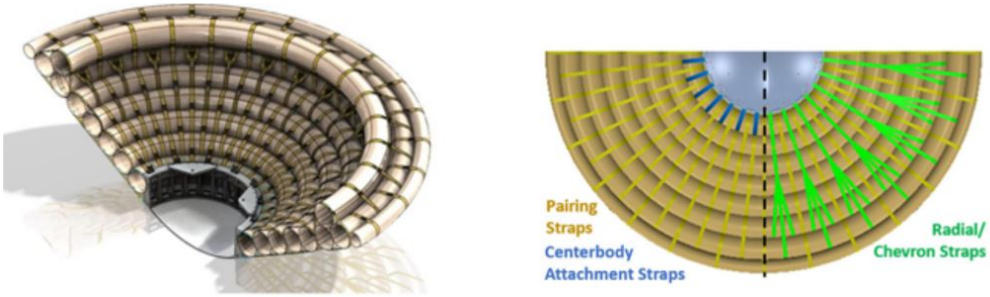

Figure 2.6: Stacked toroid elements [14]

Returning to the reference architectures of the EDL-SA study [9], architecture 2 shown in table 2.1 uses an inflatable HIAD (Hypersonic IAD) for the aerocapture and entry phase while using supersonic retro-propulsion for the terminal descent phase. This type of configuration allows for a mass savings of 25 t compared to architecture 1 due to the dual use Thermal Protection System HIAD (for entry and aerocapture), in this case the inflatable shield's diameter is 23 m and it has a lower TRL technology reliability level than the rigid aeroshell. Architecture 4, on the other hand, uses a rigid aeroshell for aerocapture and a HIAD for the entry phase eliminating the dual use, this allows for an even greater increase in surface transportable mass as the entry mass is less than 8 t, in part due to a lighter HIAD of 4 t. With this change, there is also a variation in ballistic coefficient and

consequently trajectory between the two architectures, the use of different systems for entry and aerocapture also increases technological complexity and makes the architecture less practical overall. Architectures 5 uses a single use TPS HIAD only for the entry phase and a rigid aeroshell for aerocapture, while architecture 6 a dual use TPS HIAD. The difference in these architectures is in the use of inflatables as an alternative to supersonic retro-propulsion by making them very large in diameter (68 m and 82 m respectively) to decelerate to subsonic speeds. There are again advantages in terms of entry mass, however, the mass model for inflatables is not very accurate for such large inflatables, plus the times required for EDL, particularly to get to subsonic velocities with a good margin in altitude to begin the terminal descent phase are difficult to manage compared to more classical IAD cases.

IAD diameter's choice is important as it also determines the payload mass of optimum related to the entry mass, as investigated in [10], in figure 2.7 for example it is shown that beyond 60t an IAD's diameter of 20m is no longer sufficient and it is necessary to change to a diameter of 30m, same thing beyond 80t, the diameter must become 50m. It also highlights how the use of supersonic retropropulsion alone is insuficient to the transport of large payloads.

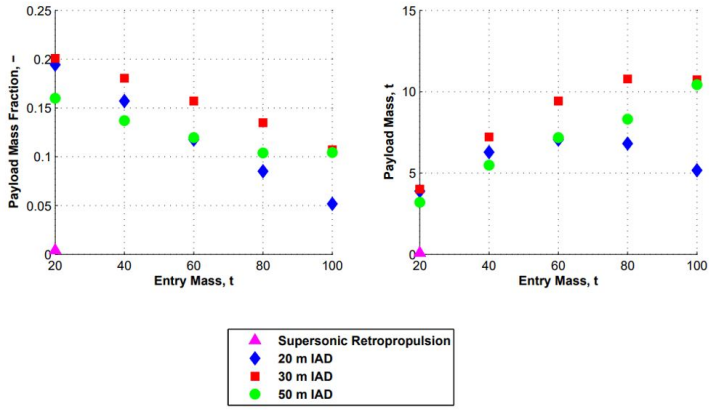

Figure 2.7: Mass savings as a function of IAD's diameter [10]

2.2.4 All-propulsive option

Architecture 3 shown in table 2.1, proposes an all-propulsive solution, and is the highest TRL and least complex architecture using only the engines. However, this option has several flaws involving the flow interaction between the structure and the engines in the hypersonic and supersonic ranges. There is not enough information about the flow separation and the resulting vehicle control dynamics, drag

and aerodynamics, and thus also thermal stress. The study carried out neglecting the drag contributions shows that nevertheless this option would be viable despite the fact that the masses on arrival are much higher than other architectures.

2.3 Ascent & Descent Generalities

The departure and arrival orbit's choice, as well as the number of stages, the type of propellant, and the thrust-to-weight ratio represent key parameters for the design of the lander and its propulsion system. NASA's technical report [15] investigates trades made to evaluate the ascent and descent missions , with the latter closely related to the EDL-SA study and the requirements imposed by the EDL phases. This study's objective concerns the development of ΔV budgets that can be used for sizing lander's systems and subsystems. What follows in this chapter will show the different options analyzed and the conclusions to which these trades led in terms of advantages and disadvantages. Numerical results will be better proposed in the next chapter 3 concerning the statistical analysis where they will be tabulated and compared together with the results of different analyses conducted in other reports and scientific articles.

2.3.1 Orbits and stages

Regarding the **Ascent Phase**, a 500x500km circular LMO Martian low orbit and a 250x33800km HMO Martian high orbit are evaluated, in both cases the trades also concern the number of stages, TPTO (Two Phase To Orbit) and SPTO (Single Phase To Orbit) options are evaluates. Both of them, in every trade, involve 3 ignitions, this is because it facilitates the choice of the line of the apsides of the arrival orbit, which must be well oriented to trace the asymptote that then brings the astronauts back to Earth.

- LMO (100 x 250km $\Rightarrow$ 250 x 500km $\Rightarrow$ 500km circ);
- HMO (100 x 250km $\Rightarrow$ 250 x 250km $\Rightarrow$ 250 x 33793km);

Some of the scientific papers investigated [16] also propose a 5 Sol orbit (250x119400 km), as shown in figure 2.8, but this kind of orbit will not be part of this study because it involves complex mission scenarios not related to a simple ascent of a small vehicle such as the one whose design is about to be investigated.

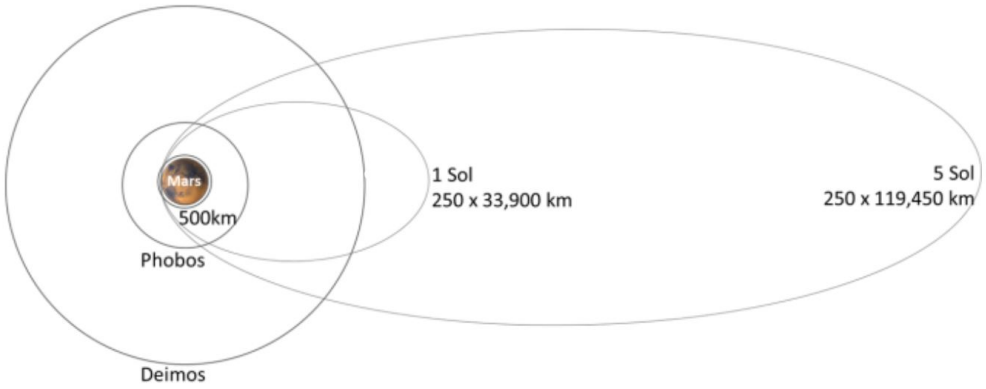

Figure 2.8: Martian Orbits [16]

Taking into account the fact that the ΔV split is given by the trajectory in the TPTO case, in figure 2.9 ΔVs required are compared in the various cases as the number of stages, arrival orbit and the thrust to weight ratio (T/W0) changes.

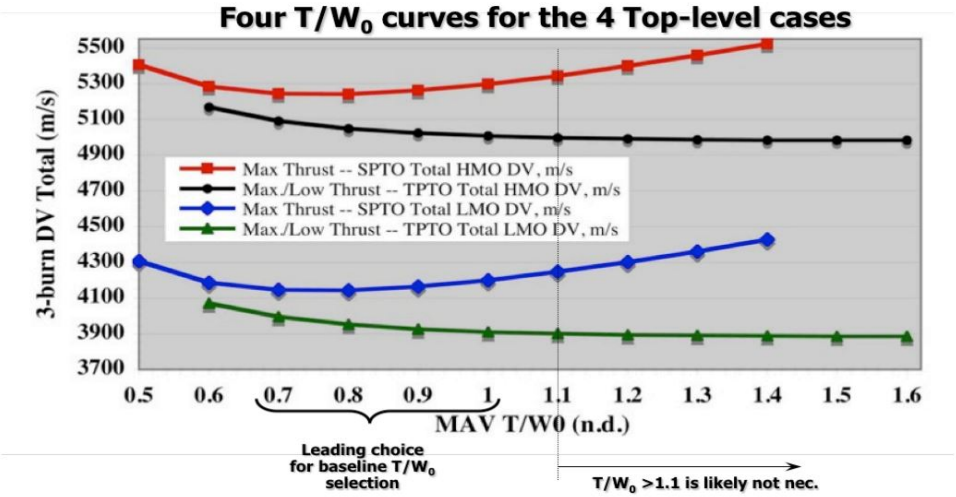

Figure 2.9: Ascent ΔV varying initial thrust-to-weight ratio, arrival orbit, and number of stages [15]

This study shows how thrust can vary greatly as the trhust to weight ratio T/W0 varies, and that there is an optimum value beyond which there is no advantage in terms of gravity losses that are instead simply dictated by the trajectory, so it is good to keep this ratio between 0.7-1, having a higher thrust can in fact also increase propulsion system masses and accelerations that cause problems for astronauts. The analysis conducted in [15] shows that by choosing either an LMO

or HMO orbit and the LOX/LCH4 propellant, the two-stage option always turns out to be less heavy than the single-stage option, and this is partly due to the efficiency that is achieved by staging.

As for the **descent**, the related subsystems' sizing depends strongly on the parking orbit and again on the choice of propulsion system. NASA's study [15] in this case, analyzes the same LMO and HMO orbits already mentioned to perform trades, considering LOX/LCH4 and LOX/LH2 as propellants as well as a payload mass varying between 10 and 40t. As already anticipated in section 2.2.2 and section 2.2.3, regarding EDL's systems, rigid aeroshell and HIAD technology are considered.

2.3.2 Propulsion system and propellants (Ascent)

Posed on the effectiveness of using two stages for ascent, NASA's study [15] compares 3 different propulsion systems with plausible values for nozzle area ratio, chamber pressure, and mixture ratio and researches the effect of specific impulse alone while holding masses, T/W0 thrust to weight ratio, and arrival orbit (HMO in this case) constant. The propellants used are

- **NTO/MMH (Isp=323 s)**: a storable configuration in which all the propellant must be carried from Earth;
- **LOX/LCH4 (Isp=355 s)**: and LOX/LH2 (Isp=440 s) which are instead two options ISRU (In-Situ Resource Utilization) using LOX that can be produced on Mars, this results in much lower masses for the vehicle than the storable configuration and are 2.5 times smaller configurations at launch from Earth.

Regarding the ISRU configuration with LOX/LCH4, an analysis is presented as the specific impulse varies, showing that the use of pressure-fed engines (Isp=340 s), pump-fed engines (Isp=355 s) or advanced engines (Isp=369 s) causes the mass of propellant required for the vehicle to ascend to vary by up to 16% between the first and last cases for a difference of only 30 seconds in the specific impulse. Thus, the conclusion is that based solely on the size of the lander and masses at departure, the configurations using propellants with ISRU capability are undoubtedly the best as they allow launching from the Earth's surface while keeping the oxidizer tanks empty, since upon arrival it will find an insitu propellant production system carried as cargo previously. However, there are several studies about less common propellants. For instance, in [17], it is pointed out how being the temperature on the surface of Mars at the equator varies between 26 C° and 111 C° depending on the season and time of the day, ISRU configurations using cryogenic propellants could be subject to boiloff, are therefore more complex to construct, make

operational and controllable, requiring a thermal system such as a cryocooler to keep the propellant in a liquid state. Martian surface temperatures related to the liquid-state operating temperatures of many propellants and oxidizers are shown in figure 2.10:

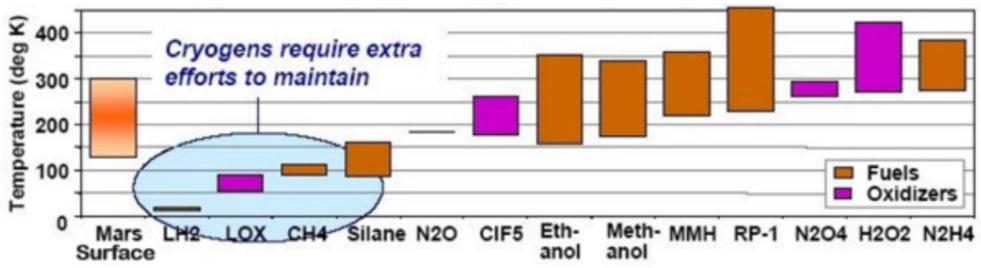

Figure 2.10: Propellant liquid temperature range and Mars Surface temperature range [17]

Another advantage of using ISRU configurations is definitely the use of non-toxic propellants such as LOX and LCH4. Disadvantages include the need for complex machinery to extract oxygen from the Martian atmosphere, which is 95% CO2, and higher power demand at the surface. The study proposes the use of a ClF5/N2H4 engine with the former used as the oxidizer, this combination allows for a high specific impulse of 370 seconds with a chamber pressure of 900 psia and a high nozzle expansion rate, this value is higher than that of conventional storable propellants as well as also denser. However, ClF5 has disadvantages, it is hypergolic in nature, which makes it difficult to be compatible with some materials, it is toxic, and it is not a very technologically developed option in terms of the engine and feed system. In the same study [17] a mission similar to the one shown in NASA's report [15] is analyzed. In this case for achieving a two-stage HMO with a thrust to weight ratio T/W0 of 1.8 and a crew of 4, the study compares the LOX/LCH4 case with the ClF5/N2H4 case and concludes that as expected the lander masses using cryogenic propellants are lighter, this also allows for easier EDL stages when using an aeroshell as it will be able to have smaller diameter. However, the storable option analyzed requires less technological development and would be a more functional and simpler system despite issues related to toxicity and high masses.

Returning to NASA's study [15] and the different trades evalueted based on number of stages and arrival orbit, from the trajectory analysis, thrust's trend as the thrust to weight ratio T/W0 changes is shown in figure 2.11. This type of analysis can be very useful in an initial sizing of the engine

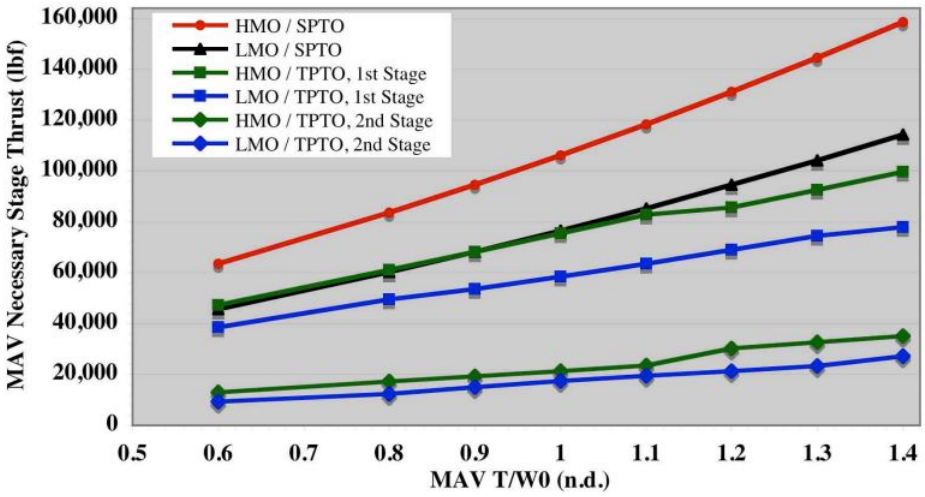

Figure 2.11: Necessary stage thrust as a function of the thrust to weight T/W0 ratio[15]

If the ISRU option is selected, given the advantages , it must still be chosen how to carry it out, so three different options are proposed that greatly vary the mass of the vehicle at launch:

- **Full ISRU**: in which both LOX and LCH4 are planned to be produced;
- **LOX ISRU**
- **No ISRU**

If the choice falls to producing only LOX, it will be sufficient to take advantage of the Martian atmosphere and then transport LCH4 from Earth by storing it in tanks until ascent. In contrast, the full ISRU option requires transporting LH2 from Earth to take advantage of the Sabatier process to produce LCH4 and LOX. Not using ISRU involves having to transport all propellant from Earth. Table 2.2 shows the differences in mass using different ISRU options.

Table 2.2: MAV masses changing the ISRU option (4 crew, T/W0=0.7, LOX/LCH4) [15]

	TPTO to LMO	**TPTO to HMO**	**SPTO to LMO**
No ISRU	28t	31-33.6t	36t
LOX only ISRU	13t	13.7-14.3t	14t
Full ISRU	9t	8.5-8.7t	9t

For ascent, the various options proposed have advantages and disadvantages, the SPTO option for example is safer guaranteeing less risk of crew loss by providing for one less event in the absence of staging. The TPTO option on the other hand allows for a lighter vehicle with lower thrust levels split over the two stages and consequently lower accelerations, risky for crew's health. Vehicles designed for LMO are smaller and lighter and allow the use of the ISRU, the HMO option on the other hand has the advantage of having to operate in a less stringent temperature environment.

2.3.3 Propulsion system and propellants (Descent)

In this case only the options involving cryogenic propellants are analyzed. The ΔV needed to perform the descent is much lower than the one needed for the ascent, and moreover it does not present all the stringent requirements related to the maintenance, since it is an event that comes to occur long before the ascent. In fact typical value for ΔV's are 798 m/s using a rigid aeroshell technology and 601 m/s using HIAD. For these reasons, making a vehicle valid for both ascent and descent would need to follow ascent's constraints choosing the propulsion system. Thus, using the same main propulsion system as for ascent, with LOX/LCH4 pump-fed propellant, the analysis shows that with a thrust to weight ratio T/W0 of 0.6-0.7 two of the MAV engines are required in the case of 10t payload and 4 in the case of 40t. These maximum values are, however, strongly influenced by lander's configuration, which can vary the required T/W0 up to even double it, leading to the need for 4 and 6 engines respectively. As a result of the analysis [15], figure 2.12 shows the thrust required in the descent phase as the final mass delivered to the surface varies.

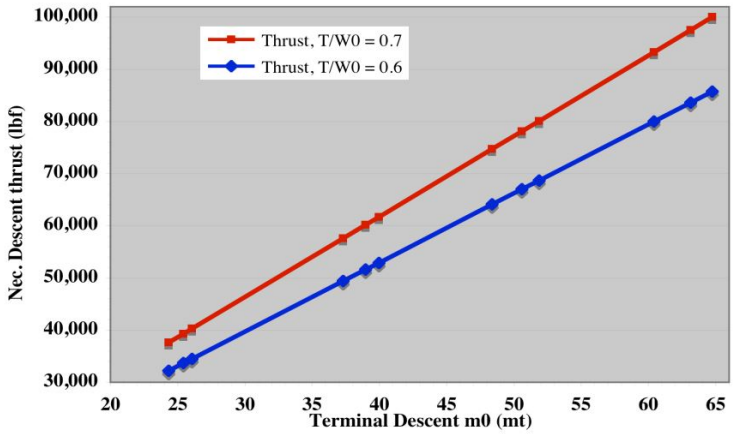

Figure 2.12: Necessary thrust for descent [15]

2.4 Mars Atmosphere

Analyzing ascent and descent missions, Mars' atmosphere is of paramount importance. By employing an atmospheric model that delineates pressure, temperature, and density, it is possible to estimate the atmospheric drag coefficient. This coefficient is crucial as it affects the acceleration and subsequently the velocity at which the lander descends or attains the parking orbit during the ascent phase.

The Martian atmosphere, a thin layer primarily composed of CO2, is significantly less dense than Earth's atmosphere. Nonetheless, similar to Earth, it hosts various chemical, thermodynamic, and fluid-dynamic processes. Importantly, the Martian atmosphere is not uniform and the flow properties fluctuate with time and altitude. The Sun heats the Martian surface, which in turn warms the adjacent fluid, transmitting heat through convection and diffusion into the atmosphere. As on Earth, pressure on Mars decreases with altitude. Temperature also decreases, reaching its peak at the surface. Density, influenced by the equation of state, varies with temperature and altitude and diminishes as well.

In April 1996, the Mars Global Surveyor developed an atmospheric model to track altitude effects on these variables, allowing for effective description of aerodynamic forces as density changes. This data collection effort was led by Jonathon Donadee of Canfield Middle School in Ohio in 1999. The curve fit for the model was developed by Dave Hiltner of St. John's Jesuit High School. This atmospheric model [18], which is utilized in ASTOS and MATLAB subroutine missions, will be further elaborated in section 4.2 and in section 5.1 in defining the aerodynamic model. The equations for calculating atmospheric temperature as a function of altitude are reported in (2.1) and (2.2), atmospheric pressure equation is reported in (2.3) and atmospheric density equation is reported in (2.4).

$$T = -31 - 0.000998 \cdot h \; [C^\circ] \;\; h < 7000 \; m \tag{2.1}$$

$$T = -23.4 - 0.00222 \cdot h \; [C^\circ] \;\; h > 7000 \; m \tag{2.2}$$

$$p = 0.699 \cdot e^{(-0.00009 \cdot h)} \; [KPa] \tag{2.3}$$

$$\rho = \frac{p}{0.1921 \cdot (T + 273.1)} \; \left[\frac{kg}{m^3}\right] \tag{2.4}$$

Where (i) T is the atmospheric temperature [C°], (ii) h is the altitude [m], (iii) p is the atmospheric pressure [KPa], (iv) ρ is the atmospheric density $\left[\frac{kg}{m^3}\right]$ The speed of sound will also be calculated based on this atmospheric model, in equation (2.5).

$$c = \sqrt{\gamma R T} \tag{2.5}$$

where (i) $\gamma = 1.29$ is the adiabatic expansion coefficient and (ii) $R = 191.8 \; [J/kg/K]$ the gas' constant. In figure 2.13 temperature, pressure, density and speed of sounds trends at varying altitudes are shown.

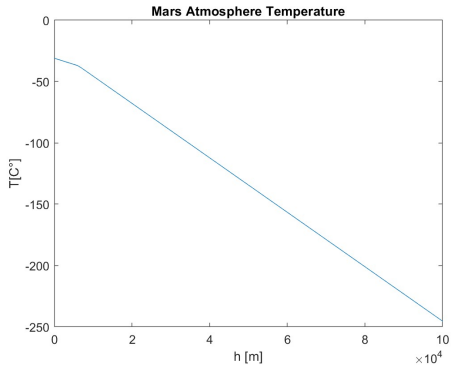

(a) Temperature

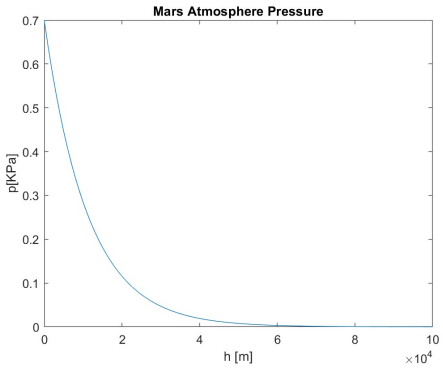

(b) Pressure

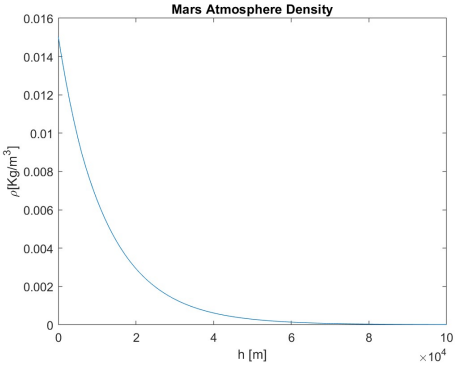

(c) Density

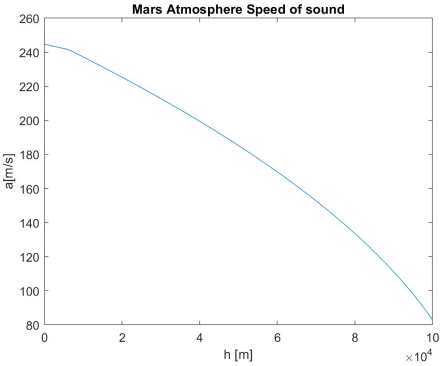

(d) Speed of sound

Figure 2.13: NASA Atmospheric model for Mars

Chapter 3
Statistical Analysis

This chapter summarizes a phase of the thesis work apt to collect useful data for lander design, starting with various configurations proposed in the literature and then dividing them into subgroups based on similarity and possibly plotting statistical trends of quantities such as dry mass or payload mass as the total mass of the lander or the number of stages and ΔV needed for example. This type of work aims to frame the state of the art about human mars landers and has these objectives:

- To serve as a starting point for preliminary design, create a design methodology that will allow initial estimates to be made primarily on the total masses and the masses of the individual subsystems. This methodology will then be updated as the work proceeds to the next iterations;
- Choice of a reference vehicle;
- Upon completion of the work, to collocate the proposed design in the current state of art.

The work related to the lander design, as far as this thesis work is concerned will be limited to this initial estimation and research of an outline methodology as more concentration will be placed on the mission analysis, which is an integral part of the methodology as it allows for various design inputs such as ΔVs and limitations on deceleration systems in terms of weight and size for example, as well as validating or not validating the proposed designs by discussing their feasibility.

3.1 Data collection in a database

The creation of the database is a crucial step in this preliminary work, considering that the study's goal is to create a lander that performs both descent and ascent

tasks, an initial study aims to collect data only on ascent related to design proposals found in the literature and will be discussed in section 3.1.1. This choice is justified from the need to save weight and search for a reusable vehicle. This vehicle is considered to be a MAV with the addition of the EDL systems, with this assumption it becomes a lander that performs both ascent and descent. MAV's statistical study will be coupled with another one concerning the masses of EDL systems in proposed designs found in literature in section 3.1.3, finding a percentage of the latter in total weight or dry mass to be added to the statistical data previously extrapolated from the study on MAVs.

3.1.1 Mars Ascent Vehicle Data

As for the MAV study, the information gathered on possible lander designs was categorized in tables 3.1, 3.2 considering TPTO, and tables 3.3, 3.4 considering SPTO, based on several inputs:

- **Type of orbit**: a rough subdivision between LMO and HMO, as already anticipated in section 2.3, HMO orbit mainly refer to orbits of 250 x 33793 km while LMO orbits often consider circular orbits ranging from 250 km to 500 km. This type of subdivision soon proved to be too heterogeneous in wanting to consider all the data, so it was preferred to categorize by ΔV;
- **Mission Duration**: the purpose of cataloging by mission duration is due to the need to frame the ultimate purpose of the vehicle, as discussed in section 1.2, in the literature it is possible to find vehicles that serve only as MAVs, others that also constitute living units on Mars, others that are simply used as descent vehicles, and still others for descent and ascent to and from the planet. By framing the duration of the mission, it is possible to understand which vehicles make sense to compare, which others need to be catalogued solely to get a general picture of the state of the art, and finally to understand if and how this duration may affect the habitable volume needed, particularly the mission durations considered here are all in the range of 7-8 days;
- **Crew number**: like the mission duration, it is a useful parameter to understand the type of vehicle, in the specific case a strong preponderance was found in the literature in choosing a number of crew passengers equal to 4, this was useful to understand that the current state of the art shows a preference towards a number of astronauts neither too small nor too large in order to both ensure the mission success without having too significant workloads, and to allow limiting the mass of payload to be carried and the weight of

the ECLSS. Only a few vehicles with passengers of 2 or 6 are present in the cataloging, which would make any statistical trend too disproportionate.

- **T/W thrust to weight ratio**: the thrust-to-weight ratio confirms what has already been learned from the literature in section 2.3.2. It is always between 0.7-1 in order to ensure a propulsion system that is not too heavy and generates higher thrusts. Few cases were found where the design deviates from these values;

- **Propellant**: almost all of the analyzed designs use LOX/LCH4 combination for the advantages in using ISRU, which the study of this thesis focuses on in analyzing the statistical trends. Some configurations propose alternative noncryogenic propellants that guarantee less complexity in maintenance, but often also difficulties related to toxicity and leading to heavier and less performing configurations (ClF5/N2H4). Much less popular are NTO/MMH and LOX/LH2 combinations, which involve higher weights and other hybrid configurations (LOX/PARAFFINS, FFA/HNO3), these options are reported in tables 3.2 and 3.3;

- **Ascent** ΔV: when orbits are too heterogeneous to be compared, comparing designs in which the ΔV to reach the ascending orbit are similar can be a good fallback method, in fact from this value starts the sizing of the propulsion system and the choice of the required thrust, similar values will indicate similar and comparable designs;

- **Payload mass**: it is crucial for the design to understand how much payload can be carried as this may be the first mission requirement, for human missions this requirement tends to be higher, this is in fact one of the parameters chosen to track statistical trends. For many designs included in the database this value is provided by references, for others it has been estimated on the basis of statistical formulas [19], in which it becomes useful to have cataloged data on mission duration and number of crew members, first the mass reserved for each crew member is estimated in equation (3.1), consider a weight of 70kg for each and and extra 42kg:

$$m_{\text{crew}} = n_{\text{crew}}(42 + 70\,\text{kg}) \tag{3.1}$$

Where n_{crew} is the number of crew members. A mass for consumables useful to the crew is also estimated on the basis of mission time, in equation (3.2).

$$m_{\text{consumables}} = n_{\text{crew}} t_{\text{mission}} \left(\frac{2.9\,\text{kg}}{\text{day}} \left(1 - \frac{70}{100} \right) + \frac{1.83\,\text{kg}}{\text{day}} + \frac{0.82\,\text{kg}}{\text{day}} + \frac{1.22\,\text{kg}}{\text{day}} \right) \tag{3.2}$$

Where (i) n_{crew} is the number of crew members and (ii) t_{mission} is the mission duration [s]. To finally find the payload mass, the cargo payload is added up, which ranges from 250kg up to even a few tons depending on the type of mission and consists of specific instrumentation or mission useful materials.

- **Total Mass**: collecting information on total mass, again makes it possible to identify what type of vehicle is being cataloged, and its purpose, but also to identify maximum and minimum values within which to choose a reference vehicle. This value in particular is used to plot statistical trends when represented by varying other masses (dry mass, inert mass, payload mass) or other useful characteristics such as Thrust, these trends are reported in section 3.1.2;

- **Dry Mass**: the vehicle total mass minus propellant and payload mass, typically the most difficult to estimate but also the most significant for weight estimates since it represents the sum of the masses of the systems. The main aim is to find a percentage of dry mass for these system mass estimation. In the database this mass is reported as a single mass, but where possible it has also been divided among the various subsystems into percentages of the total in order to estimate the weights of each and enter preliminary design methodology;

- **Inert Mass**: by keeping track of this value it is possible to trace the dry mass as can be seen in equation (3.3). If the specific design in the literature does not specify it, as well as the payload mass

$$m_{inert} = m_{payload} + m_{dry} \tag{3.3}$$

  Where (i) $m_{payload}$ is the payload mass [kg] and (ii) m_{dry} is the dry mass [kg].

- **Propellant mass**: closely related to propellant type and dry mass, information collected to get an initial estimate on the amount of propellant needed if the ΔV or propellant performance parameters were not known so that the weight of the tanks could also be estimated. Typically when not provided by the references, it was estimated using rocket equation shown in (3.4).

$$m_{prop} = m_{final} \cdot \left(e^{\frac{\Delta V}{I_{sp} g0}} - 1 \right) \tag{3.4}$$

  Where (i) m_{final} is the final stage mass [kg], (ii) ΔV is the speed increase provided [m/s], (iii) I_{sp} is the propellant's specific impulse [sec] and (iv) g0 is the standard earth's gravitational acceleration [m/s^2];

- **Thrust**: mainly related to the first stage, the heaviest one, kept track mainly for propulsion system sizing.

Table 3.1 shows an initial data collection, with the most important parameters, regarding MAV vehicles using LOX/LCH4 as propellant and ascending to various HMO orbit (or LMO with similar ΔV), most of the data comes from NASA's technical report [15] in which numerous designs with different thrust-to-weight ratios, payload masses, dry masses, etc. are proposed and where presented in the previous chapter. Similarly, the designs referenced in [17] and [16] have a higher ΔV requirement and in the second case a higher payload, but since these are similar vehicles the trend is respected. The vehicle referenced in [20], on the other hand, is extremely interesting, it concerns a vehicle very similar to the one whose design is intended to pursue, namely a multifunction vehicle that performs both ascent and descent, but whose only ascent data were reported. Such a vehicle performs ascent toward a 390.5 km periastrum altitude of an HMO 1 Sol orbit, the heterogeneity of the data compared to other designs is to be found in the need to create subsystems capable of accommodating the descent requirements in some cases more stringent, in the higher ΔV resulting in greater propellant needs, and in the use of more conservative approaches to design.

Table 3.1: LOX/LCH4 Mission Data Table (MAV)

Mission	**Thrust 1st Stage [kN]**	**T/W**	**Ascent ΔV (m/s)**	**Payload mass(kg)**	**Total mass (kg)**	**Dry mass (kg)**	**Inert mass (kg)**	**Propellant mass (kg)**
TPTO to HMO [15]	292	0.9	3777	826.77	33034	10067	10893.77	22967
TPTO to HMO [15]	232	0.7	3845	826.77	33638	9239.23	10066	23572
TPTO to HMO [15]	262	0.8	3802	826.77	33253	9239.23	10066	23187
TPTO to HMO [15]	292	0.9	3777	826.77	33034	9240.23	10067	22967
TPTO to HMO [15]	323	1.0	3761	826.77	32897	9240.23	10067	22830
TPTO to HMO [15]	355	1.1	3751	826.77	32808	9240.23	10067	22741
TPTO to HMO [15]	366	1.2	3744	826.77	31014	9239.23	10066	20948
TPTO to HMO [15]	395	1.3	3741	826.77	30983	9239.23	10066	20917
TPTO to HMO [15]	425	1.4	3738	826.77	30965	9238.23	10065	20900
TPTO to HMO [15]	292	0.9	3777	826.77	33033	9240.23	10067	22966
TPTO to HMO [15]	279	0.9	3777	676.77	32500	9340.23	10017	22483
TPTO to HMO [15]	232	0.9	3777	826.77	33132	9338.23	10165	22967
TPTO to HMO [15]	304	0.9	3777	1265.16	34445	9200.845	10466	23979
TPTO to HMO [15]	309	0.9	3777	826.77	34880	9240.23	10067	24813
TPTO to HMO [15]	292	0.9	3777	826.77	33034	9240.23	10067	22967
TPTO to HMO [15]	279	0.9	3777	826.77	31528	9239.23	10066	21462
TPTO to HMO [15]	231	0.7	3845	826.77	33639	9240.23	10067	23572
TPTO to LMO [15]	230	0.9	3777	802.28	25981	9170.72	9973	16008
TPTO to LMO [15]	251	1.0	3766	802.28	25496	9170.72	9973	15523
TPTO to HMO [20]	371		4698	783.11	60808	15700	16483	45108
TPTO to HMO [17]	235	1.8	5137	792.00	36152	8649	9441	26478
TPTO to HMO [16]	300		5413	1106.00	42900	8894	10000	32900

As anticipated, configurations with different propellants such as LOX/LH2, as well as noncryogenic, and storable propellants without ISRU capability have also been found in literature and are reported in table 3.2. Cataloguing these designs is complicated as these are unique configurations to which there is no

comparison in the literature, and certainly with quite different results from those obtainable with the LOX/LCH4 combination in terms of design preventing them from being related. These designs are reported in the database and subsequent graphical representation for the pure purpose of framing the state of the art and contemplating future design developments.

Table 3.2: Other propellants and atypical Missions Data Table (MAV)

Mission	**Thrust 1st Stage [kN]**	**T/W**	**Propellant**	**Ascent ΔV [m/s]**	**Payload Mass**	**Total Mass [kg]**	**Dry Mass [kg]**	**Inert Mass [kg]**	**Propellant Mass [kg]**
TPTO to HMO[15]	330	0.9	NTO/MMH	3777	826.77	37332	9239.23	10066	27266
TPTO to HMO [15]	230	0.9	LOX/LH2	3777	826.77	26082	9240.23	10067	16015
TPTO to HMO [21]	375		LOX/PAR.WAX	5274	635.00	6749	3426	4061	2688
TPTO to HMO[17]	175	1.8	ClF5/N2H4	5137	792.00	27188	6315	7107	20081

Following a similar approach, data are also collected for the single stage option. From the literature analysis this option appears to be much less selected because of the higher total masses, the need to carry more propellant not being able to enjoy the advantages of staging, with the possibility of releasing tank or engine masses in case these are empty or have fulfilled their purpose with the disadvantage of higher complexity. Since Martian missions, especially human missions, as seen in the literature review in chapter 2, are very focused on mass saving as there is a need for transport of higher payloads and heavy systems for human support, this option is not typically contemplated in most cases, in fact the number of hypothetical designs found in the literature is very small. Again, as far as propellant is concerned, most configurations opt for a LOX/LCH4 combination given the possibility of using ISRUs, but there are also several more cutting-edge configurations aimed at proposing alternative solutions for savings in weight and technological complexity. Table 3.3 shows data regarding SPTO missions using LOX/LCH4, while table 3.4 concerns same missions type but involving other propellants.

Table 3.3: Single Stage LOX/LCH4 Missions Data Table (MAV)

Mission	**Thrust [kN]**	**T/W**	**Propellant**	**ΔV (m/s)**	**Payload Mass (kg)**	**Total Mass (kg)**	**Dry Mass (kg)**	**Inert Mass (kg)**	**Propellant Mass (kg)**
SPTO to HMO [15]	410	0.9	LOX/LCH4	4016	826.77	46224.00	10195	11022	35202
SPTO to HMO[15]	315	0.7	LOX/LCH4	4036	827.77	45966.00	10195	11022	34944
SPTO to LMO[15]	295	0.9	LOX/LCH4	4016	802.28	33300.00	9264.72	10067	23233
SSTO to LMO [22]	101		LOX/LCH4	5700	833.23	18000.00	3166.77	4000	14000

Table 3.4: Single Stage Other Propellants Missions Data Table (MAV)

Mission	**Thrust [kN]**	**Propellant**	ΔV **(m/s)**	**Payload Mass (kg)**	**Total Mass (kg)**	**Dry Mass (kg)**	**Inert Mass (kg)**	**Propellant Mass (kg)**
SSTO to HMO [23]	135	NTO/MMH	5209	140.00	14093.00	2620.5	2760.5	11332.5
SSTO to LMO [16]	300	NTO/MMH	4176	1049.00	24400.00	4951	6000	18400
SSTO to LMO [24]	72	FFA/HNO3	4830	212.00	4190.00	580	792	3398
SSTO to LMO [25]	250	MMH/MON25	4200	982.00	26292.00	6632	7614	18678

3.1.2 MAV Data Graphical Representation

Once the MAV data have been collected, the study proceeds with a graphical representation of the most useful design variables and the comparison of these variables where possible shown in figure 3.1. Having in fact categorized the design architectures according to number of stages, propellant, and arrival orbit allows regression lines to be drawn for the variables between similar architectures, regression lines' equations are reported in table 3.5 where y is the total mass, and in table 3.6 where y is the dry mass.

Table 3.5: MAV Statistical Equations Payload Mass - Total Mass

Mission Type	ΔV	**Equation** y	R^2
SSTO LOX/LCH4	4000 m/s	$y = 43.588x$	0.905
TSTO LOX/LCH4	5200-5400 m/s	$y = 41.113x$	0.9938
TSTO LOX/LCH4	3700-3800 m/s	$y = 38.987x$	0.9663

Table 3.6: MAV Statistical Equations Payload Mass - Dry Mass

Mission Type	ΔV	**Equation** y	R^2
SSTO LOX/LCH4	4000 m/s	$y = 12.076x$	0.9991
TSTO LOX/LCH4	5200-5400 m/s	$y = 9.0174x$	0.9777
TSTO LOX/LCH4	3700-3800 m/s	$y = 10.885x$	0.9834

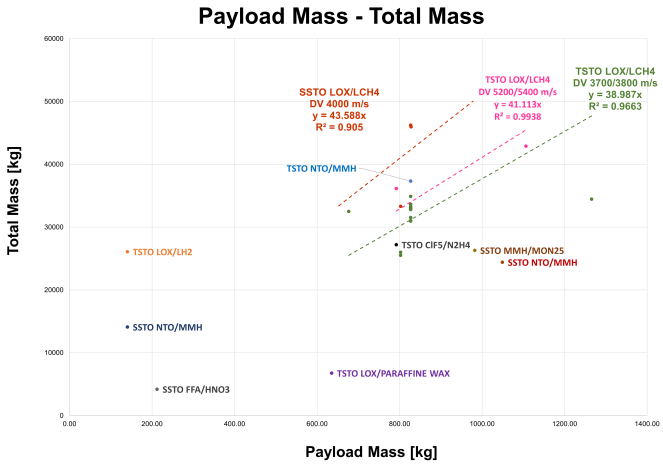

(a) Payload Mass - Total mass

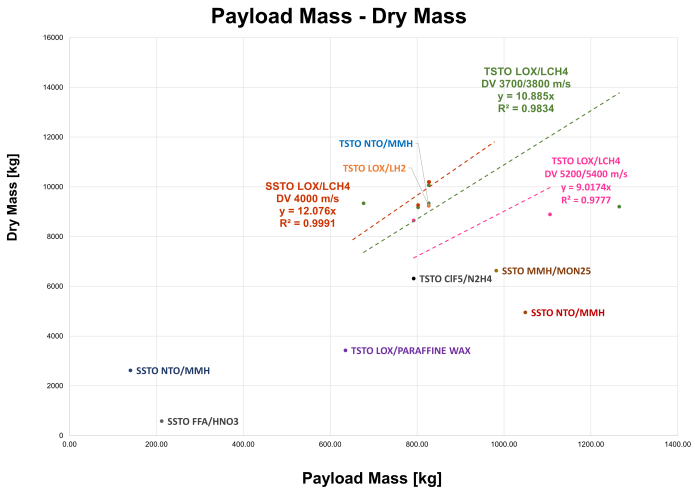

(b) Payload Mass - Dry Mass

Figure 3.1: MAV Statistical Trends & State of Art

Given the large discrepancy found on some of the variables due to slightly different arrival orbits, and different mission architectures for reaching the same orbit, these regression lines has been plotted only between designs with similar ΔV. These statistical trends provide a very first rough estimate of certain variables, in figure 3.1, (a) and (b) show the trends for the total mass and dry mass of the MAV as a function of the payload mass, which is one of the design parameters that indicates how much useful mass can be transported to Martian orbit and is strongly dependent on the mission objective, taking this value as input as a requirement it will be possible to estimate a total mass and a dry mass for the lander and

then enter a first sizing cycle for the subsystems by dividing these masses among each of them, this following a properly validated design methodology. Dry mass in this sense is much more useful for this purpose, representing primarily the mass of the latter. It should be noted how important it is to be able to identify reference missions and vehicles to ensure a truthful output value, and that the heterogeneous nature of many of these missions and architectures precludes having a large enough statistical base for some of the trends tracked, which is why many architectures are reported solely to frame the current technological state about human Martian missions and it is useful to include them in the study in order to be able to collocate the design being studied in this master's thesis within the bigger picture when the work is completed. Specifically, the reference vehicle's choice from among those proposed turned out to be the correct way to begin preliminary sizing in order to then use more accurate design methodologies in subsequent iterations.

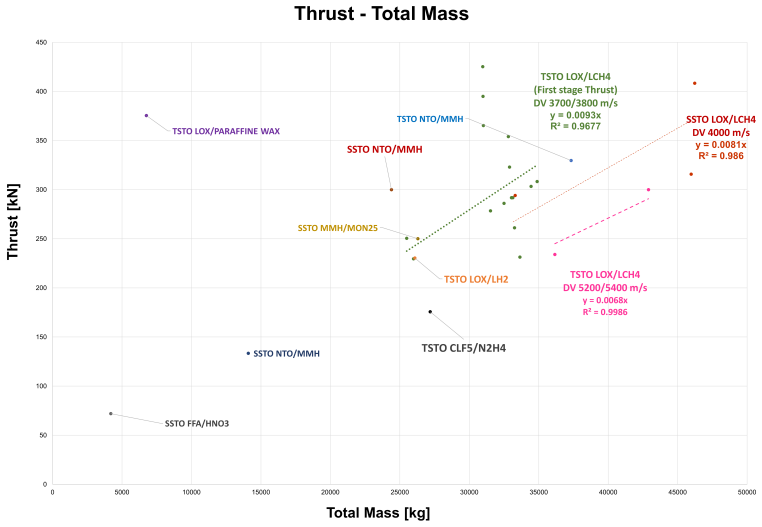

Figure 3.2: MAV Statistical Trends: Thrust - Total Mass

Another represented parameter is the overall or first stage thrust depending on the architecture, as the total mass varies, represented in figure 3.2. Although from the value of ΔV it is still possible to have a first estimate of thrust for the lander, it is still useful to have an order of magnitude to rely on in the first iterations to size the propulsion system plotting a regression line whose equations are reported in table 3.7, where y is the thrust.

Table 3.7: MAV Statistical Equations: Thrust - Total Mass

Mission Type	ΔV	**Equation** y	R^2
SSTO LOX/LCH4	4000 m/s	$y = 0.0081x$	0.986
TSTO LOX/LCH4	5200-5400 m/s	$y = 0.0068x$	0.9986
TSTO LOX/LCH4	3700-3800 m/s	$y = 0.0093x$	0.9677

3.1.3 EDL Systems Data Collection

Having so far catalogued only data on ascent modules (MAVs), this statistical analysis cannot be said to be complete in seeking to qualitatively represent the masses of a lander subsystems as subdivided from dry mass. In fact, a MAV is not equipped with the systems for EDL that were discussed extensively in section 2.2 regarding the EDL-SA study conducted by NASA and explored in depth later in numerous publications on the subject [9] [15]. EDL systems use technologies that involve IAD, rigid aeroshells, heat shields, F-TPS etc, furthermore, it is assumed that some subsystems such as TPS have masses that differ from those of a simple ascent vehicle due to different operating environments and relative constraints. In order to have a first estimate of their masses, a cataloging was carried out by taking as reference again hypothetical designs from the literature, data are reported in table 3.8, this time concerning descent modules. The interest here relates only to these system's masses. Data are cataloged as follows:

- **Total Mass**: note how it is much higher than those analyzed for the ascent module, in fact in the literature it is possible to find configurations of landers involving also the ascent mission, however the vast majority of them carry with them as payload or cargo entire habitation modules, rovers, MAV vehicles completely independent and without interchangeable systems, often these are the same vehicles that are used for the Mars Transfer repurposed for descent scenario;

- **Dry Mass**: for the same reasons listed above it is much more useful then to analyze the dry mass to make estimates about the weights of the subsystems;

- **TPS & Deceleration System Mass**: from data sheets of the designs found in the literature, a magnitude that should be evaluated as the objective of the analysis.

Table 3.8: EDL Mass Distribution

Lander Reference	**TPS & Deceleration System Mass [kg]**	**Total Mass [kg]**	**Dry Mass [kg]**
[26]	4608	62791	21565
[27]	6706	77516	26280
[9]	6000	109000	57400
[9]	25700	133500	84700
[28]	8658	60435	21355
[28]	3762	57233	20190
[29]	5499	63921	27937
[29]	6373	75000	26270
[29]	7025	68277	19781
[22]	6800	62000	40190
[20]	3025	41715	25815

3.1.4 EDL Systems: Data Graphical Representation

Having thus operated the graphical representations of these values in figures 3.3 and 3.4, the work proceeds again drawing the regression lines in order to extrapolate a percentage for the mass of these systems on the total or dry mass, the equations are shown in table 3.9. This type of analysis is very relative, in fact covering different systems for deceleration, as can be seen in figure **??**, it covers countless technologies, and therefore with different characteristics, advantages and disadvantages discussed in chapter 2 talking mainly about IAD and rigid aeroshell. This implies that this first very rough estimate is valid to be able to initially frame the impact that the mass of these systems has on the design and as first to give a general picture on the current state of the art, it is a figure to be updated later after further more specific research regarding the design of these types of technologies for descent that will not be the subject of study of this master thesis that will later deal mainly with mission analysis, assisting with a work conducted in parallel just on subsystem design that will take this concept further.

Table 3.9: EDL Statistical Equations: Dry Mass/Total Mass - Dec. Sys & TPS Mass

Mass	**Equation** y	R^2
Total mass	$y = 0.1126x$	0.8205
Dry Mass	$y = 0.2326x$	0.876

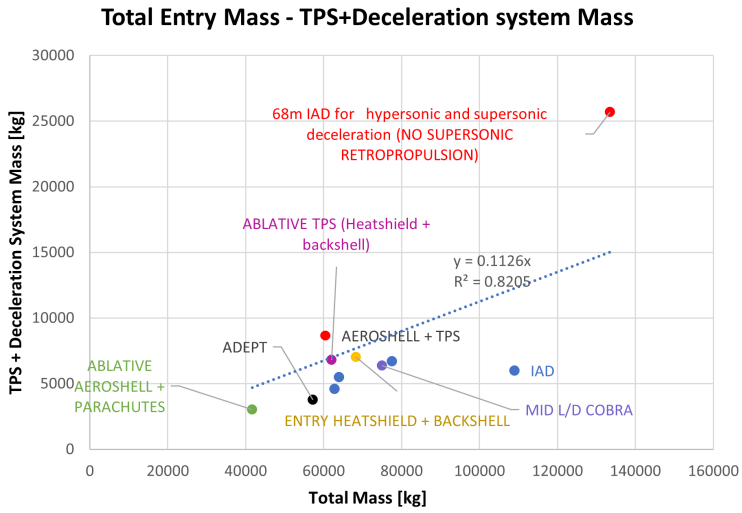

Figure 3.3: Statistical trend: TPS Mass & Dec.Sys Mass - Total Mass

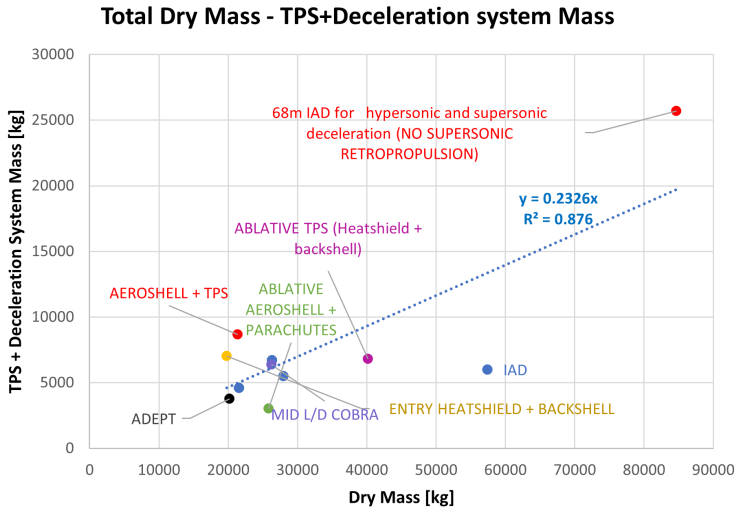

Figure 3.4: Statistical Trend: TPS Mass & Dec.Sys Mass - Dry Mass

3.2 First Design Methodology & Starting Point

As a final result of the statistical analysis it is possible to draw up an initial rough design methodology, with the information collected in the databases for ascent and descent vehicles, by investigating the data sheets of each of the mentioned

references it is possible to derive percentages of the total mass/dry mass of all the systems/subsystems, considering of course also the presence of the deceleration system for the EDL. This type of information is appropriately supplemented with another design methodology concerning, however, multipurpose landers that also perform the interplanetary transfer [30] from which absent data and those whose discrepancy between different designs made it impossible to plot statistics are estimated. This type of methodology is to be used with great care, it simply serves to create an outline, an initial imagery of what is the incidence of a given system or subsystem in the design, the validations for mission analysis that will be carried out in this thesis work in fact will use for the first iterations a reference vehicle, another output of this statistical analysis, as it is chosen according to the type of mission i.e. dual purpose, an interchangeable vehicle capable of performing ascent and descent reusing as much as possible systems/subsystems saving in mass. The vehicle in question [20] is the one that was given special attention in section 3.1.1 for this very reason. This will be the starting point for the first iteration for what concerns the mission analysis model. Then as already explained in the introductory chapter the design work will be carried out in parallel in another thesis work and continue in the development of a reliable and validated methodology. A summary for the statistical analysis' work is shown in figure 3.5, that also highlights how, starting from this point, the work is split in order to lay the foundations for mission analysis and design's routines.

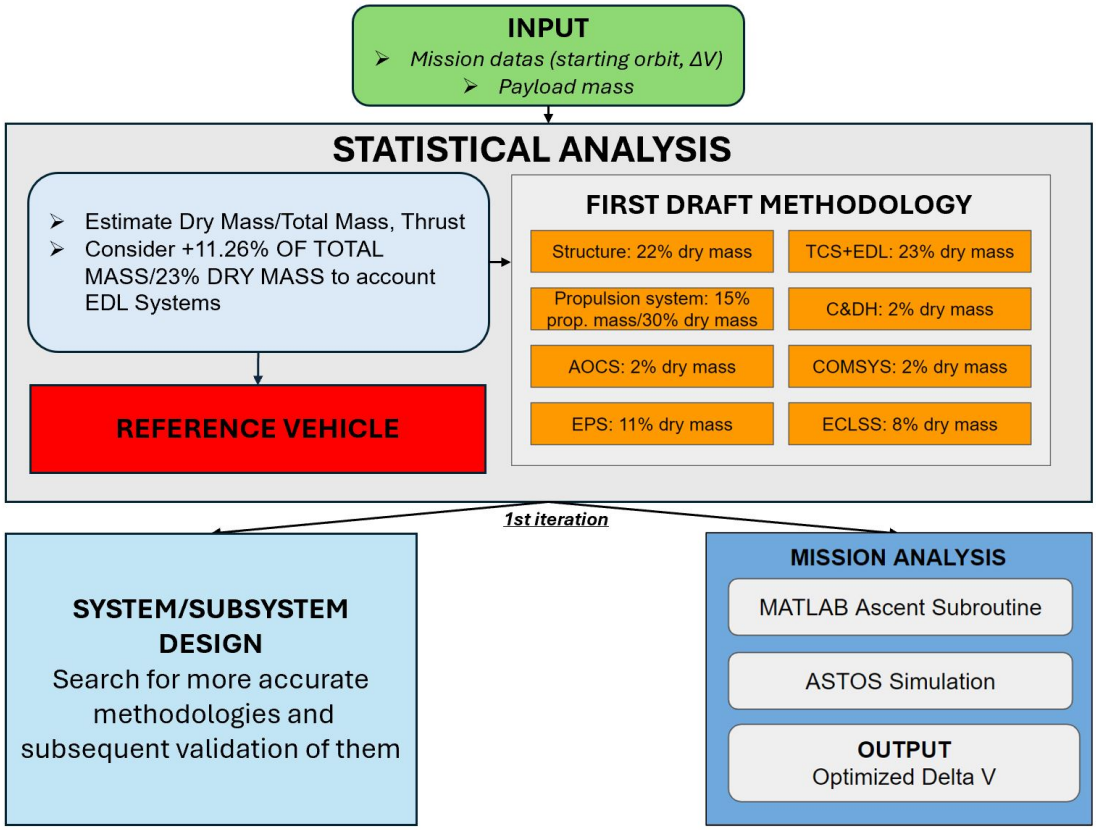

Figure 3.5: Statistical analysis summary work & next steps

Chapter 4

Mission Analysis: Ascent Scenario

This chapter will discuss the ascent scenario's modeling from the Martian surface to a Low Mars Orbit (LMO), following the mission and reference lander described in [20] and investigated during the statistical analysis in chapter 3. The main objective of the model is to estimate the ΔV required for the ascent, taking into account atmospheric and gravity losses. This is crucial for providing significant input for the lander sizing's routine and for verifying the overall feasibility of the mission based on the design taken as reference. To achieve this, a model for the Martian atmosphere will first be created based on the one developed by NASA [18], already mentioned in section 2.4. A valid drag coefficient for ascent will then be modeled to evaluate atmospheric drag, this will be discussed in section 4.2. After selecting an appropriate mission architecture that divides the ascent into propulsive and non-propulsive phases to ensure orbit is reached in section 4.3, the actual simulation will be carried out. Ascent mission's simulation and its subsequent optimization will be performed twice, using two different software tools and considering slightly different initial assumptions:

- **MATLAB Subroutine**: In this initial and simplified model, the goal is to create a very fast code that can immediately provide an initial estimate for the ΔV and losses. A set of simplified, 2-degree-of-freedom equations of motion will be integrated, taking the thrust angle, engine throttle, and duration of certain phases as input values to be optimized against an objective function. This model is better investigated in section 4.4;
- **ASTOS Simulation & Optimization**: This model will be more complex, with 3 degrees of freedom, taking the lander's dynamic attitude, duration, and throttle in each phase as inputs. The program allows the ascent to be simulated without optimization, given an initial estimate of these inputs.

When the initial estimate provided by the simulation yields a good ascent and velocity profile consistent with the expected arrival orbit, it will then be possible to optimize following a set of appropriately selected optimization constraints. This optimization is slower and more sensitive to the initial estimate, but it is also much more accurate. The reference section for this study is section 4.5.

Once both models are completed and good results are obtained on both of them, results will be compared in section 4.6.

4.1 Reference Lander Mission Summary

Starting with the reference vehicle [20], it is useful to provide an overview of the mission for which it is designed and to report its main characteristics and parameters used in the mission analysis conducted here. The reference Human Mars Lander (HML) is part of a larger and more complex mission architecture that involves other vehicles, particularly a Service Module (SM) that transfers from Earth to a circular Martian reference orbit with a radius of 7020 km. From there, the SM transfers to an orbit with a periapsis of 390.5 km altitude and an apoapsis of 3630.5 km altitude. On this orbit, the Mars Vehicle for Interplanetary Cruise (MAVERIC) will later be placed, which the crew of four astronauts will use to arrive on Mars and subsequently return to Earth. The SM is sent ahead to dock with the interplanetary vehicle and transfer the crew to the HML. The SM then performs a Hohmann transfer to place itself in a 200-km circular orbit from which the Entry, Descent, and Landing (EDL) of the HML takes place, and it proceeds to undock. The HML is then repurposed to a Mars Ascent Vehicle (MAV) on the Martian surface by removing the landing systems and Thermal Protection System (TPS), refueling the tanks with LOX/LCH4 propellant produced in situ. This propellant is used for the ascent to the periapsis of the interplanetary vehicle orbit. For simplicity, the arrival orbit will be considered to be circular with an altitude of 390.5 km. The main data used to test the model in MATLAB and ASTOS concern generic information about the propulsion system, wet and dry masses of the lander, and reference diameters for modeling atmospheric drag. The HML, as treated here, is a two-stage vehicle in its configuration for ascent. For both descent and ascent maneuvers, it uses a chemical propulsion system with a combination of LOX and LCH4, which, as previously discussed, ensures in-situ production on the planet, adequate thrust-to-weight ratio (T/W), high Technology Readiness Level (TRL), as well as being a safe system for the crew and cost-effective when used for both maneuvers. The system consists of a total of seven thrusters, each capable of producing 53142 N, with dimensions of 1.8 meters in length and 4 meters in

diameter. The study reports that 265 kN, equivalent to the use of five thrusters, is actually sufficient for the first stage of ascent. However, the use of the two additional thrusters provides more safety and allows for the reduction in the size of the thrusters. In the second stage, no thrusters are released, and no further information is provided about the thrust requirement. The difference between the two stages lies in the release of four cylindrical tanks, each weighing 771 kg. To ensure the reuse of the models in MATLAB and ASTOS, it was assumed that the thrust required in the second stage would be decreased, following the indications given in the literature, due to the lower weight and lower atmospheric density in the second stage. Only four thrusters and a thrust of about 212 kN were considered for performing the mission analysis. Launch site selected is Hebrus Valley, located at 20.2° N latitude and 126.4° E longitude. A summary of the most important information used in the mission analysis on both software is given in table 4.1 while figure 4.1 shows a representation of reference's lander.

Table 4.1: Summary of Mission Analysis Data [20]

Stage Number	**Thrust [N]**	**Wet Mass [kg]**	**Propellant Mass [kg]**	**Reference Diameter**
1st Stage	265000	60808	30808	8
2nd Stage	212000	26556	14300	8

Figure 4.1: Reference Lander [20]

4.2 Atmospheric & Aerodynamic models

As for the atmospheric model, NASA's model [18] mentioned in section 2.4 is implemented. Importantly, the atmospheric drag which is one of the forces that will be included in the equations of motion, is closely related to how this model is constructed. Atmospheric drag can be calculated as in equation (4.1).

$$D = \frac{1}{2} \cdot \rho \cdot V^2 \cdot A_{wet} \cdot C_D \tag{4.1}$$

Where (i) ρ is the atmospheric density [kg/m^3], (ii) V is the vehicle's velocity [m/s], (iii) A_{wet} is the wet area [m^2] and (iv) C_D is the drag coefficient. It is therefore closely related to the Martian atmosphere's density, which in the implemented model depends on pressure and temperature, varying with altitude, as shown in equation (2.4) plotted in figure 4.2.

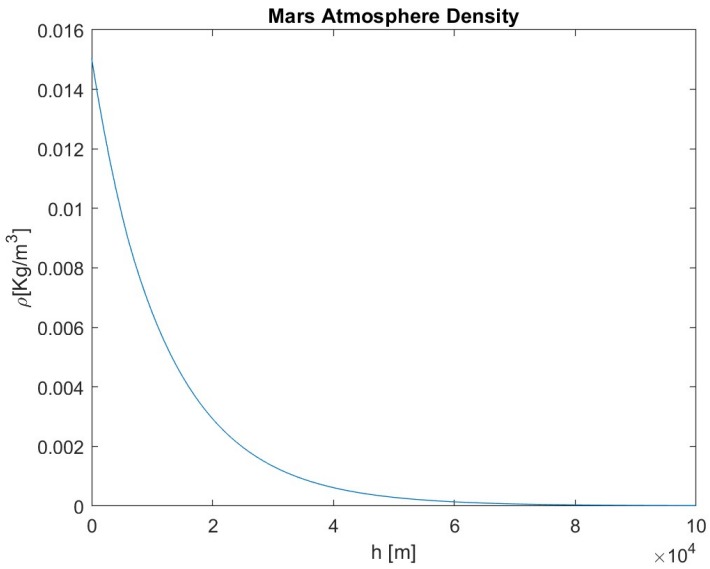

Figure 4.2: Mars Atmospheric Density

Density, like temperature, decreases with altitude. Since temperature decreases until it is very close to the value of -273.1 K in this model, it is necessary to implement a maximum altitude in MATLAB and ASTOS beyond which the atmospheric model is deactivated and aerodynamics are considered fixed. This prevents computational problems in the code due to imaginary numbers. In MATLAB, for each radius computed from the integration of the equations of motion as time varies, the values of temperature, pressure, and density are computed. Beyond 100 km,

fixed values are set for these parameters. In ASTOS, the atmospheric model is passed through tabulated data, and values up to the altitude of 100 km are set as constant. Knowing density value as altitude varies, it is necessary to know the drag coefficient trend as velocity varies, in order to evaluate the atmospheric drag. Aerodynamics plays a critical role the HML's design, and it is important to evaluate this parameter to understand the losses due to it when computing ΔV. When the atmospheric drag coefficient needs to be evaluated, it is usually estimated by considering multiple contributions, a **base drag** at the base of the vehicle due to flow separation, a **friction drag** due to viscous effects and shear stresses in the fluid, a **boat-tail drag** generated by the rear of the vehicle as it narrows toward the engine nozzle, and a **supersonic and transonic wave drag** due to the shock waves generated in these motion regimes [31]. However, in this particular case, considering that no one has ever launched a vehicle into orbit from the Martian surface, atmospheric drag coefficient's behaviour remains unknown and therefore needs to be modeled based on experimental data. From a literature review conducted in the landmark study [20], a vector of 78 elements is created to define the Mach numbers. Depending on the flight regime, different ranges of variation are identified with a constant step to provide more resolution in the most critical flight phases.

- **Subsonic Range**: M = 0 to M = 0.6 with a fixed step of 0.2;
- **Transonic Range**: M = 0.7 to M = 1.9 with a fixed step of 0.1, this is the most critical range, here is the maximum variation and the peak value of C_D;
- **Supersonic Range**: M = 2 to M = 10 with a fixed step of 0.2;
- **Hypersonic Range**: M = 11 to M = 30, a wider range is implemented here since the C_D from statistics turns out to be almost constant.

By evaluating from literature a C_D for each Mach, it is possible to interpolate these values on MATLAB and represent them graphically as shown in figure 4.3.

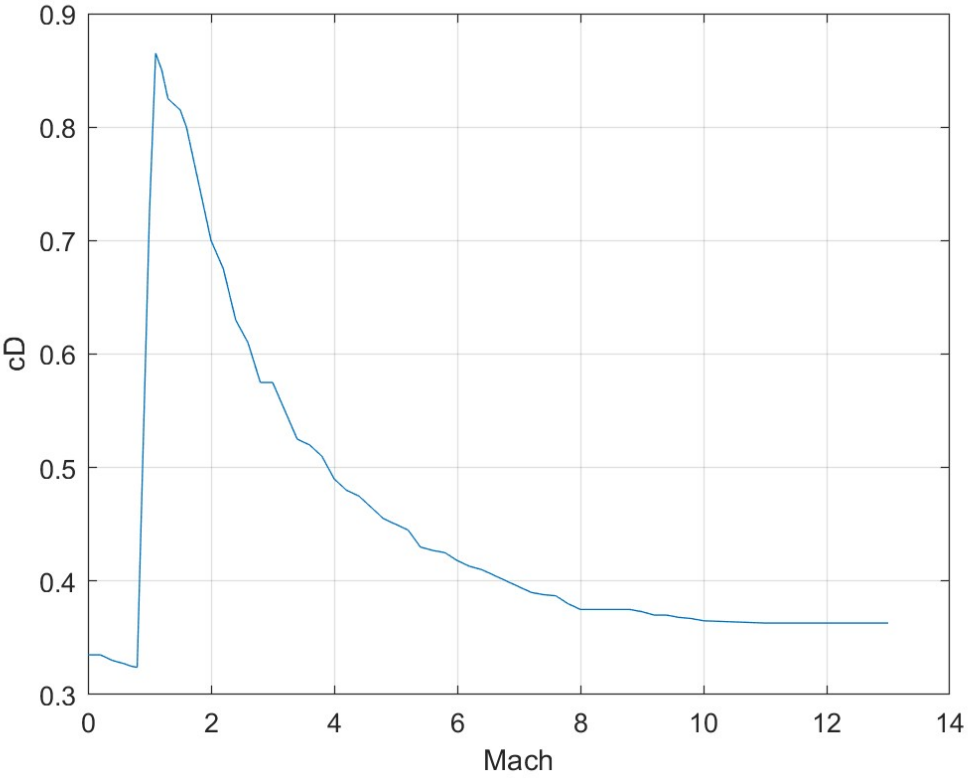

Figure 4.3: Ascent Drag Coefficient

So in MATLAB's subroutine, this interpolated function is used to evaluate the C_D by first calculating the Mach and then evaluating the drag, which is useful to have an estimate of drag losses. In ASTOS, C_D's data are tabulated and used to evaluate drag and drag losses.

4.3 Mission Phases Definition

The phases that constitute the ascent mission from the Martian surface are very similar to those that characterize an ascent from the Earth's surface, with the differences being mainly in their duration and the attitude that needs to be given to the vehicle. The reference mission uses a simplified approach to validate the ascent by not considering non-propelled coasting phases. In that case study, an initial phase is considered in which the thrust angle is set at 90° to ensure vertical takeoff for the first 250 meters, followed by two long gravity turn phases with engines on for both stages, separated by the release of the first stage tanks. This type of approach is very simplifying and is probably suitable for a larger study that does

not focus exclusively on the ascent and descent missions. In the study carried out in this thesis work, the coasting phases will also be modeled, following a subdivision inspired by Earth and Moon ascent. In particular, the mission architecture of the VEGA launcher will be used as reference. This study relies on the document provided by ASTOS, which provides a tutorial for Conventional Launcher [32] to create a scenario already optimized for the VEGA launcher. The following steps will then be considered:

1. **Lift-Off**: the MAV begins its ascent with a thrust angle of 90°, this phase simulates vertical take-off and in the case of terrestrial and lunar ascent has a duration on the order of 10s;

2. **Pitch-Over**: following a certain rate, the pitch angle begins to decrease, lasting only a few seconds;

3. **Constant-Pitch**: the pitch angle is kept constant so as to align the thrust with the velocity and mitigate the occurrence of destructive loads, this phase lasts few seconds as the previous one;

4. **First stage Burn**: propulsive phase, the engines burns propellant until it runs out (the one intended for the first stage), typically on Earth this phase is a Gravity Turn Phase, no maneuvering is performed by the vehicle letting gravity vary the pitch angle. As it will be explained later in section 4.5.2, actually in the models presented here a certain thrust angle is imposed for the Martian ascent in order to meet the constraints;

5. **Coasting**: a coasting phase with engines off that is useful for releasing the first stage tanks;

6. **Second Stage 1st Burn**: similar to the first burn, not all second stage propellant is used and the pitch angle is maneuvered;

7. **Second Coasting**: a stage similar to the previous one useful for reaching the arrival orbit;

8. **Second Stage 2nd Burn**: there is a second burn apt to circularize the orbit and meet the imposed altitude and velocity constraints.

In the simplified MATLAB model presented in section 4.4, pitch angle will be passed as an input function valid for the propelled phases and will not consider the Lift-Off, Pitch-Over and Constant-Pitch phases, however, it will be set as a 90° decreasing pitch as a replacement. In the ASTOS scenario, all phases will be modeled, and later in section 4.5.2 this will be better discussed.

4.4 MATLAB Optimization Subroutine

Having defined the key information about the atmospheric, aerodynamic model and concerning the mission scenario in section 4.2 and in section 4.3, the main objective now is the creation of a simplified and fast code to have a first approximation about the trajectory of the HML in its configuration for ascent in order to derive its ΔV and losses. In fact, before moving onto the mission analysis routine to be implemented in ASTOS, it is useful to estimate by a good margin the data that ASTOS will require as input related to mission performance. The mission analysis subroutine on MATLAB takes as input a range of information related to the mission design itself and its architecture and returns as output ΔV, drag losses, and gravity losses, as shown in figure 4.4.

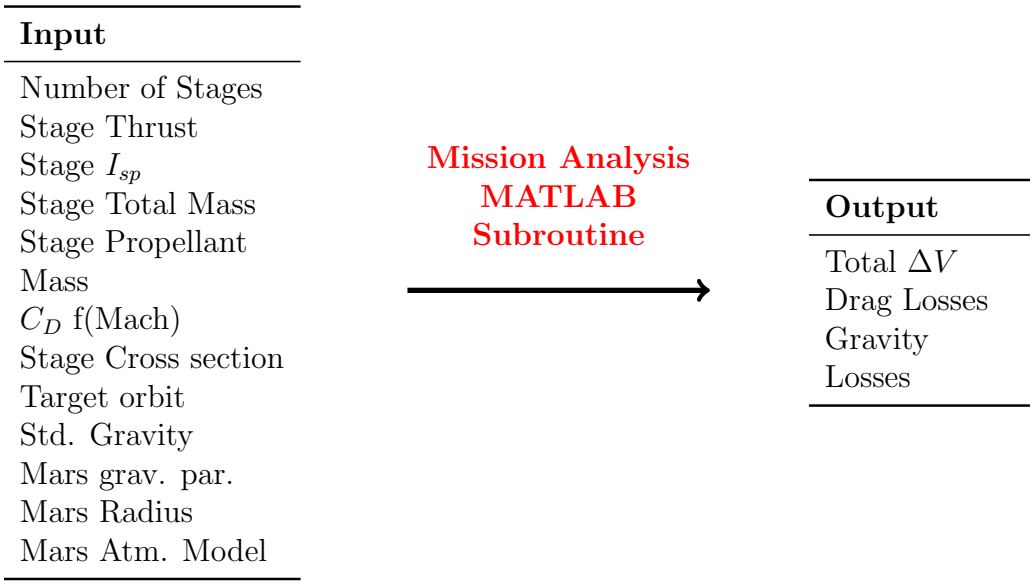

Figure 4.4: MATLAB Subroutine: Input & Output

4.4.1 Trajectory Model: Equations of Motion

The trajectory model used in this study is derived from the classical equations of motion written in a planet-centered and planet-fixed system considering only 2 degrees of freedom, see figure 4.5. This approach was chosen in agreement with studies done for lunar ascent that shows how this approximation can be useful and conservative for finding a first iterations result [33].

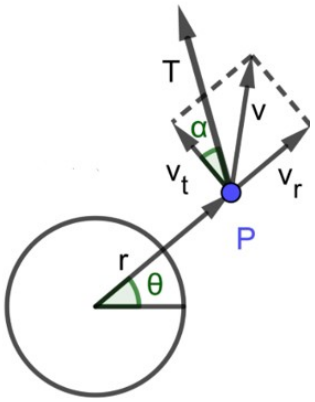

Figure 4.5: Reference frame, trajectory variables [33]

Simplified 2-dof equations of motion are reported from equation (4.3) to (4.6):

$$dr = v_{\text{rad}} \quad [\text{m/s}] \tag{4.2}$$

$$d\theta = \frac{v_{\text{tan}}}{r} \quad [\text{m/s}] \tag{4.3}$$

$$dv_{\text{rad}} = \frac{v_{\text{tan}}^2}{r} + \frac{\delta\,\text{Thr}}{m}\sin\alpha - \frac{GM}{r^2} - \frac{1}{2}\rho C_D\sqrt{v_{\text{rad}}^2 + v_{\text{tan}}^2}\,A\,v_{\text{rad}} \quad [\text{m/s}^2] \tag{4.4}$$

$$dv_{\text{tan}} = \frac{v_{\text{rad}}\,v_{\text{tan}}}{r} + \frac{\delta\,\text{Thr}}{m}\cos\alpha - \frac{1}{2}\rho C_D\sqrt{v_{\text{rad}}^2 + v_{\text{tan}}^2}\,A\,v_{\text{tan}} \quad [\text{m/s}^2] \tag{4.5}$$

$$dm = -\frac{\delta\,\text{Thr}}{g_0 I_{\text{sp}}} \quad [\text{kg/s}] \tag{4.6}$$

Where:

- **r**: Vehicle's distance from the center of Mars [m];
- θ: Angle between the vehicle and a reference point on the ground, in this case the launch site (Hebrus Valley located at 20.2° N latitude and 126.4° E longitude) [deg];
- v_{rad}: Radial component of velocity [m/s];
- v_{tan}: Tangential component of velocity [m/s];
- **GM**: Standard gravitational parameter of Mars $[m^2 \cdot s^{-2}]$;
- **m**: Total mass of the vehicle [kg];
- **Thr**: Total thrust considering all engines [N];

- α: Thrust angle (pitch) [deg];
- δ: Engines throttle;
- g_0: Acceleration at sea level on Earth [m/s^2];
- C_D: drag coefficient;
- **A**: cross sectional area [m^2];
- I_{sp}: Specific Impulse [s].

All equations are given in incremental form, as they will be integrated into the code as will be explained in section 4.4.2 and in section 4.4.4. The expression for the change in mass is derived from the definition of the specific impulse, while the expressions for the change in radial and tangential velocities are composed of the centripetal and centrifugal acceleration term, the acceleration dictated by Thrust in the radial and tangential directions decomposed according to the thrust angle, and the acceleration given by atmospheric resistance, which opposes motion. Obviously, in the expression concerning the change in radial velocity, there is also the term of gravity acceleration, dependent on the radius squared and the standard gravitational parameter of Mars.

Expressions for changes in ΔV and losses due to drag and gravity are also included within the formulation, reported in equations (4.7), (4.8) and (4.9) respectively, so that they can later be evaluated on an instant-by-instant basis.

$$d\Delta V = I_{\text{sp}}\, g_0 \ln\left(\frac{m}{m+dm}\right) \quad [\text{m/s}^2] \tag{4.7}$$

$$d\Delta V_{\text{drag}} = \frac{\text{Drag}}{m} \quad [\text{m/s}^2] \tag{4.8}$$

$$d\Delta V_{\text{gravity}} = \frac{g_{0,\text{Mars}}}{\left(\frac{r}{R_{\text{Mars}}}\right)^2} \sin\gamma \quad [\text{m/s}^2] \tag{4.9}$$

Where (i) dm is the change in mass instant-by-instant, (ii) $g_{0,\text{Mars}}$ is the standard gravity acceleration for Mars and

(iii) $\gamma = acos\left(\frac{v_{tan}}{\sqrt{v_{tan}^2+v_{rad}^2}}\right)$ is the flight path angle [deg].

4.4.2 Code overview

A general overview of how the MATLAB code works is proposed here, useful in understanding its overall operation. In subsequent sections what is hinted at here will go into the specifics, covering how input variables are defined and which of them are optimized, the method used for integrating the equations of motion, and finally the optimization method.

The trajectory is divided into five phases, three propulsive phases, one for the first stage and two for second stage ignition, and two coasting phases. The first coasting phase allows for the first-stage tanks to detach, the second one aims to reach the arrival orbit before performing a second burn designed to circularize it. The code works on each of these stages sequentially with a for loop, taking as input the initial values for each stage of the state vector, and the variables related to the vehicle at that particular stage (Thrust, Wet Mass, remaining propellant mass, Specific Impulse, wet Area). These values are inputs to the ODE45 function in MATLAB, along with the equations of motion, the integration duration (the phases' duration is appropriately calculated based on the time it takes the engine to burn the propellant, or given as input as a variable to be optimized), and some variables to be optimized that appear in the equations of motion (δ, α). The final results of the integration, thus the final state vector, is used to calculate the orbital parameters needed to evaluate the optimization objective function, which is constructed to have zero value when the desired orbit has been reached. Constraints are also imposed on the radial velocity, which must be zero when the desired circular orbit is reached, and on the tangential velocity, which should have the value relative to the target orbit.

4.4.3 Input variables

It is possible to subdivide code input variables into multiple categories:

- **Variables related to lander design**: All variables that phase by phase depend on lander design itself and the sub-rocket considered, thus Thrust, wet mass, propellant mass, resistant area, stage-specific impulse (360s for both stages). They are defined as vectors of 5 elements and updated according to the stage;
- **Global variables related to Mars**: The planet's radius, universal gravitation parameter, its mass;
- **Variables for the aerodynamic model**: Drag coefficient and the corresponding Mach, previously defined and useful for evaluating drag. They are defined as vectors with the same indices;

- **Initial state vector**: The code integrates the equations of motion and thus needs an initial value for each variable. The state vector is thus defined at the beginning:

$$\mathbf{p}_0 = \begin{bmatrix} r_0 \\ \theta_0 \\ v_{r0} \\ v_{t0} \\ m_0 \\ t_0 \\ drag_{\text{loss}} \\ gravity_{\text{loss}} \\ \Delta v \end{bmatrix} = \begin{bmatrix} R_{\text{Mars}} \\ 0 \\ 0 \\ 0 \\ \text{Wet Mass 1st Stage} \\ 0 \\ 0 \\ 0 \\ 0 \end{bmatrix}$$

These are the initial values for the aforementioned variables presented in section 4.4.1;

- **Variables to be optimized**: A x_0 vector of variables that will be optimized using MATLAB "fmincon" function

$$\mathbf{x}_0 = \begin{bmatrix} \delta_{1\text{st}} \\ \delta_{2\text{nd}} \\ \alpha_{01} \\ \alpha_{f1} \\ \alpha_{02} \\ \alpha_{f2} \\ \alpha_{03} \\ \alpha_{f3} \\ a_1 \\ a_2 \\ a_3 \\ \xi_1 \\ \xi_2 \\ \xi_3 \\ t_{\text{coast1}} \\ t_{\text{burn}} \\ t_{\text{coast2}} \end{bmatrix} = \begin{bmatrix} 0.99 \\ 0.99 \\ 75^\circ \\ 60^\circ \\ 40^\circ \\ 37^\circ \\ 7^\circ \\ 0^\circ \\ 100 \\ 100 \\ 100 \\ -0.5 \\ 0.5 \\ -0.7 \\ 44\,\text{s} \\ 160\,\text{s} \\ 460\,\text{s} \end{bmatrix}$$

Where (i) δ_{1st} and (ii) δ_{2nd} are engines' throttle for the two stages , (iii) a and (iv) ξ are variables that define the shape of 3 functions that describes α's (thrust/pitch angle) trend as time varies, for the 3 propelled stages, (v) α_{ij} are the initial and final pitch values in these 3 phases [deg], (vi) t_{coast1}

and (vii) t_{coast2} are the coasting phases duration [s], and (viii) t_{burn} is the first stage ignition duration [s], useful for defining the integration time.

The variables related to the 3 functions just mentioned present in the x_0 vector will now be investigated and explained. The code aims to optimize the thrust angle, or pitch angle, as input to the equations of motion from an initial guess. However, in order to provide more continuity in the results and to allow this value to vary over time so as to reach the circular orbit of arrival, rather than considering constant angles to be optimized for each phase, 3 tangent bi-linear functions were modeled to describe this angle's time dependence, function is shown in equation (4.10), and the optimization concerns its parameters.

$$\alpha(t) = \arctan\left(\frac{\left(\tan(\alpha_{\mathrm{f}}) - a^{\xi}\tan(\alpha_0)\right)\frac{t}{t_{\mathrm{fin}}} + a^{\xi}\tan(\alpha_0)}{(1-a^{\xi})\frac{t}{t_{\mathrm{fin}}} + a^{\xi}}\right) \tag{4.10}$$

A bi-linear tangent function is a function with the properties of both bi-linear and tangent functions, bi-linear indicates that it is linear with respect to its two arguments when the other is held fixed while tangent because it is constructed trigonometrically on the basis of the tangent of the input angles. As highlighted in [34], the implementation of a tangent bilinear guidance law can improve launch vehicle performance by providing precise and stable control, reducing deviations from the optimal trajectory and optimizing propellant utilization. Specifically, three such functions are used by passing as input the initial and final values of the angles for each propelled phase and the values of a and ξ, these values are initially assumed.

- **Parameter** a: Part of the product a^{ξ}, it is a multiplicative constant that modulates the influence of the initial angle α_0 with respect to the final angle α_f in calculating the angle $\alpha(t)$ as a function of time. A higher value of a increases the contribution of the initial angle to the total function, while a lower value decreases it;

- **Parameter** ξ: exponent of a (i.e., a^{ξ}), indicating that the influence of a is enhanced or diminished depending on the value of ξ. If it is positive and greater than 1, it amplifies the effect of a while if it is between 0 and 1, it attenuates it. If it is negative, it reverses the effect of a. This allows fine modulation of the influence of the initial angle versus the final angle along the time interpolation curve.

Also, t_{fin} is the final phase time. In MATLAB $\alpha(t)$ functions are modeled as function handles and will be input to the equations of motion during the integration.

4.4.4 Integration Method

The code uses a for loop that gives as input each phase's data to MATLAB ODE45 function along with the equations of motion and the variables to be optimized. ODE45 is an ordinary differential equation solver (ODE) based on the **Runge-Kutta method, order 4/5** (Dormand-Prince method). This method is a variable step method, which means that the algorithm automatically adjusts the size of the integration step to keep the integration error within specified bounds. This is a particularly suitable method for nonrigid problems, that is, problems in which the solutions change smoothly and are not too sensitive to small variations in the parameters. The method estimates the derivative of the function at multiple points within each integration interval using a combination of predefined coefficients. Two estimates of the solution are calculated: one of fourth order and one of fifth order. The difference between these two estimates is used to estimate the integration error. An interval for integration over time must be defined, ODE45 carries on the integration by continuously adapting the step and estimating the derivatives until it reaches the specified time interval.

Depending on the mission stage, the integration time to be given as input to the function is defined. In section 4.4.3, the the coasting phases' duration times and the first ignition of the second stage duration time were also included among the variables to be optimized, which are then simply given as input as integration times. Regarding the propelled phases of the first stage and the second stage second ignition, the integration time is calculated from the specific impulse definition based on the propellant of the specific remaining stage, as shown in equation (4.11).

$$t_{phase} = \frac{I_{sp} \cdot g_{0,\text{Earth}} \cdot m_{\text{fuel}}}{\text{Thr}} \tag{4.11}$$

Where (i) I_{sp} is the specific impulse [sec], (ii) g_0 is standard earth gravity acceleration [m/s^2], (iii) m_{fuel} is the propellant mass [kg], and (iv) Thr is the thrust [N]. If it is a non-propelled phase in addition, a null value of throttle ($\delta = 0$) is given as input to the equations of motion. The time vector is updated at each iteration on the for loop as well as the state vector so that results for the entire trajectory can be saved.

4.4.5 Optimization Method & Objective Function

The FMINCON function in MATLAB is used for optimization. This function is often used to solve constrained nonlinear optimization problems. It is one of MATLAB's most powerful tools for optimization and can handle problems that include equality and inequality constraints. It requires as input an **objective function**, the previously defined **vector** x_0 with the variables to be optimized,

lb and ub vectors of lower and upper bounds on the variables, and a **function representing nonlinear constraints**, here called mycon. As for the lower and upper bounds on the variables to be optimized:

- **Initial and final angles of the bilinear tangent functions**: vary between $-90°$ and $+90°$;
- **Variables related to the bilinear tangent functions**: ξ varies between -1 and 1 while a varies between 50 and 150;
- **Throttle**: δ varies between a minimum value of 0.01 and 1;
- **Phase Duration**: the reference value is an initial guess, evaluated from the literature and testing the integration of the equations without optimization iteratively, a plausible boundary of that value is chosen.

The objective function, on the other hand, is calculated based on the equations' integration, at each iteration the code that integrates the equations of motion is launched, the final values of the integration are used to estimate, known the final state vector, the specific mechanical energy (E) [J/kg] as shown in equation (4.12), the specific angular momentum (h) $[m^2/s]$ reported in equation (4.13), the eccentricity (e) highlighted in equation (4.14), the periapsis and the apoapsis' radius [m] shown in equations (4.15) and (4.16).

$$E = \frac{\sqrt{v_r^2 + v_t^2}^2}{2} - \frac{\mu_{\text{mars}}}{r} \tag{4.12}$$

$$h = r \cdot v_t \tag{4.13}$$

$$e = \sqrt{1 + \frac{2Eh^2}{\mu_{\text{mars}}^2}} \tag{4.14}$$

$$r_p = \frac{h^2}{\mu_{\text{mars}}} \left(\frac{1}{1+e} \right) \tag{4.15}$$

$$r_a = \frac{h^2}{\mu_{\text{mars}}} \left(\frac{1}{1-e} \right) \tag{4.16}$$

Where (i) μ is the Standard Gravitational Parameter $[m^3 \cdot s^{-2}]$, (ii) r is the vehicle's radius [m], (ii) v_r is the vehicle's radial velocity [m/s], (iii) v_t is the vehicle's

tangential velocity [m/s]. These values are useful in evaluating the constructed objective function, reported in equation (4.17), this function has zero value if the target orbit is reached.

$$\text{objective} = \left(\frac{r_a}{1000} - \frac{\text{Target}}{1000}\right)^2 + \left(\frac{r_p}{1000} - \frac{\text{Target}}{1000}\right)^2 \tag{4.17}$$

Where (i) r_a is the apoapsis' radius [m], (ii) r_p is the periapsis radius [m] and (iii) Target is the target orbit radius [m]. As for nonlinear constraints, only equality constraints are imposed on the radial velocity, which must be zero on arrival, and on the tangential velocity, which must have a value dictated by the altitude of 390.5km and the circularity of the orbit. FMINCON proceeds with iterations as long as, within a certain tolerance, the objective function is not zero, then searching for minima. Feasibility is also evaluated based on the imposed equality constraints, solution is feasible if all the equalities are exactly satisfied. If the equalities are not exactly satisfied, the measure of violation can be calculated as the absolute value of the difference from the required value, a feasibility of at least 10^{-6} is sought.

4.4.6 Results

The results of the optimization are now reported in graphical form from figure 4.6 to 4.11, a feasibility of the order of 10^{-7} and a value of the objective function of the same order of magnitude is achieved in about 10 minutes. As can be seen from the graphical representation, the trajectory shown in figure 4.6 and velocity profile shown in figure 4.11 meets what is expected, the circular orbit of 390.5 km is achieved, and this can be verified by checking the plot of altitude and velocities, which assume the hoped-for values.

The values assumed by the total ΔV, drag and gravity losses on arrival represent the most important result of this evaluation as previously anticipated in section 4.4. They are an initial estimate for sizing and will be used to verify the validity of the code when compared with the results obtained on the later discussed and more accurate ASTOS model.

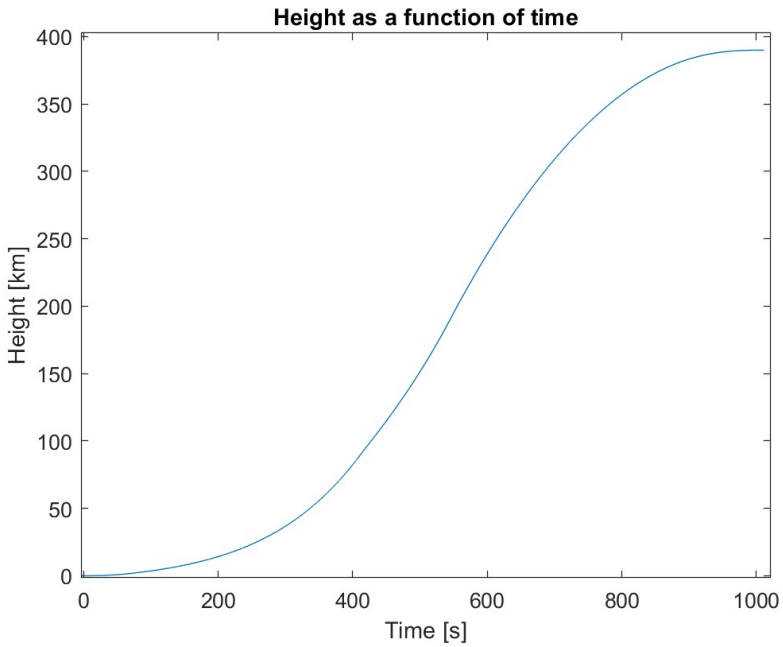

Figure 4.6: MATLAB Results: Height

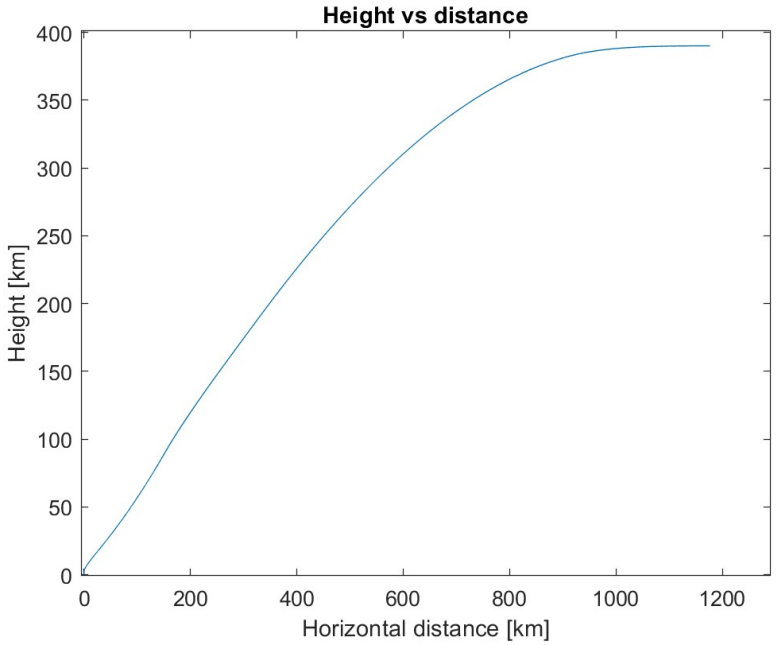

Figure 4.7: MATLAB Results: Horizontal distance

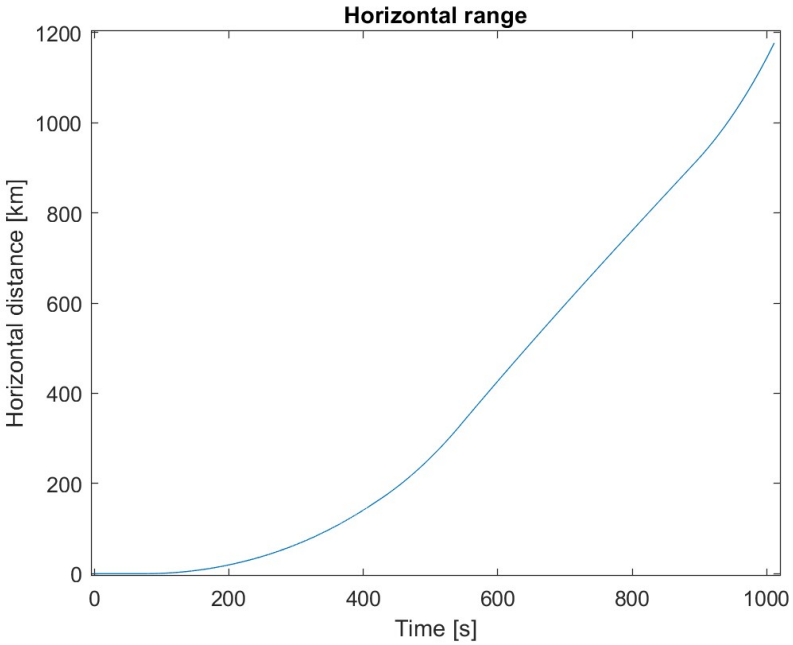

Figure 4.8: MATLAB Results: Horizontal range

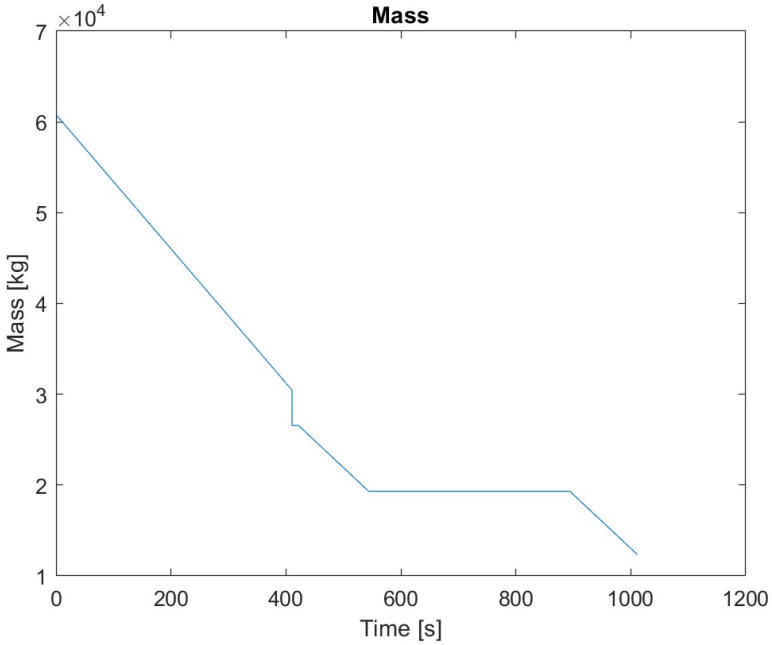

Figure 4.9: MATLAB Results: Mass

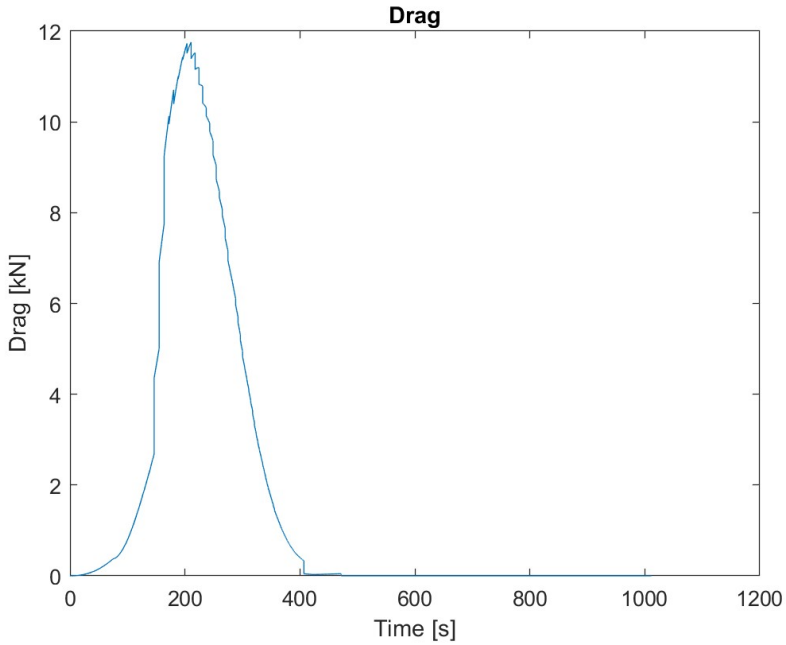

Figure 4.10: MATLAB Results: Drag

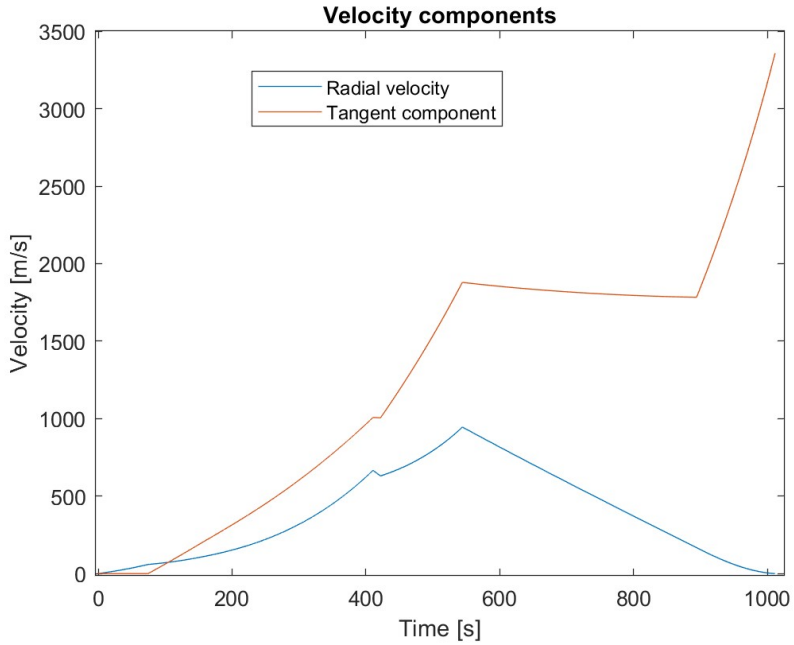

Figure 4.11: MATLAB Results: Velocity

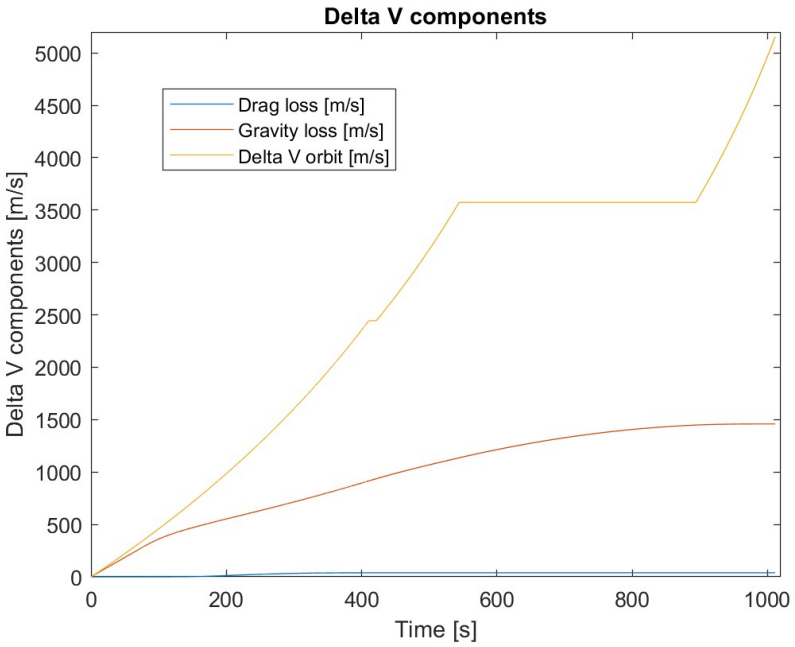

Figure 4.12: MATLAB Results: ΔV components

The numerical values of these three variables are given in table 4.2.

Drag Losses	38.91 [m/s]
Gravity Losses	1459.14 [m/s]
Total ΔV	**5155.75 [m/s]**

Table 4.2: MATLAB: Drag Losses, Gravity Losses e Total ΔV

4.5 ASTOS Model

The final design routine uses ASTOS software for ascent modeling and optimization, this is because it provides a much more accurate simulation of the mission using a 3-degree-of-freedom model that can better evaluate the design routine inputs in terms of gravity and drag losses and modeling all the phases. ASTOS is a powerful simulation and optimization tool compared to the subroutine in MATLAB, it allows:

- **Accurate gravitational modeling**: depending on the planet;
- **More accurate aerodynamic modeling**;
- **More realistic vehicle simulation** with more detailed specifications on engines, stages, modeling of vehicle mass and its changes during flight, such as separation of tanks or engines;
- **Simulation of flight dynamics** including attitude and stability controls;
- **Mission Constraints and Phases Management**, path constraints can be inserted on the different phases and multi-objective optimization can be implemented on multiple variables simultaneously, and cost functions can be inserted;

In section 4.5.1 it is shown how the model is created, in section 4.5.2 a dynamic configuration was assigned to the various mission phases, and in section 4.5.3 constraints were imposed on the phases for optimization.

4.5.1 Vehicle Parts, Properties & POIs Definition

All lander's components and models are defined:

1. **Thrusters**: thrusters' parameters for the first and second stages are defined by entering values for nozzle area, specific impulse, and thrust in vacuum, as shown in figure 4.13;

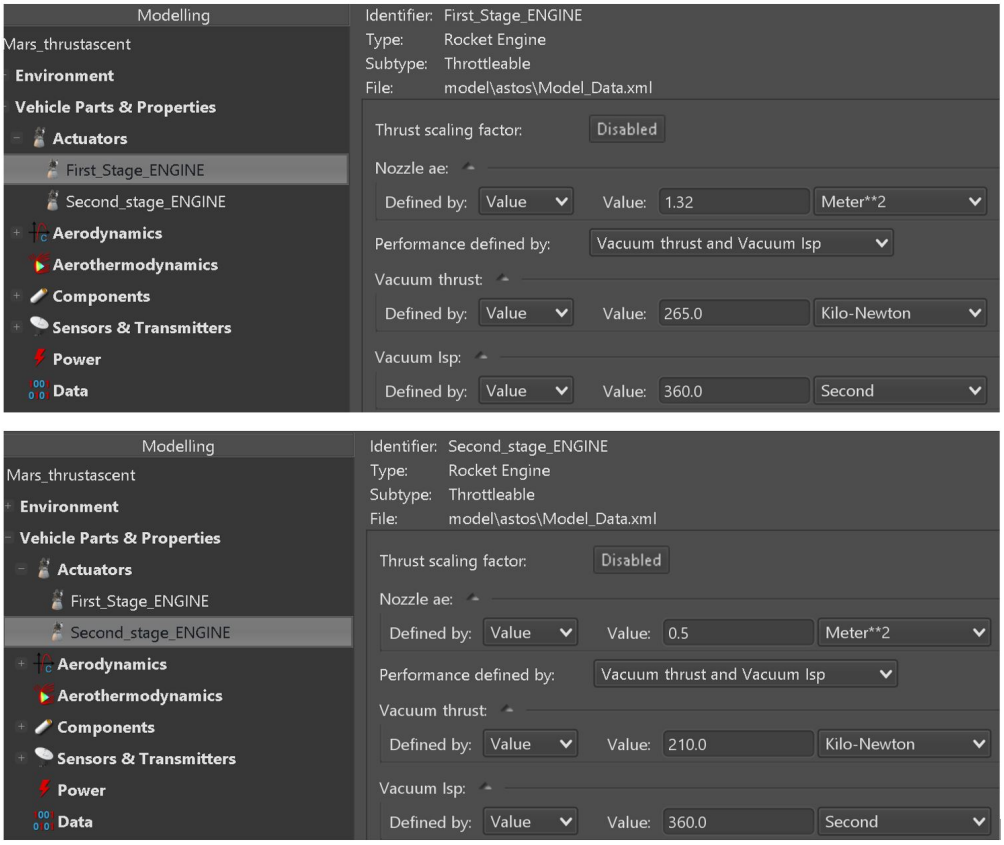

Figure 4.13: ASTOS Model: Thrusters

2. **Aerodynamics**: having already defined the C_D as a function of Mach, tabulated values from excel are entered to define the aerodynamics for ascent using the reference diameter of 8m;

3. **Components**: the crew module and the two stages are defined by entering the reference vehicle values related to masses and propellant as in figure 4.14;

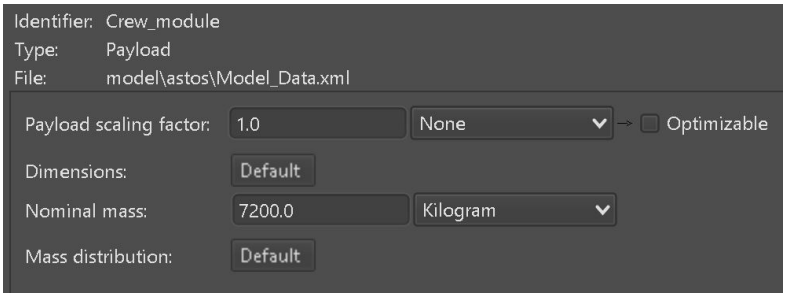

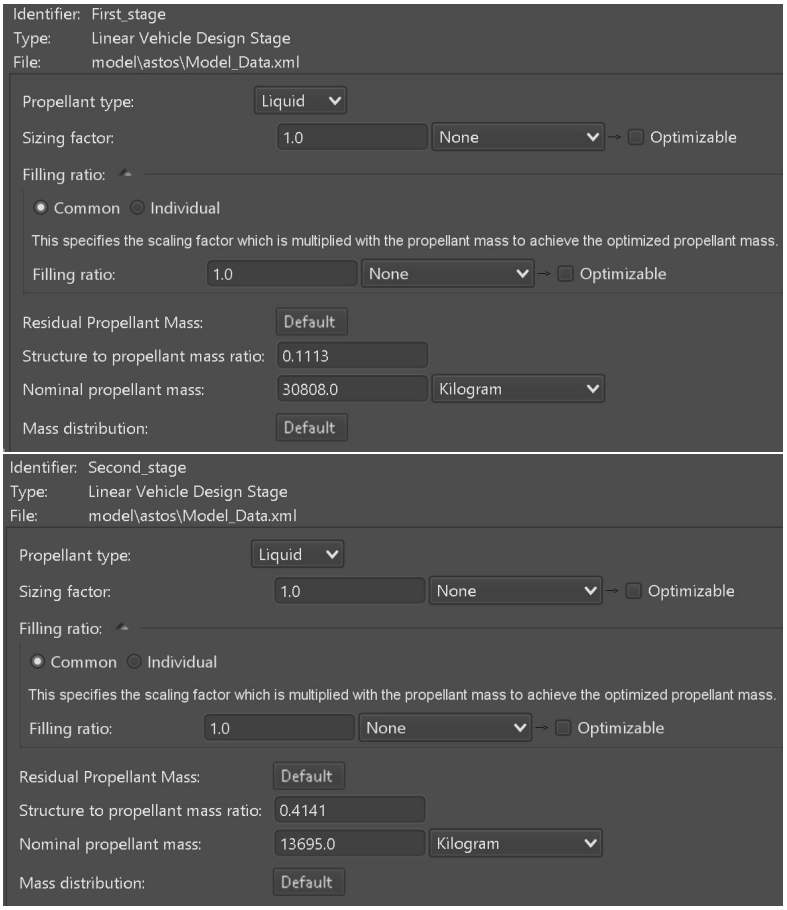

Figure 4.14: ASTOS Model: Components

4. **Vehicles & POIs Definition**: after defining all components and related properties, the lander in its ascent configuration is assembled on ASTOS, as shown in figure 4.15.

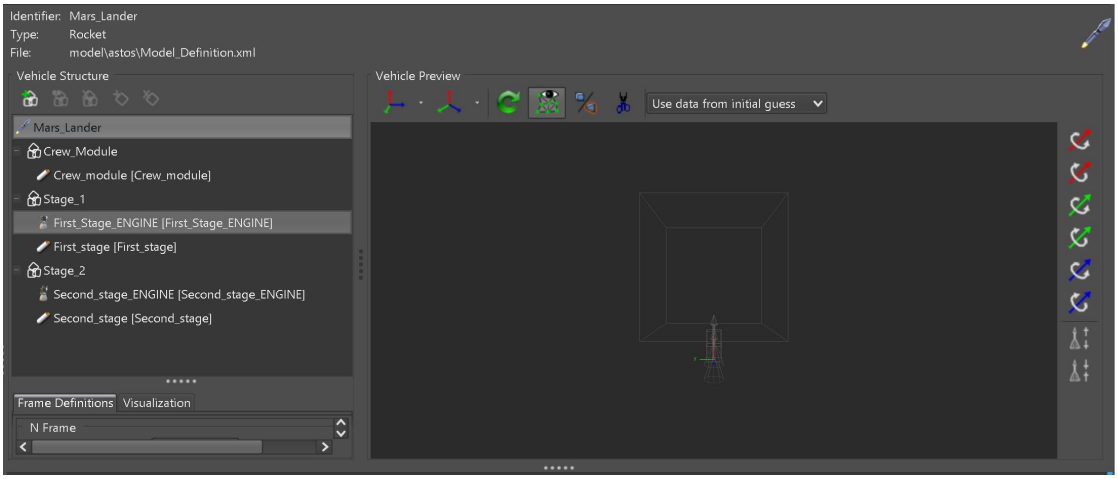

Figure 4.15: ASTOS Model: Vehicle Assembly

4.5.2 Dynamics Configuration

The mission phases have been implemented in the model exactly as described in section 4.3, this time all phases are included and the initial guess on their duration is entered as input, ASTOS will optimize the duration of each of them starting from these values. Having defined the phases and their duration settings, their dynamics are defined, in terms of which engines are turned on, which components are released, and which control laws are implemented to define the attitude via the yaw angle and to define the pitch for each of the phases. Starting with the definition of the phases and their duration, table 4.3 shows all the phases and the initial guess on duration from which ASTOS will start the optimization.

Mission Phase	**Duration Guess**
Lift-Off	20s
Pitch-Over	7s
Constant Pitch	7s
1st Stage Burn	377.5s
Coasting	12s
2nd Stage 1st Burn	60s
Second Coasting	184s
2nd Stage 2nd Burn	180s

Table 4.3: Mission Phases and Their First Guess Durations

The initial guess choice is given both by the results obtained from MATLAB

subroutine discussed in section 4.4.6 and by an iterative process of simulation on ASTOS. In fact, without launching the optimization, several simulations were launched aimed at searching for durations that would guarantee good results with regard to reaching the arrival orbit, iterating the simulations until an adequate value of altitude, radius of periapsis and apoapsis, and radial and tangential velocity was found.

As for the definition of phase dynamics, it starts initially by defining the initial state of the vehicle. The **initial state** is defined in terms of position and velocity, the position is described using a planet-centered planet-fixed reference system PCPF in polar representation shown in figure 4.16, this is the same system used in MATLAB in two dimensions to define the initial state vector and integrate the equations of motion, but in 3 dimensions.

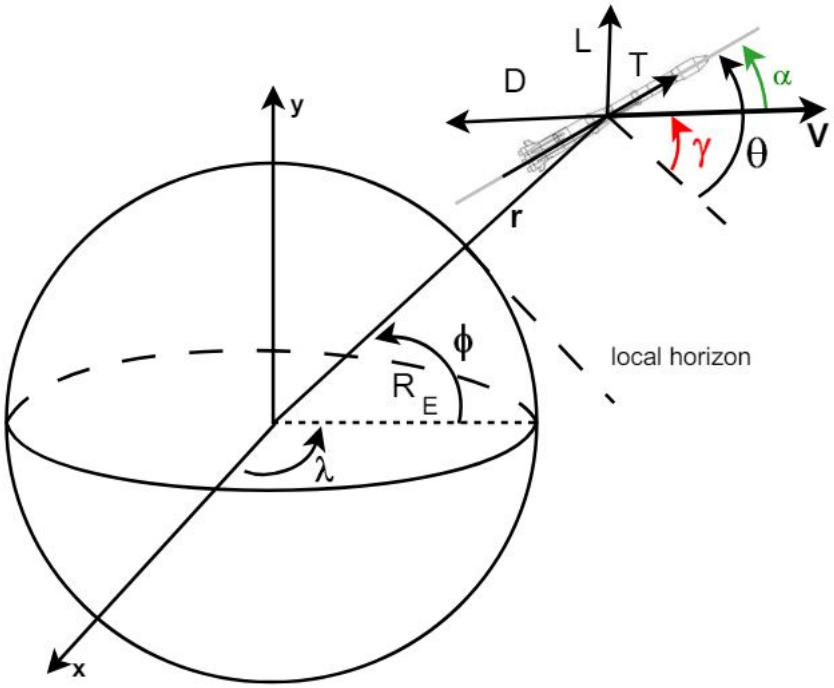

Figure 4.16: ASTOS Model: PCPF Reference Frame[33]

Note how this system is non-inertial and rotating, this implies that the MATLAB subroutine carries with it an additional error in addition to that related to the simplicity of the 2-degree-of-freedom model, in fact the velocity gain due to the rotation of the planet, directly related to the latitude of the launch site, is also neglected. These errors can be considered acceptable as long as they are contained within 15% compared to a more complete model such as ASTOS, the MATLAB

model in fact simply has to give an initial estimate of the losses and is not part of the final design routine. Although it is possible to input data in a PCPF reference system as it is more convenient, in reality the equations of motion integrated by ASTOS are equations of motion in a Cartesian inertial system, as is the graphical representation of the results that will be presented next.

Then the altitude, latitude, and longitude of the launch site (**Hebrus Valley**) and the radial, northward, and eastward velocities are set for the initial state in the PCPF Reference Frame, as shown in table 4.4

Position	
Altitude	0 [m]
Longitude	126°
Latitude	20°

Velocity	
Radial	0 [m/s]
North	0 [m/s]
East	0 [m/s]

Table 4.4: Position & Velocity Initial State

After setting as default for all the phases the reference aerodynamics as previous modeled in section 4.2, the settings for all phases in terms of control laws, active engines, and components released are next set:

1. **Lift-Off**: the first stage engines are ignited, for the attitude a control law is set for the yaw angle aimed at achieving the target orbit inclination of 20°, for the pitch angle a control law of "Vertical Take-Off" is set to have an angle of 90° and get out of the denser layers of the atmosphere, the angle is set as optimizable;

2. **Pitch Over**: the first stage engines continues to burn, the yaw angle has a constant and optimizable control law while the pitch angle follows a linear law and decreases with a rate of 2 deg/sec, again the angles values are optimizable;

3. **Constant Pitch**: two constant and optimizable laws are set;

4. **1st Stage Burn**: again, the laws are set to a constant value, unlike Earth ascents, the need to keep the angle at a certain constant value with a control law rather than performing the Gravity Turn has emerged, this is because the low gravity also the effect of a classical gravity turn, which is highly effective in a stronger gravitational field such as Earth's. Consequently, a constant thrust angle control can provide a more stable trajectory during the initial ascent. As emerges in [35] during the high-speed launch phase, the use of open guidance with predefined roll, pitch and yaw angles is crucial

to maintain stability and trajectory accuracy. This approach is preferable to gravity turn, especially in low-gravity environments such as Mars, where aerodynamic forces are less predictable and influential. At the end of this phase, the release of the first stage is set;

5. **Coasting**: in the first stage of coasting, the engines are turned off and a constant control law is set for yaw angle and a linear law for pitch with an optimizable final value of 10°; this choice is preparatory to increasing tangential velocity in subsequent burns in which it will be necessary to push to circularize;

6. **2nd Stage 1st Burn**:with the second stage engines burning, two constant and optimizable laws;

7. **Second Coasting** engines off, stage preparatory to reaching the arrival orbit before circularization precisely for this reason a linear control law is set with final value equal to 0° optimizable;

8. **2nd Stage 2nd Burn**: again engines on and two constant and optimizable laws in order to circularize the orbit reached the desired altitude.

4.5.3 Optimization: Cost Function & Constraints

The optimization method implemented is CAMTOS (Computer Aided Multidisciplinary Tool for Optimization of Spacecraft), an advanced tool used for multidisciplinary spacecraft optimization. It is in fact designed to address optimization problems involving multiple engineering disciplines including aerodynamics, propulsion, and flight dynamics, plus it includes advanced simulation capabilities to analyze spacecraft behavior during different mission phases. CAMTOS uses advanced optimization algorithms, such as genetic algorithms, stochastic optimization, and nonlinear programming methods. These algorithms are chosen for their ability to find optimal solutions in complex, nonlinear design spaces. The integration method is again the Runge-Kutta 4/5 method as on MATLAB, and the integration error set is on the order of 10^{-8}. The optimization is done by imposing certain constraints, exactly as was done in the MATLAB Subroutine, however this time they are more specific and detailed given the optimization algorithm and related to the phase. Constraints are modeled in this way:

- **Initial Latitude, Longitude, Altitude**: defined as the initial state, set as initial boundary of the first phase;

- **Initial Velocities**: set as initial boundary of the first phase to null values (North,East, Relative Radial)

- **Eccentricity**: set as the final boundary of the last phase a value very close to zero on the order of 10^{-4} to ensure circularity of the orbit;
- **Apoapsis Altitude**: an upper bound in altitude of 390.5km is set as the initial boundary of the second coasting phase;
- **Coasting Path Altitude**: the same upper boundary is set on the whole path of the second coasting phase;
- **Final Apoapsis Altitude**: related to the final altitude of the vehicle, set as the final boundary of the second stage coasting with the reference value of 390.5km;

A cost function on the maximum transportable payload is also included. The cost function is a mathematical function that maps a set of parameters to a scalar value that represents a "cost" associated with those parameters. The goal of optimization is to find the parameters that minimize this cost function, which is the guide for the optimization algorithm. A scaling with a value of 10^{-4} is inserted; this parameter is used to facilitate optimization by avoiding numerical problems.

4.5.4 Results

Results are shown from Figures 4.17 to 4.22 where it is possible to follow the vehicle's ascent trajectory at each stage. Figures 4.17 and 4.18 show the altitude reached by the lander and the periapsis and apoapsis radii of the final orbit. Both coincide with the final altitude value of 390.5 km, indicating that the optimization was successful. Figure 4.20 depicts the mass trends of the two stages and the vehicle as a whole. Abrupt changes in mass indicate the release of the first stage, while the linear decrease in mass indicates propellant consumption. Figure 4.21 shows the atmospheric drag, slightly different from the more simplified mass-based subroutine, with a peak in the first stage. The pitch trend is shown in figure 4.19, where there is a significant difference from modeling with bilinear tangent functions in MATLAB, especially in the early stages, where it is more discontinuous. This difference contributes to the variations in drag and losses. Finally, Figure 4.22 shows the trend of the inertial velocities, the profile of which is very similar to the MATLAB subroutine, reaching the expected values of tangential and radial velocities required for the circular orbit.

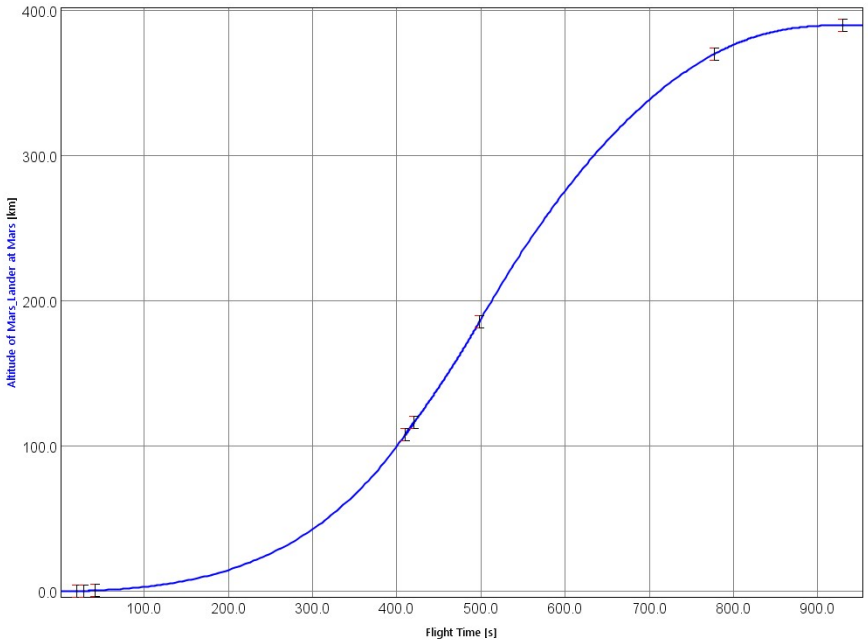

Figure 4.17: ASTOS Results: Height

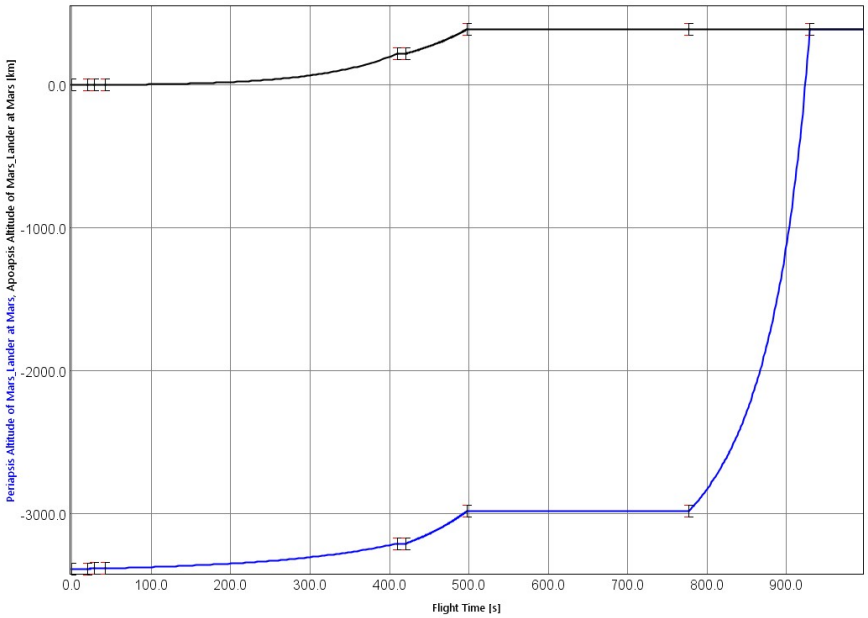

Figure 4.18: ASTOS Results: Periapsis & Apoapsis Altitude

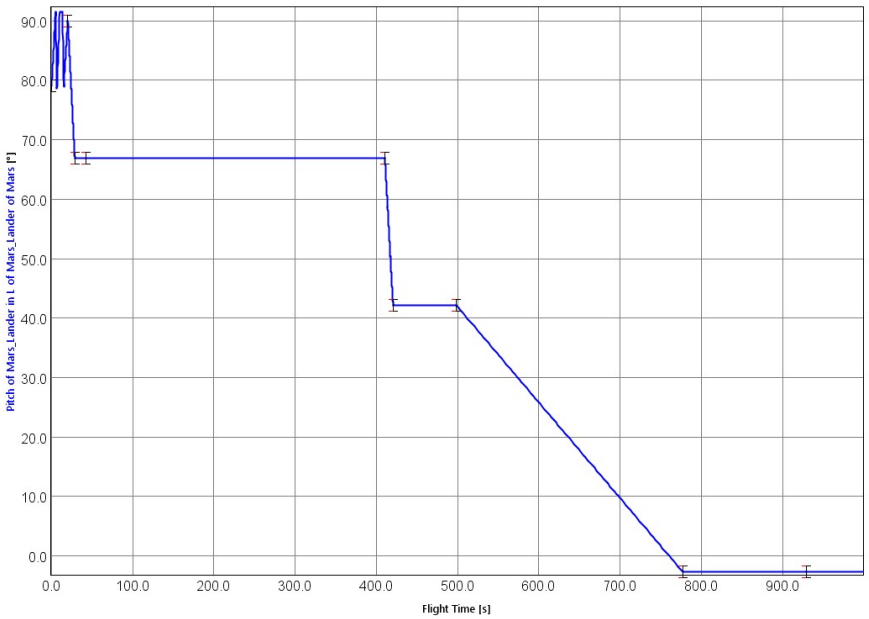

Figure 4.19: ASTOS Results: Pitch

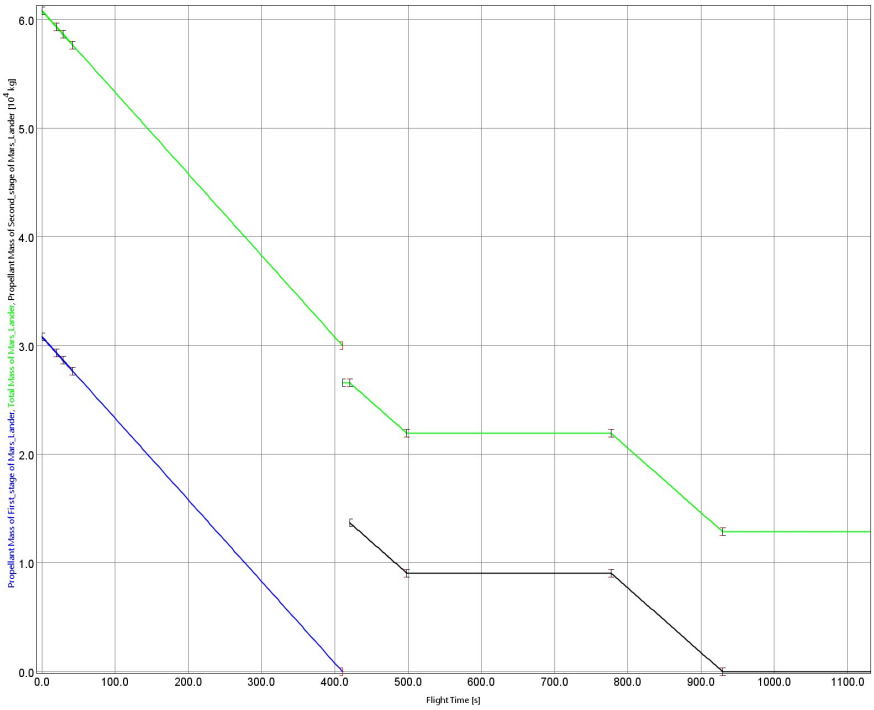

Figure 4.20: ASTOS Results: Total Mass (Green), First Stage Mass (Blue), Second Stage Mass (Black)

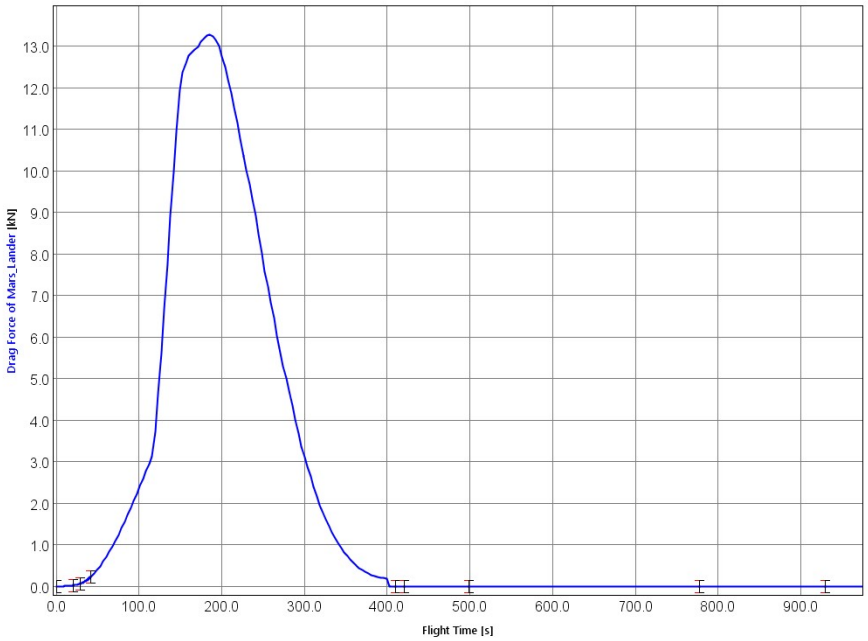

Figure 4.21: ASTOS Results: Drag

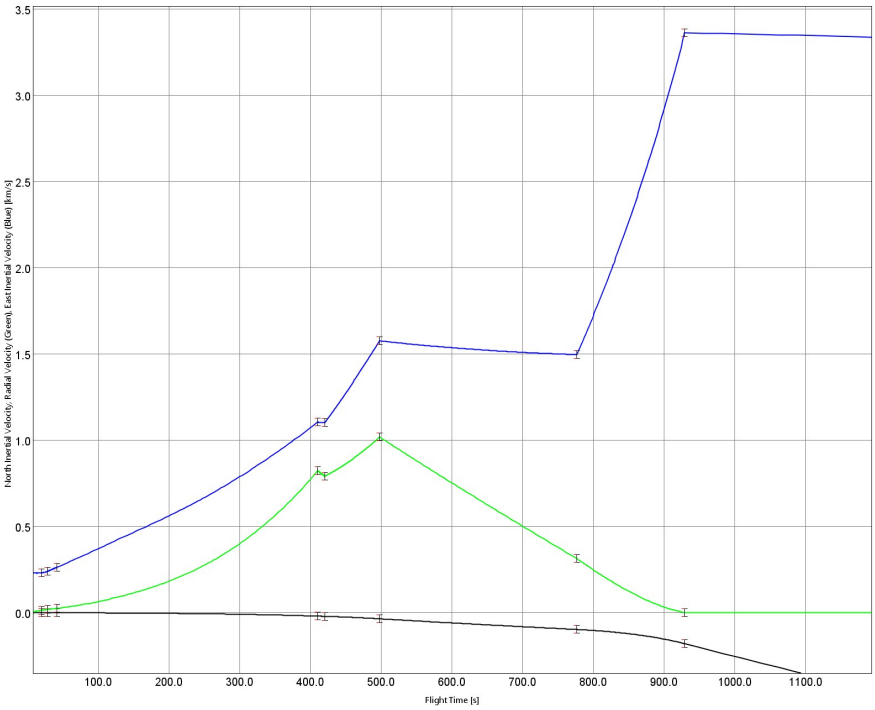

Figure 4.22: ASTOS Results: East Inertial Velocity (Blue), Radial Velocity (Green), North Inertial Velocity (Black)

In addition, in the following figures 4.23 and 4.24, the three dimensional representation of the ascent is shown, where it is possible to concretely see the achievement of the circular orbit of arrival.

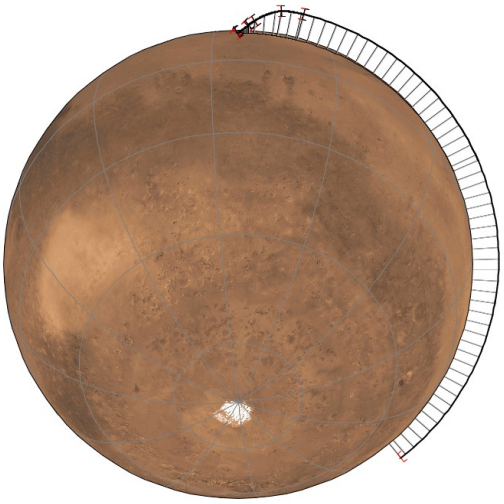

Figure 4.23: ASTOS Results: 3D Representation

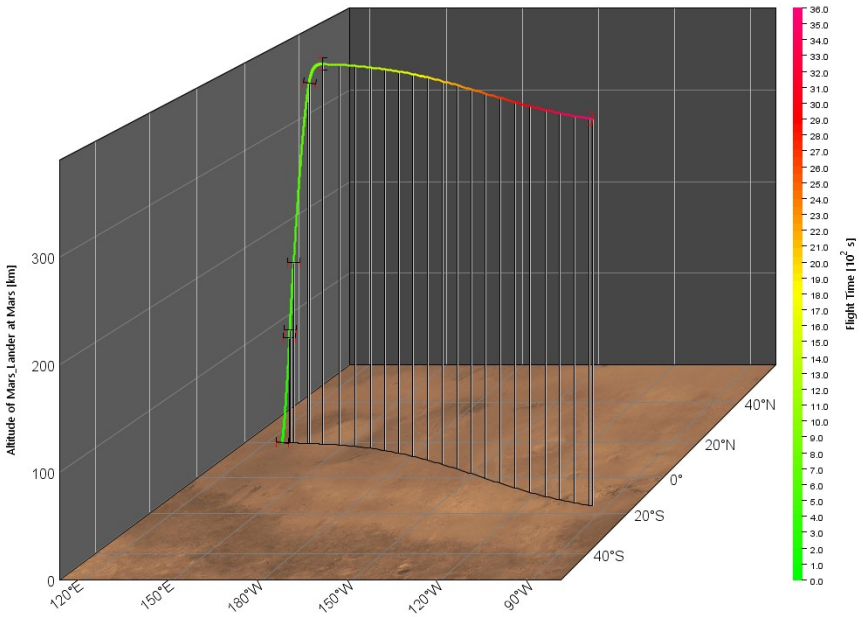

Figure 4.24: ASTOS Results: Latitude, Longitude, Altitude Plot

Table 4.5 shows the optimized phase data in terms of durations, mission times, and masses.

Phase	Time [s]	Duration [s]	Initial Mass [kg]	Propellant Consump. [kg]	Jettisoned Mass [kg]
1.	0 - 20.00	20.00	60803	1501.2	0
2.	20.00 - 28.59	8.59	59301.8	644.5	0
3.	28.59 - 41.96	13.37	58657.3	1003.6	0
4.	41.96 - 410.43	368.47	57653.6	27658.6	3428.9
5.	410.43 - 420.43	10.00	26566.1	0	0
6.	420.43 - 498.24	77.81	26566.1	4628.4	0
7.	498.24 - 777.10	278.85	21937.7	0	0
8.	777.10 - 929.52	152.42	21937.7	9066.6	0

Table 4.5: ASTOS Optimized Mission and Vehicle Data

Figure 4.25 shows the total ΔV which also includes gravity and atmospheric losses, this is the main output of the design routine that is used for lander sizing. Numerical values are reported in table 4.6.

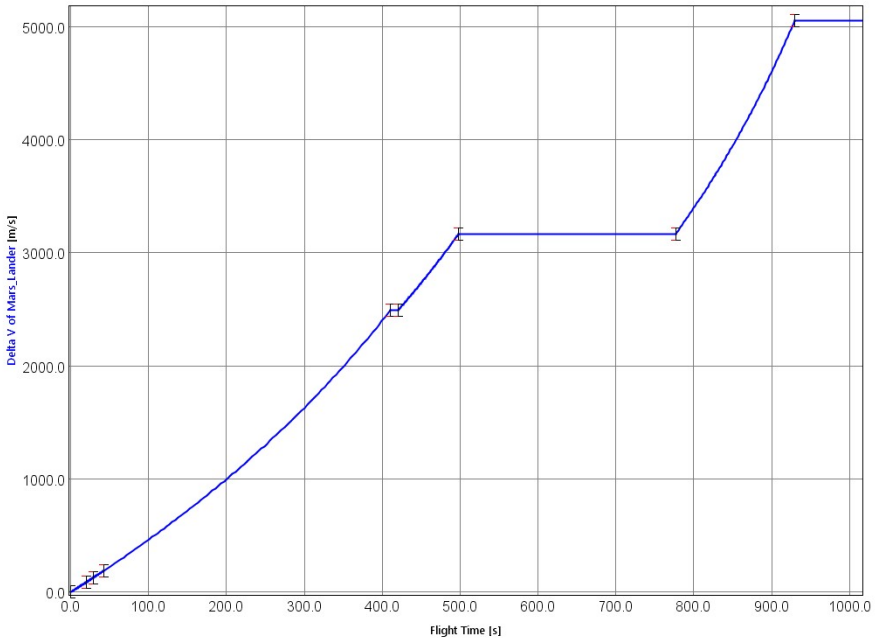

Figure 4.25: ASTOS Results: ΔV

Drag Losses	42.18 [m/s]
Gravity Losses	1451.35 [m/s]
Total ΔV	**5050.3 [m/s]**

Table 4.6: ASTOS: Drag Losses, Gravity Losses e Total ΔV

4.6 Comparisons and final considerations

The results for the two MATLAB and ASTOS models compared are shown in figures from 4.26 to 4.28 , as can be seen the altitude and velocity profiles are very similar as are the durations of the various phases. In the velocity profile some discrepancies can be seen mainly due to three factors, the MATLAB model is simplified and in two dimensions, this implies that North Velocity is not contemplated, in ASTOS it is also slightly different from zero, this is due to the inclination of the orbit which in MATLAB is not evaluated. Another factor that leads the profiles to be slightly different is the reference system, in MATLAB it is non-inertial (PCPF) and does not take into account in the representation the velocity given by the rotation of the planet at the given latitude while in ASTOS inertial velocities are reported. The last factor is the phase modeling, which is more punctual in ASTOS especially in the very early Lift-Off, Pitch-Over and Constant-Pitch phases, totally absent in MATLAB, but also in the attitude dynamics which in MATLAB is modeled with tangent bi-linear functions while in ASTOS by more specific and better optimized control laws, as explained in section 4.5.2. These discrepancies in the velocity profile and consequently in the altitude profile, although minimal lead to slightly different trajectories in the atmosphere phase causing different atmospheric drag and also to a different influence of gravity given by the direction of thrust, these contributions cause the losses to differ between the two models leading to different ΔV.

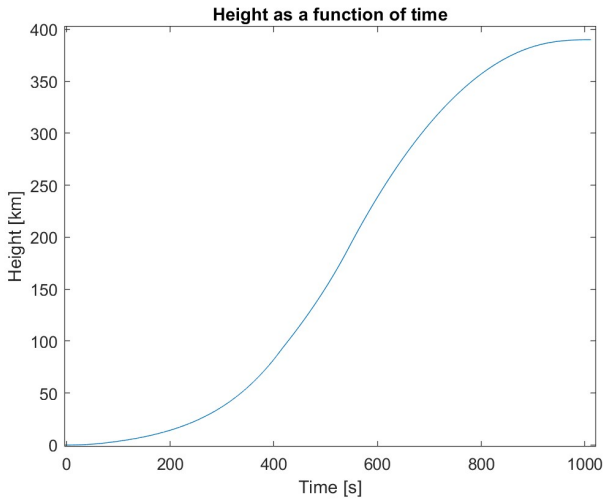

(a) MATLAB Height

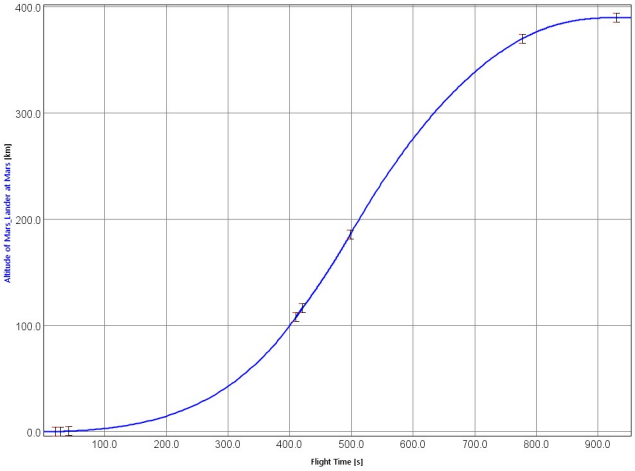

(b) ASTOS Height

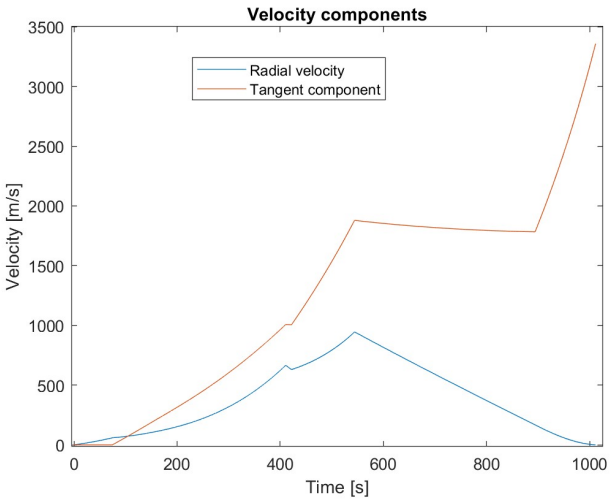

(c) MATLAB Velocities

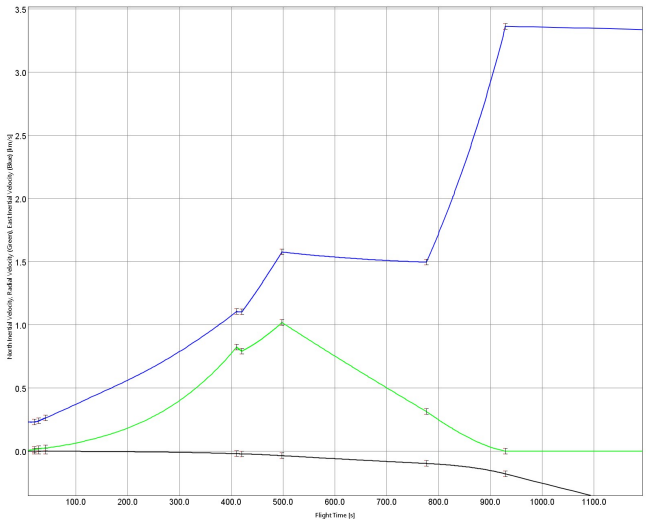

(d) ASTOS Velocities

Figure 4.26: ASTOS-MATLAB Comparison: Height & Velocities

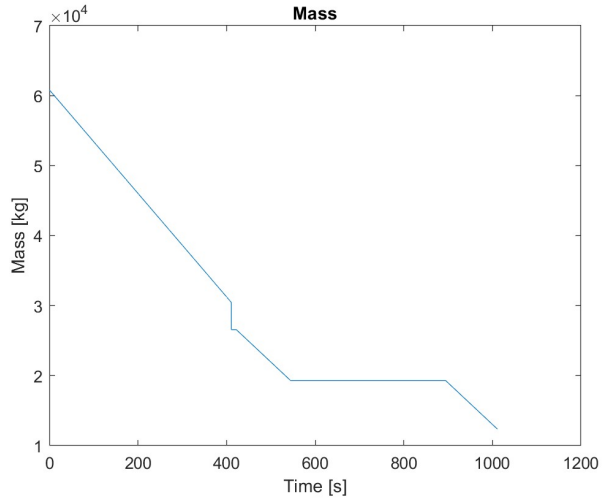

(a) MATLAB Masses

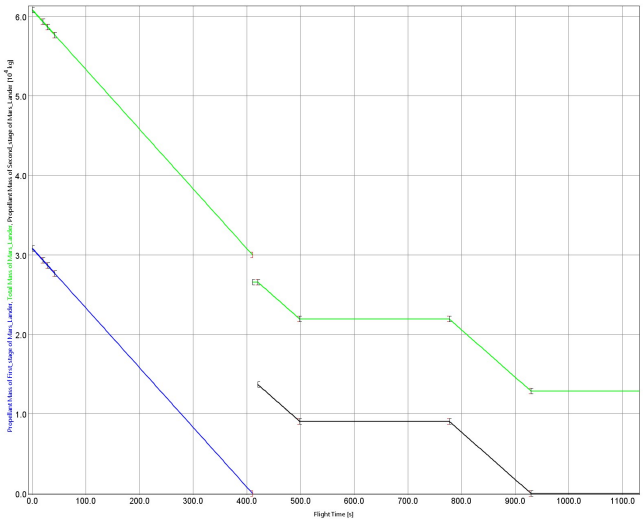

(b) ASTOS Masses

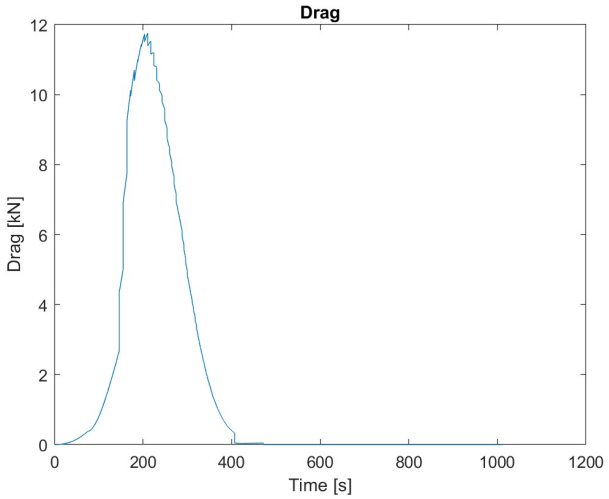

(c) MATLAB Drag

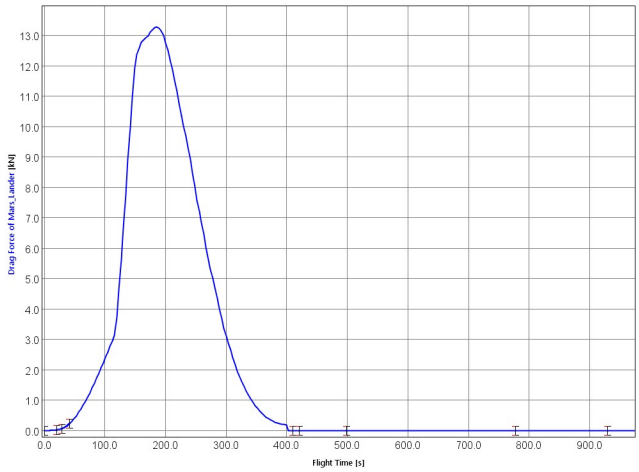

(d) ASTOS Drag

Figure 4.27: ASTOS-MATLAB Comparison: Masses & Drag

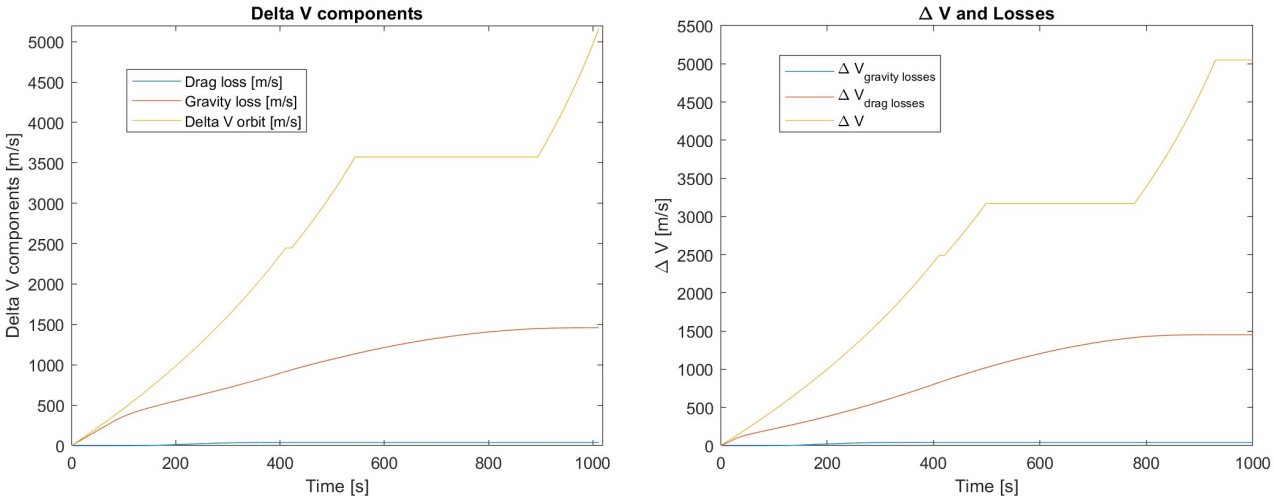

(a) MATLAB ΔV (b) ASTOS ΔV

Figure 4.28: ASTOS-MATLAB ΔV

To validate the MATLAB subroutine and the ASTOS model the total ΔV of the mission is compared between the two models in table 4.7, to verify that the relative error between ASTOS and MATLAB is less than 15% so as to ensure a plausible value for sizing.

	ASTOS Results	**MATLAB Results**
Drag Losses	42.18 [m/s]	38.91 [m/s]
Gravity Losses	1451.35 [m/s]	1459.14 [m/s]
Total ΔV	**5050.3 [m/s]**	**5155.75 [m/s]**

Table 4.7: Drag Losses, Gravity Losses e Total ΔV: ASTOS vs MATLAB Results

$$\text{Error } \% = \frac{|\Delta V_{ASTOS} - \Delta V_{MATLAB}|}{\Delta V_{ASTOS}} \cdot 100 = 2.09\% \tag{4.18}$$

Chapter 5

Mission Analysis: Descent Scenario

This chapter will discuss the Mars descent mission, in particular the Entry, Descent & Landing (EDL) phases will be analyzed. The objective is mainly to create a valid aerodynamic model by calculating the drag coefficient using established theoretical models. The trend of the coefficient as the altitude and flight Mach change will be plotted, thus including a specific evaluation on the flight regime and involving the calculation of the Reynolds number and viscosity of the Martian atmosphere from altitude using the atmospheric model already presented in section 2.4. After modeling the aerodynamics in section 5.1, the chapter will cover mission modeling on ASTOS in section 5.2, definition of the vehicle in its components in section 5.2.2, choice of mission phases in section 5.2.3, initial guess on their duration, attitude dynamics, and finally the imposition of constraints for optimization in section 5.2.4.

5.1 Aerodynamic Model for EDL

As anticipated in creating the aerodynamic model for ascent in section 4.2, usually the drag coefficient depends strongly on the vehicle configuration and size, and is estimated as a sum of several contributions. However, as for the ascent scenario, the choice was to use an experimental dataset at varying Mach in different flight regimes. For descent, on the other hand, the choice is to follow a theoretical model that deals with the drag coefficient C_D in different flow regimes whether continuous or rarefied, valid for the spheres [36]. Assuming then the lander as a sphere, the study plots correlation equations of the coefficient with the flow regime that are simplified at their limits allowing an eager computer calculation when compared to classical formulations. This study presents 3 correlation equations:

- **Subsonic Flow**: valid for all subsonic regimes;
- **Supersonic Flow**: valid for supersonic regimes with Mach> 1.75;
- **Linear Interpolation**: valid between Mach 1 and 1.75, linearly interpolates the drag coefficients.

This different approach taken in descent, with the use of theoretical models rather than the use of experimental data, is mainly because having no evidence of launches from Mars, ascent may often involve specific vehicle configurations with different mission phases, multiple stages, the flight path during ascent may vary significantly depending on the specific mission. The set of these factors may not be fully captured by generic theoretical equations, whereas for descent, the availability of established and validated equations for a wide range of flow regimes, along with experience from previous missions, makes theoretical equations a reliable choice.

5.1.1 Subsonic Flow Regime

In the subsonic regime, the model implements the following equation (5.1):

$$\begin{aligned} C_D = 24 & \left[Re + S \left\{ 4.33 + \left(\frac{3.65 - 1.53\frac{T_w}{T}}{1 + 0.353\frac{T_w}{T}} \right) e^{-\frac{0.247Re}{S}} \right\}^{-1} \right] \\ & + e^{-\frac{0.5M}{\sqrt{Re}}} \left[\frac{4.5 + 0.38\left(0.003Re + 0.48\sqrt{Re}\right)}{1 + 0.03Re + 0.48\sqrt{Re}} + 0.1M^2 + 0.2M^8 \right] \\ & + \left[1 - e^{-\frac{M}{Re}} \right] 0.6S \end{aligned} \tag{5.1}$$

All the figurative terms are analyzed below:

- **Re (Reynolds Number)**: depends on the sphere diameter, viscosity and flow velocity;
- **S (Molecular Speed Ratio)**: is equal to $M \cdot \sqrt{\frac{\gamma}{2}}$ where γ is the ratio of specific heats;
- **Tw**: is the temperature of the sphere considered to be isothermal [K];
- **T**: is the temperature of the flux [K].

This correlation equation considers different subsonic flow regimes:

- **Subsonic Continuum Flow**: Fluid particles interact frequently, allowing the flow to be described by continuous flow equations, such as the Stokes-Oseen equation ($C_D = 24Re^{-1} + 4.5$). This simplification holds for Reynolds numbers high enough to ensure continuous flow but low enough to avoid significant inertial effects. A new correlation, applicable up to the laminar-turbulent transition, has been developed to account for both inertial and compressibility effects (the term within the brackets of the second part). The inertial components align with the standard curve, while the compressibility components are in agreement with the Bailey and Hiatt data;

- **Subsonic Free Molecular Flow**: In this regime, the Reynolds number is extremely low, indicating infrequent interactions between fluid particles. This is typical of highly rarefied conditions where molecules behave as free particles. The first term of the equation simplifies to the molecular flow equations of Langevin and Epstein at zero Reynolds number. Values of 1.0 and 0.89 are used for the coefficient of thermal accommodation (describing the efficiency with which thermally moving gas molecules interact with a solid surface) and the fraction of diffusely reflected molecules (describing the behavior of gas molecules when they collide with and bounce off a surface), respectively. The third term, when Re tends to zero, has a value of $0.6S$, approximating the compressible subsonic flow equations of Stalder and Zurick in combination with the equations of Epstein and Langevin;

- **Subsonic Slip and Transition Flow - Incompressible**: This regime occurs when the flow is neither fully continuous nor entirely molecular, but in a transitional phase between the two. Particles begin to slip past each other, and the flow can be regarded as incompressible. A three-constant equation of the form proposed by Millikan is used in this region. One constant is selected to approach the molecular flow equation in the limit, the second constant is chosen to align with the modified slip-flow equation of Millikan, and the third constant is utilized to best fit Millikan's experimental data, which span the entire slip-flow and transition flow regime across different Reynolds numbers.

- **Subsonic Slip and Transition Flow - Compressible**: This regime is similar to the previous one but considers the compressibility of the fluid, meaning the variation in fluid density with pressure. The exponential factors in the second and third terms of the equation are derived to match the experimental data of Bailey and Hiatt.

5.1.2 Supersonic Flow Regime

As anticipated, two equations are used for the supersonic regime, one for Mach>1.75 and one valid between Mach 1 and 1.75 that linearly interpolate the drag coefficients. For **M>1.75** the following equation (5.2) applies:

$$C_D = \frac{0.9 + \frac{0.347}{M_\infty^2} + 1.86\left(\frac{M_\infty}{Re_\infty}\right)^{\frac{1}{2}}\left[2 + \frac{2}{S_\infty^2} + \frac{1.058}{S_\infty}\left(\frac{T_w}{T}\right)^{\frac{1}{2}} - \frac{1}{S_\infty^4}\right]}{1 + 1.86\left(\frac{M_\infty}{Re_\infty}\right)^{\frac{1}{2}}} \tag{5.2}$$

The subscripts ∞ refer to free stream conditions. Again, the equation is adapted according to the flow regime and involves:

- **Supersonic Molecular Flow**: Reynolds number is low and consequently the equation at its limit tends to keep only the terms in the parentheses, respecting the theoretical results predicted by Stalder and Zurick in this regime;
- **Supersonic Continuum Flow**: Reynolds number is high, and when the Mach at the limit tends to zero it is simplified to just the first two terms at the numerator. This is an expression derived from the sum of the correlation equations for afterbody drag and forebody drag, which respects the experimental data set of Bailey and Hiatt;
- **Supersonic Slip and Transition Flow**: in these regions between the two regimes, the proposed equation returns results in agreement with Bailey and Hiatt's experimental data, obtained over the entire slip-flow regime and a large part of the transition regime.

As for the cases where $1 < M < 1.75$ the following interpolation in equation (5.3) is used

$$C_D(M_\infty, Re_\infty) = C_D(1, Re) + \frac{4}{3}(M_\infty - 1)[C_D(1.75, Re_\infty) - C_D(1, Re)] \tag{5.3}$$

In which (i) $C_D(1, Re)$ is the coefficient calculated from the subsonic equation posed mach unitary and (ii) $C_D(1.75, Re_\infty)$ is the coefficient calculated from the supersonic equation just discussed with Mach equal to 1.75.

5.1.3 Drag Coefficient Estimation

A MATLAB code is implemented with as input a vector for Mach numbers set exactly as was done for ascent and a vector with different reference altitudes,

see section 4.2. Starting from the altitude, the atmospheric model [18] is again exploited to calculate density and temperature. Applying Sutherland's formula reported in (5.4), the temperature-dependent dynamic viscosity of Mars' atmosphere is calculated:

$$\mu(T) = \mu_0 \left(\frac{T}{T_0}\right)^{\frac{3}{2}} \frac{T_0 + S}{T + S} \tag{5.4}$$

- μ_0 is the dynamic reference viscosity at temperature T_0, equal to $1.37 \cdot 10^{-5}$ Pa·s
- T is the temperature of the gas [K].
- T_0 is the reference temperature (273.15K)
- S is the Sutherland constant, which for Mars is 222K

Taking advantage of the viscosity just calculated, the lander's reference diameter, the velocity calculated from Mach number, and the temperature and density given by the atmospheric model, the Reynolds number is estimated in equation (5.5):

$$Re = \frac{\rho v L}{\mu} \tag{5.5}$$

Where (i) ρ is the atmospheric pressure [kg/m^3], (ii) v is the flux's velocity [m/s] and (iii) L is the reference variable [m]. Given the values of Reynolds and viscosity, in order to apply the correlation equations as a function of Mach it is necessary to estimate the specific molecular velocity in equation (5.6), posed $\gamma = 1.29$ on Mars:

$$S = M \cdot \sqrt{\frac{\gamma}{2}} \tag{5.6}$$

Where (i) M is the mach number and (ii) is the aforementioned specific molecular velocity. And also it is necessary to evaluate the ratio $\frac{T_w}{T}$, taking up the study from which the correlation equations were derived [36], a dependence of the latter on Mach number is made explicit in figure 5.1, following this approach the model uses a null ratio for $M > 6$, equal to 3 for $M > 3.5$, in all other cases it is considered unit ratio.

Table 1 Comparison of correlations with experimental drag coefficients

Data set	Range of M	Range of Re	Range of T_w/T_∞	No. of points	Maximum percentage deviation			
					Carlson	Crowe	Korkan	Henderson
Standard curve	–	$10^{-2}-10^{4}$	1	12	48	4	13	6
Molecular flow	$10^{-2}-6$	–	1	14	66	22	39	5
Slip and transition	$5\times10^{-7}-6\times10^{-6}$	$10^{-7}-10^{-5}$	1	50	9	13	23	3
Subsonic	$0.15-0.5$	$200-10^{4}$	1	19	53	21	15	8
Subsonic	$0.6-0.99$	$100-10^{4}$	1	31	54	28	18	15
Supersonic	$1.03-1.55$	$20-5\times10^{3}$	1	35	135	30	32	16
Supersonic	$1.75-2.55$	$5-5\times10^{3}$	1	14	117	31	14	13
Supersonic	$2.55-6$	$15-5\times10^{3}$	1	35	114	42	13	6
Supersonic	$3.5-6$	$10-100$	2-4	9	102	31	9	2

Figure 5.1: $\frac{T_w}{T}$ Ratio as a function of flow regime and Mach number[36]

5.1.4 Results

It can be seen from the results in figure 5.2 that as Mach increases, there is a peak in the drag coefficient with a value of about 1, for Mach equal to about 1.8, then settling to a constant value around 0.9 for very high Mach. Details for the single altitude are reported in figure 5.3.

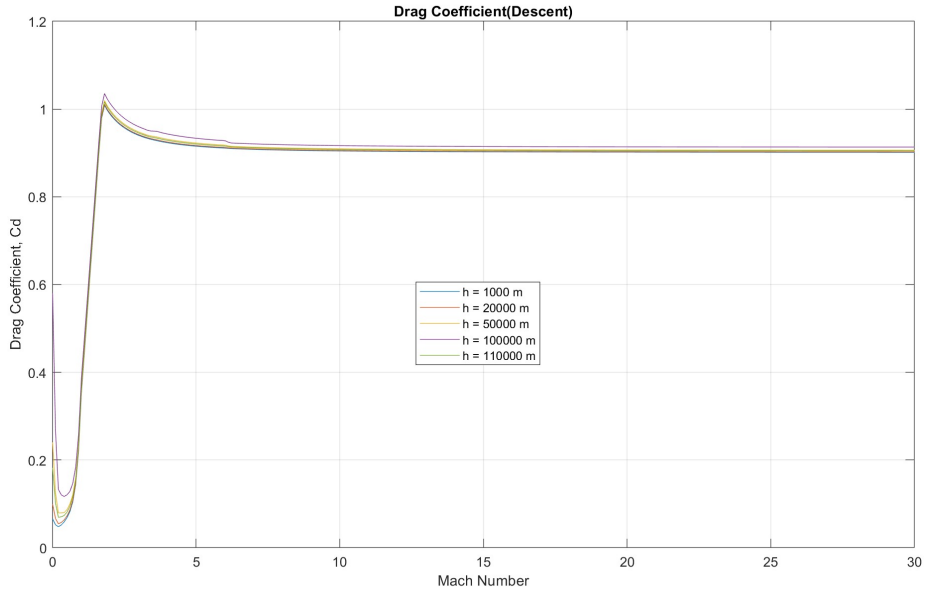

Figure 5.2: Descent C_D for various altitudes

The effect of altitude resulting in a change in Reynolds given the decrease in temperature and density results in a shift of the peak toward higher mach and higher values, however, this effect is not very influential. The effect of altitude is much more interesting for low Mach numbers, for low altitudes the coefficient has

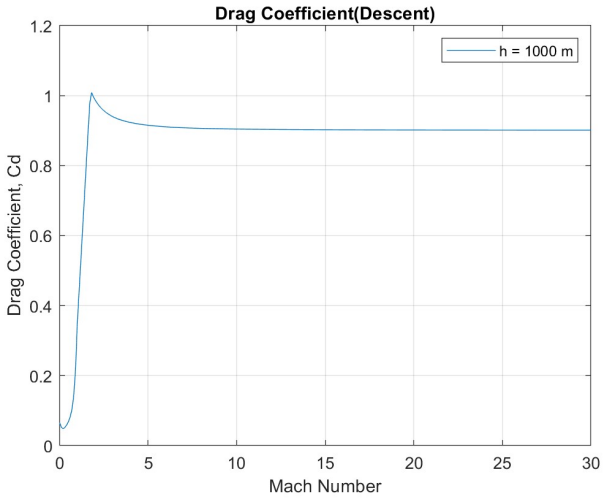

(a) h = 1000m

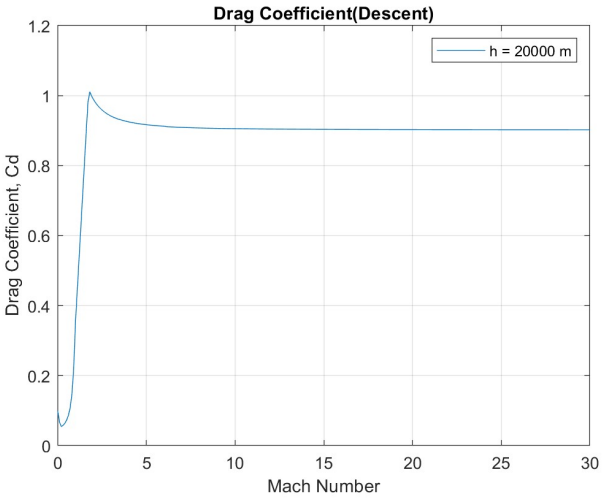

(b) h = 20000m

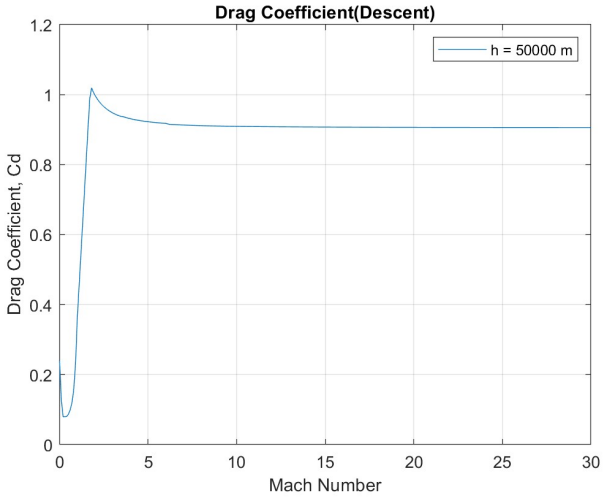

(c) h = 50000m

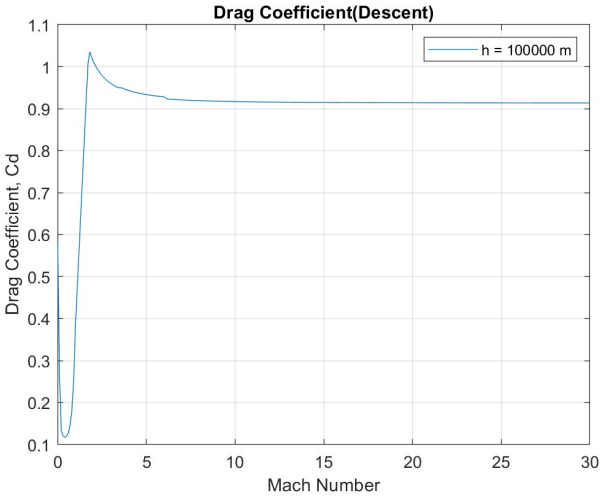

(d) h = 100000m

Figure 5.3: Descent C_D for each altitude

lower values and gradually loses the decreasing trend in subsonic. This effects are shown in figure 5.4.

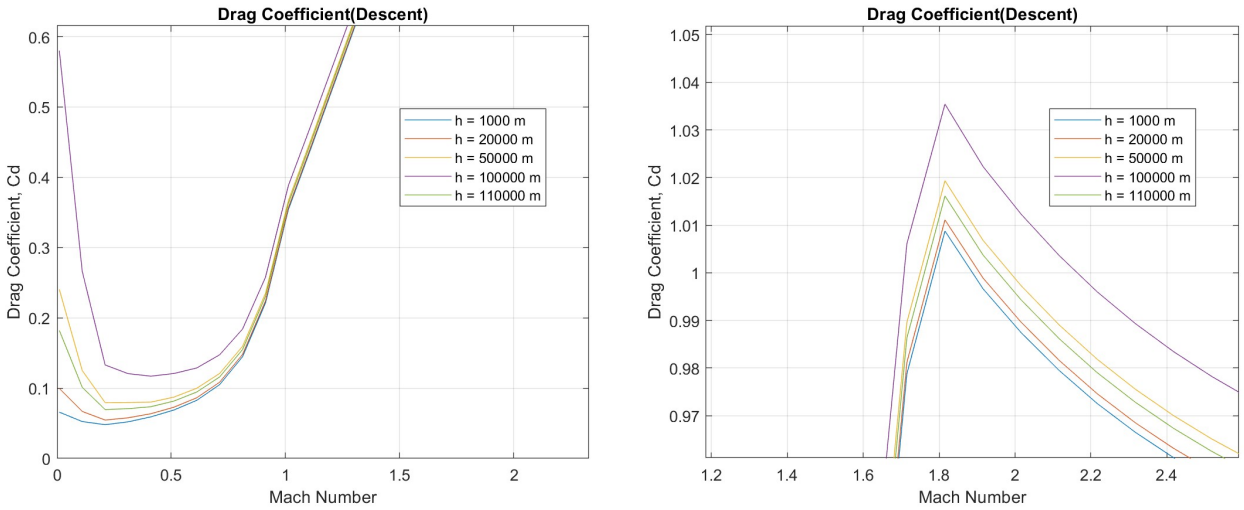

(a) Altitude Effect: low mach number

(b) Altitude Effect: peak

Figure 5.4: C_D Details for low mach numbers and peak

5.2 ASTOS Descent Scenario Model

As done for the ascent model, starting from the reference mission described in section 5.2.1, the scenario is replicated in ASTOS by defining all the vehicle's characteristics in section 5.2.2, and implementing the aerodynamic model just described in addition to the same atmospheric model used for ascent. Based on the reference missions covered in Chapter 2, the mission phases and trajectory to be followed by the lander during descent are chosen in section 5.2.3, constraints for optimization are set in section 5.2.4, and initial guess values are sought in section 5.2.5.

5.2.1 Reference Mission

In the reference mission [20] the EDL phases begin at an altitude of 200km, the chosen landing site is again **Hebrus Valley** at the coordinates of 20° N and 126° E. The lander is initially on a circular orbit and therefore needs an initial phase of waiting in orbit to reach a good latitude and longitude to land at Hebrus Valley. Engines performs an initial maneuver to initiate EDL aimed at reducing periapsis. The lander is equipped with a 16m diameter IAD in the hypersonic flight phase

that slows down to supersonic speeds. For supersonic Mach around values of 3-4 a supersonic parachute of 30m in diameter is deployed. Such a configuration for the EDL, shown in figure 5.5, is representative of the most classic choices found in the literature and discussed in the chapter 2, the parachute slows to subsonic velocities to allow safe release of the rigid nose heat shield and subsequent retropropulsion. Note that the TPS is composed by the rigid nose and by the F-TPS on the inflatable. It appears from the literature and the study conducted by the reference mission that the supersonic parachute release should occur between 10-20km altitude. The lander should perform both ascent and descent, so as far as propulsion is concerned, the same thrusters designed for the MAV are used (7 thrusters providing 53kN as in the reference mission, also considering redundancies to ensure safety).

Figure 5.5: Reference lander in EDL configuration [20]

All of the reference mission's notable variables used to create the model are shown in table 5.1.

Lander Variable	Value
Crew Module Mass	15726 [Kg]
Propellant Mass	8200 [Kg]
TPS, IAD & Parachute Mass	3314 [Kg]
Nose Heatshield Mass	223 [Kg]
IAD Diameter	16 [m]
Parachute Diameter	30 [m]
Reference Lander Diameter	8 [m]
Thrusters	7x53 [kN]

Table 5.1: Reference lander variables and their values in EDL configuration

5.2.2 Vehicle Parts, Properties & POIs Definition

As already done for the ascent scenario, the various lander's components are defined on the ASTOS software, see figure 5.6. As for the thrusters, the presence of a single actuator capable of providing all the thrust of the 7 engines is considered, the actuator is set as throttable and the throttling value as optimizable, for simplicity the nozzle output area is set equal to $0.5m^2$.

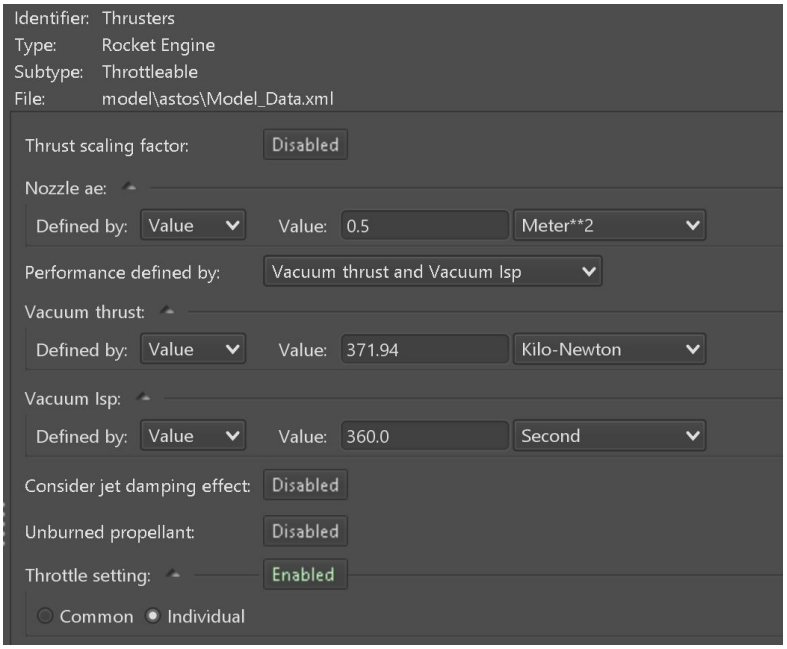

Figure 5.6: Engines definition on ASTOS (Descent)

Unlike ascent, where the aerodynamic model is fixed because the reference

diameter does not vary due to parachute deployment or heat shield and inflatable release (see section 4.2), it is necessary to define 3 aerodynamic models considering different reference diameters and tabular values of C_D

- **Aerodynamics with IAD**: the reference diameter is 16 meters relative to the inflatable, it is active until the deployment of the parachutes, the tabulated values for the C_D are implemented, and a shape coefficient for the infaltable of 0.69 is considered;
- **Aerodynamics with parachutes**: the reference diameter is assumed to be sum of the IAD diameter of 16 meters and the parachute diameter of 30 meters, in this case to consider the presence of the parachutes, a shape coefficient of 0.9 is added to the tabulated values of C_D
- **Aerodynamic payload**; which considers only the lander reference diameter and the tabulated values for the C_D.

The definition of the basic components of the lander, such as the crew module, the descent stage, a component called the IAD that includes inflatable and parachute's masses, and a component including the nose heatshield mass is then conducted. By defining these components it will be possible to release the nose and the masses related to the deceleration and protection systems in the last stages, the descent stage is not released as the tanks are reused for ascent. Figures 5.7, 5.8, 5.9 and 5.10 show the components as defined on ASTOS.

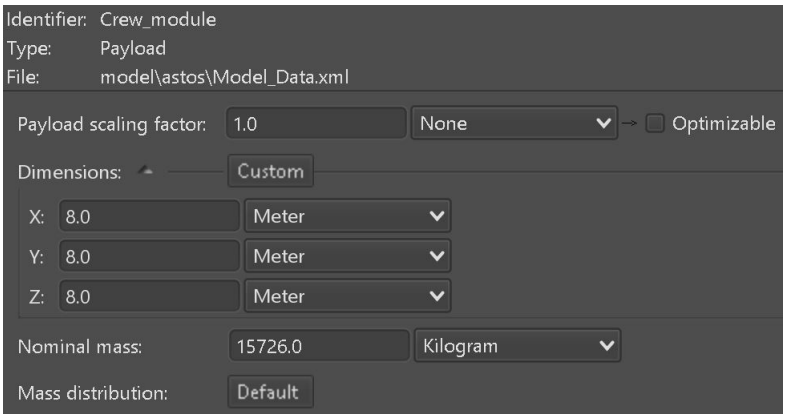

Figure 5.7: Crew Module definition on ASTOS (Descent)

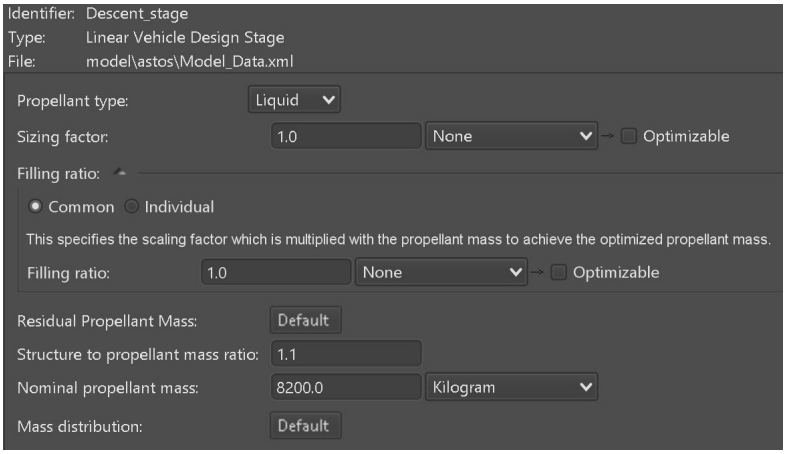

Figure 5.8: Descent stage definition on ASTOS

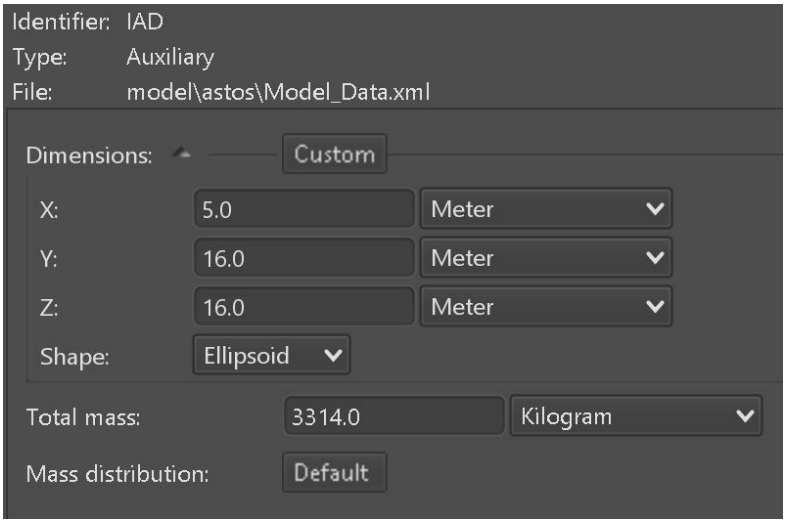

Figure 5.9: Dec. Sys definition on ASTOS

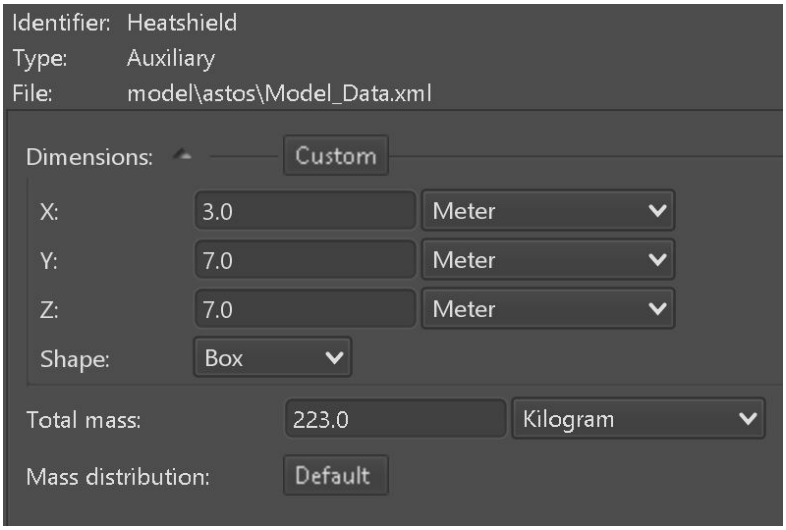

Figure 5.10: Rigid Nose Heatshield definition on ASTOS

Once all components have been defined, they are assembled on ASTOS to define the vehicle as one (vehicle & POIs definition), see figure 5.11.

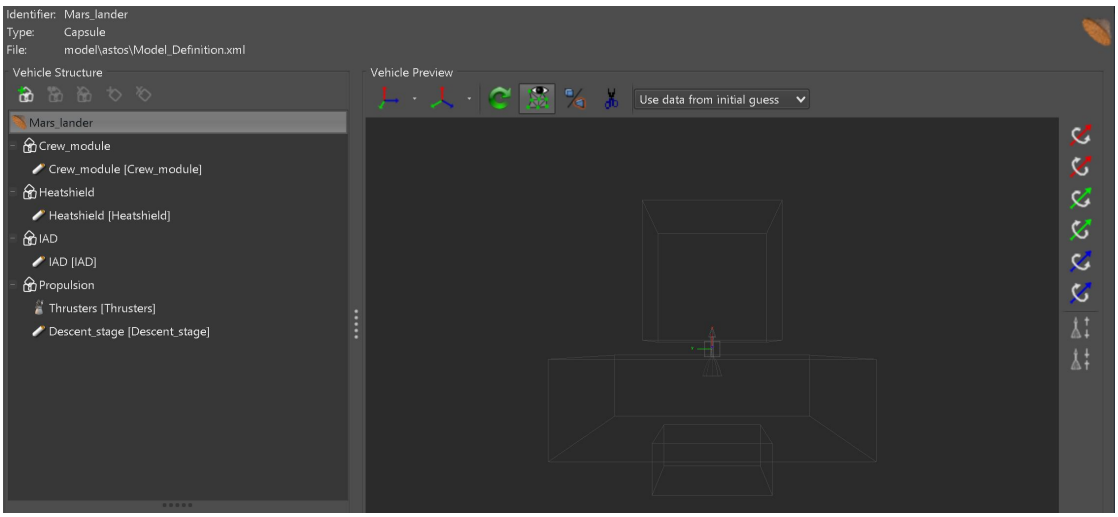

Figure 5.11: Vehicle & POIs definition

5.2.3 Dynamics Configuration

For the modelling of the descent phases, the starting point is what already described in section 2.2.1. In fact, from the literature, the definition of the phases is very similar to that characteristic of the descent of Viking missions, with the

use of propulsive deceleration and parachutes, with the need to introduce a rigid aeroshell or an inflatable. Therefore, taking a cue from the phases as described in section 2.2.1, the proposed model is simplified, and the phases are defined in ASTOS as follows:

1. **Orbiting**: the lander is on the circular starting orbit of 200km altitude, orbiting until it reaches the optimal conditions to reach the landing site;

2. **Decrease Periapsis**: a short propulsive phase in which the thrusters slow down the lander to bring the periapsis to lower values and begin the descent;

3. **Coast to periapsis**: a phase in which the inflatable is used to decelerate, activating the aerodynamics associated with it in ASTOS and decreasing the periapsis again to values very close to the Mars radius but with a negative sign. The objective being to reach an altitude and mach suitable for deploying the supersonic parachute (around 20 km);

4. **Coast with Parachute**: this phase utilises the aerodynamics associated with the presence of the parachute, slows the lander down further and decreases the periapsis;

5. **Coast to Impact**: similar to the previous one, but the rigid nose is jettisoned and the thrusters are ignited, periapsis reaches the aimed value;

6. **Braking**: having reached subsonic Mach and altitudes in the order of 5-10km, the trhusters are ignited again in a vertical direction to further reduce radial velocity and allow the lander a soft landing.

As already done for ascent in section 4.5.2, the dynamics of each phase are defined by choosing the attitude, in terms of yaw angle and pitch angle indicating the direction of velocity with respect to the vehicle axis and thrust with respect to the horizon. Starting from the **initial state**, this is defined as a state vector of orbital elements, an elliptical Keplerian orbit is set and the values for the 200km circular orbit are entered, as in figure 5.12.

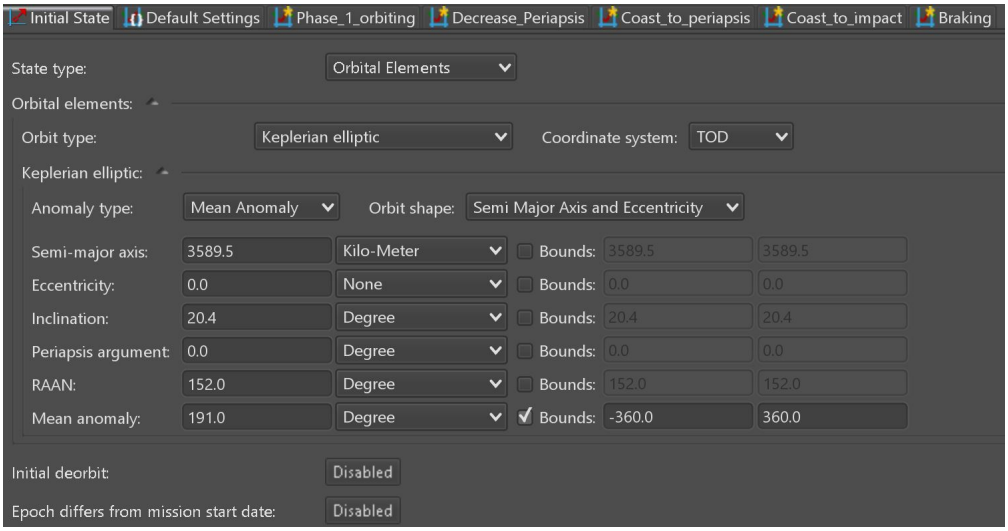

Figure 5.12: Descent initial state

The reference frame used to define the orbital elements is a TOD (True of Date) frame shown in figure 5.13, an astronomical reference used in astrodynamics and astronomy to describe the positions and motions of celestial objects as a function of the specific date of observation. It is a very accurate system that defines the position of the vehicle relative to the centre of the reference body. It is a non-inertial system that incorporates planetary rotation, precession and nutation. As a time reference, the mission start date is set arbitrarily to 18 February 2030, considering the NASA's Evolvable Mars Campaign [1] that envisages Mars missions in 2030.

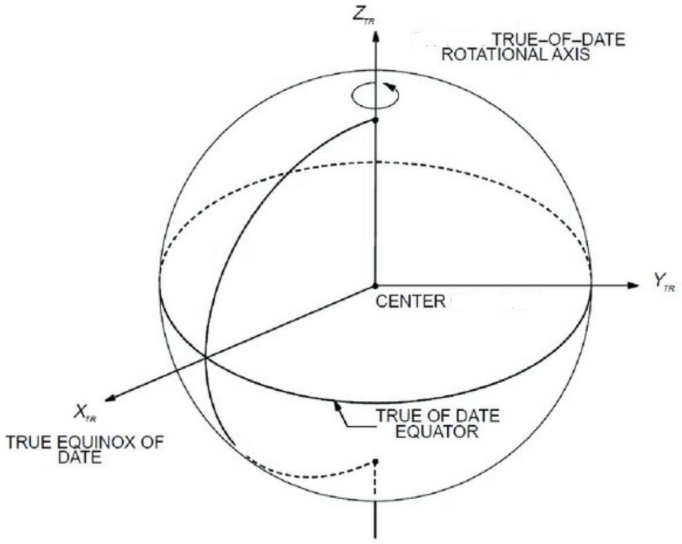

Figure 5.13: TOD Reference Frame [37]

With regard to the dynamics of the subsequent phases, the values for pitch and yaw angles are set. In the initial **orbiting** phase, a value of zero is entered, which can be optimised so that the software decides the most suitable values if different, both the atmospheric and aerodynamic models are deactivated given the altitude. In the **decrease periapsis** phase, a constant law is set for the pitch with a value of 180 degrees, that can be optimised to be sure that the thrust provided is useful to slow down and reduce the periapsis, the pitch is set as the same as the previous phase and optimised. In this case the atmosphere is reactivated as well as the thrusters. The **coast to periapsis** phase sees the aerodynamics relative to the inflatable activated in the model, the yaw angle has a constant and optimisable control law with a reference value of -90°, as well as the pitch angle is set equal to the previous phase and optimisable. The **coast with parachute and coast to impact** phases see the activation of the aerodynamics that takes into account the parachute, the control laws are constant and optimisable and with initial values equal to the previous phase. In addition, the component called "Heatshield" in the model is released at the end of the first phase and the component called "IAD" is jettisoned at the end of the second one, comprising the inflatable and the parachute. After the rigid nose release, the thrusters are ignited to initiate the retropropulsion. The last phase of **braking** once again involves the ignition of the thrusters, the activation of the aerodynamics relative only to the crew module, the yaw angle has a control law defined as in the previous coasting phases while a linear law is implemented for the pitch with a final value of 90° so as to land vertically and slow down by directing the thrust in a radial direction.

Following control laws for constant pitch and yaw angles is useful for maintaining vehicle stability during different stages of the descent. These laws predefine the pitch and yaw angles to be maintained, reducing the complexity of the control system. This approach is effectively followed and investigated in section [38]. It emerges the importance of allowing ASTOS to optimise these laws according to the trajectory and specific phase in order to maintain vehicle stability.

The table 5.2 shows all initial guess durations for the phases. This time, these durations are chosen directly on the basis of an iterative process of simulations without implementing optimisation, seeking the desired trajectory and velocity profiles, aiming for the lowest possible values for the 3 inertial velocities at arrival, as well as altitude and Mach values on a phase-by-phase basis in accordance with the considerations made previously in the definition of the phases and based on the literary analysis in section 2.2.1. The periapsis and apoapsis values were also observed in the various simulations, aiming to have a value of $-R_{Mars}$ for the former and zero for the latter.

Phase	**Duration Guess**
1. Orbiting	35 min
2. Decrease Periapsis	17 s
3. Coast to Periapsis	3083 s
4. Coast with Parachute	10 s
5. Coast to Impact	60 s
6. Braking	15.5 s

Table 5.2: Phases and their duration guess (Descent)

5.2.4 Optimization: Cost Function & Constraints

The optimization method implemented is again CAMTOS, as already extensively discussed for ascent in section 4.5.3, as explained this tool allows a multidisciplinary approach and implements several optimisation algorithms valid for space missions. Once again the integration method is the Runge-Kutta method of order 4/5 as for ascent, already mentioned in section 4.4.4 where a brief explanation of how it works is given and in section 4.5.3. Again, phase-specific constraints are imposed as initial or final boundary conditions, this helps the algorithm to optimize by following the impositions necessary for the correct development of the trajectory. The constraints implemented for descent are as follows:

- **Final Altitude**: final boundary for the last phase, the final equatorial altitude has 0 metres as its reference value;

- **Final Latitude & Longitude**: final boundaries for the last phase, these are position constraints regarding the landing site, the coordinates of Hebrus Valley are entered using a PCPF reference system, already mentioned in section 4.5.2, its latitude is equal to 20.4 ° while its longitude is equal to 126.23°;
- **Final Pitch**: final boundary for the last phase, it is necessary for the lander to land vertically with respect to its local reference system, for this reason this constraint is set on the final pitch and must have a reference value equal to 90°;
- **Final Radial, East Relative & North Velocities**: the final inertial velocities must indicatively have a value of zero to guarantee a soft landing, in this case to relax the constraints, reference ranges between -5 m/s and +5 m/s are imposed as final boundaries for the last phase for these velocities.
- **Parachute Deploy altitude**: as the final boundary of the phase called *Coast to Periapsis* and the initial boundary of the phase called *Coast with Parachute*, the latter is the phase in which the parachute aerodynamics is activated in the model. This constraint aims to impose an upper boundary and a lower boundary relative to the altitude at which this phase begins, as already mentioned in section 5.2.3 in fact it should take place in a certain range where Mach is supersonic and the altitude is such that this deceleration device is effective from an aerodynamic point of view. To relax the constraint, this range is between 5km and 20km;

  A cost function on the maximum transportable payload is also included, as done for the ascent in section 4.5.3. The scaling value is used to facilitate optimization by avoiding numerical problems and is set to a value of 10^{-4}, the main objective is to maximize payload mass.

5.2.5 Simulation Results

The results of the last simulation carried out as part of the iterative process previously described in section 5.2.3, aimed at finding the best initial guess for optimisation, are shown. These results can be appreciated in the figures from 5.14 to 5.19. The reason why these results are proposed rather than the optimised ones is the problem encountered in optimising the model given the defined constraints, this result is attributable to a number of factors, first of all the problems found slowing down the incoming lander further, which despite reaching a discrete result appreciable in figures 5.18 and 5.19 with values of 27. 8 m/s for the East Inertial Velocity and -15.5 m/s for the radial velocity does not allow the software to optimise, despite the fact that the final altitude of approximately zero value is reached

after the braking phase as can be observed in figure 5.14. From the figure 5.15 it can be observed that the periapsis reaches a negative value equal to the radius of Mars while the apoapsis reaches a null value on arrival. The figure 5.16 shows the atmospheric drag which reaches its peak when the aerodynamic model for the parachutes is activated. In fact, by iteratively changing the phase duration, only better values can be obtained for the previously mentioned velocities but never for both, resulting in a Mach variable between 0.3 and 0.6 on arrival, the graphical representation of which in all flight phases is shown in figure 5.17. Another factor is the established need for advanced technologies to slow the descending lander down in human missions, as shown in the literature review in chapter 2, and it is likely that a simplified treatment of EDL technologies as discussed here would require more in-depth study. However, we do not exclude the possibility that one of the factors why optimisation is not successful is due to the attitude dynamics input to the software, which should be evaluated in more detail in order to reduce the computational load on the optimising software by providing more accurate initial guesses. Finally, the ASTOS software is very sensitive to the initial guess, and hardly able to provide an exhaustive answer when the optimisation fails, making troubleshooting complex when a good profile for trajectory and speed is achieved as in this case.

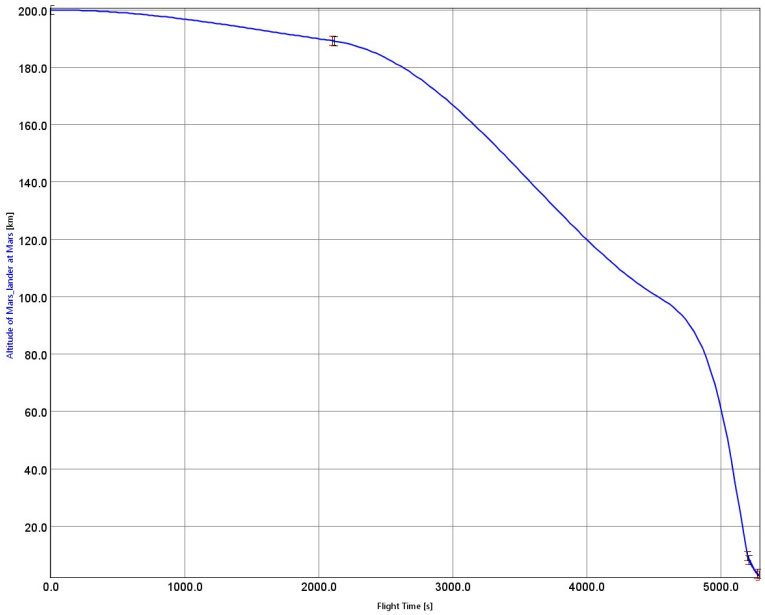

Figure 5.14: ASTOS Descent Results: Altitude

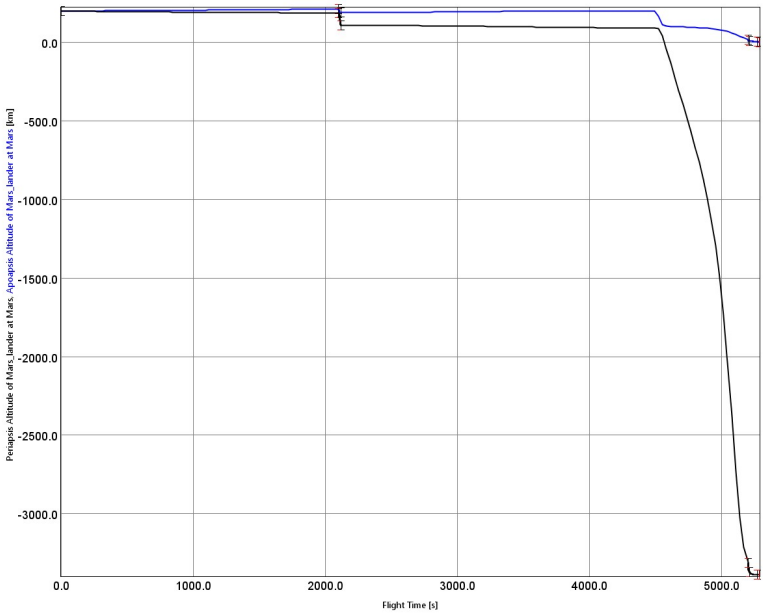

Figure 5.15: ASTOS Descent Results: Periapsis & Apoapsis Altitude

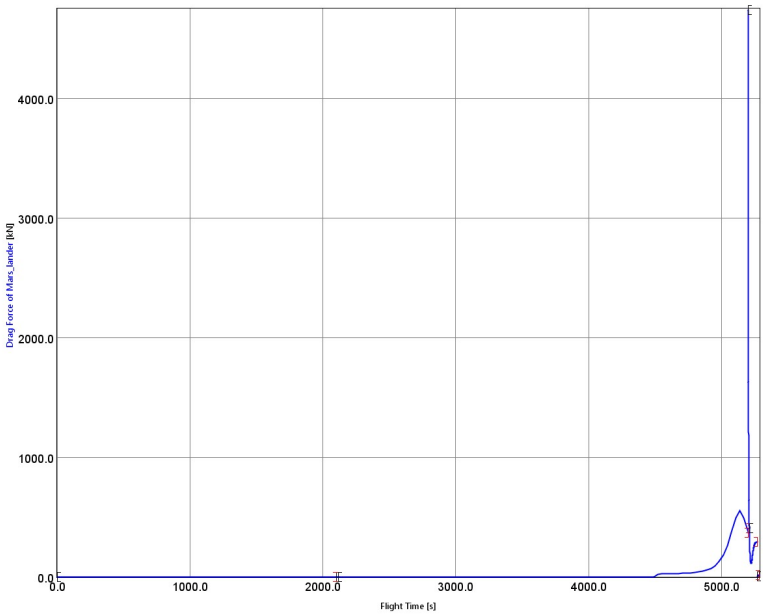

Figure 5.16: ASTOS Descent Results: Drag

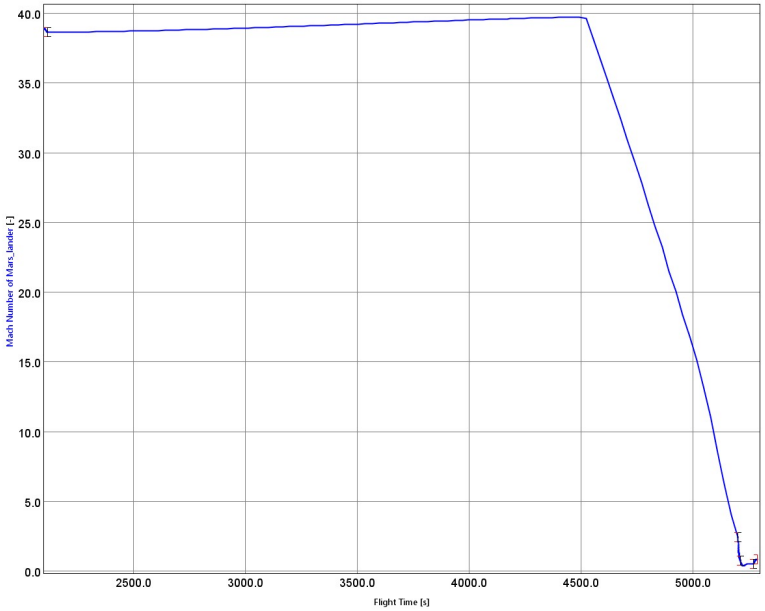

Figure 5.17: ASTOS Descent Results: Mach

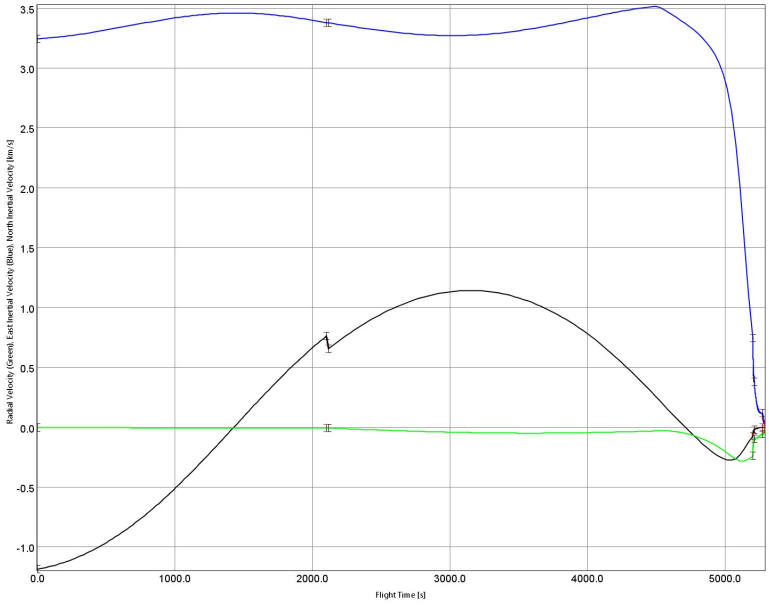

Figure 5.18: ASTOS Descent Results: East Inertial Velocity (Blue), Radial Velocity (Green), North Inertial Velocity (Black)

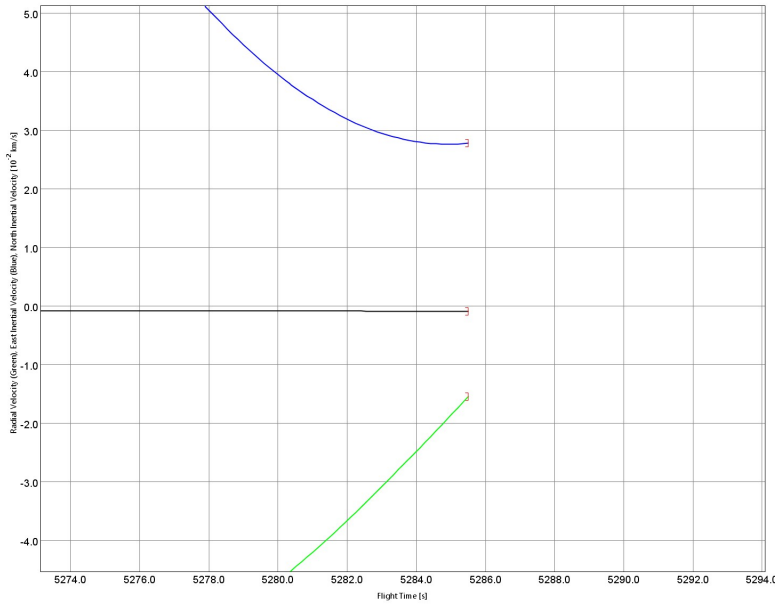

Figure 5.19: ASTOS Descent Results: Arrival Velocities; East Inertial Velocity (Blue), Radial Velocity (Green), North Inertial Velocity (Black)

Figure 5.20 shows a three-dimensional representation of the descent to the planet in all its phases.

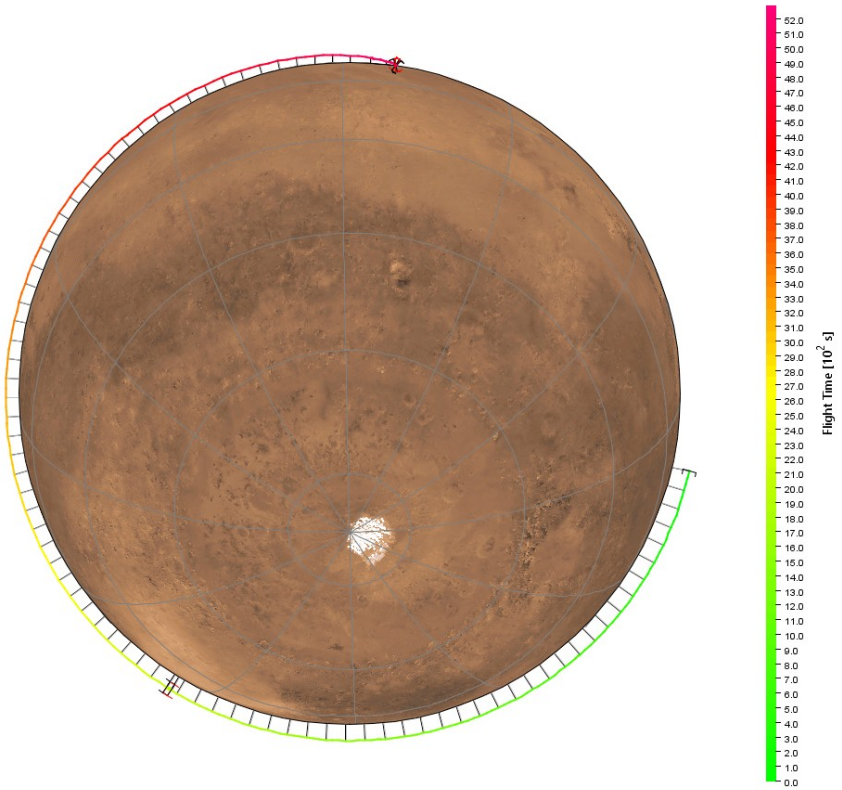

Figure 5.20: ASTOS Descent Results: Three-dimensional representation

Due to the unsuccessful optimization, the data cannot be considered valid for the sizing of the vehicle descent module. In this case the design values exploitable for a vehicle design routine would again be the ΔV usable for subsystem sizing, the duration of the entire descent, and the lander total mass. The simulation results, although unusable, are shown in figures 5.21 and 5.22 for the propellant mass. In figure 5.21 it can be seen that the value of ΔV required for the descent is 751.17 m/s, although this is a non-optimised result, when compared to the values found in literature shown in section 2.3.3 which vary between 600 m/s and 800 m/s depending on the technology used, it is a good result in terms of initial guess as already shown by the other trends, and that the model can be used as a starting point for the creation of a working model.

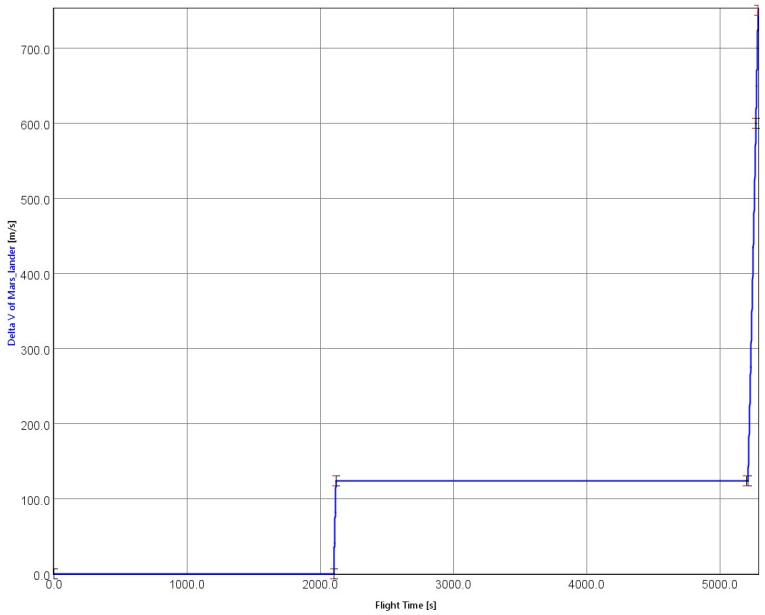

Figure 5.21: ASTOS Descent Results: ΔV

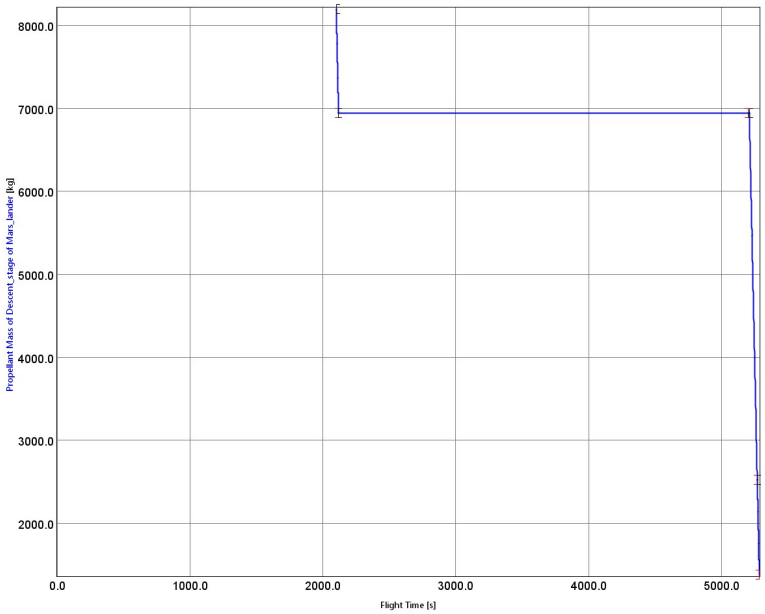

Figure 5.22: ASTOS Descent Results: Propellant Mass

Chapter 6
Conclusions

In this chapter, the final discussions of the thesis work will be reported, starting with a general summary of the results that will be presented in section 6.1, the pivotal points addressed in the previous chapters will be recalled, paying attention to the contribution that this project can make in addressing the ascent and descent missions. Subsequently the results will be discussed and compared with the existing literature analysed in the chapter 2. This discussion naturally leads to investigating the limits of the treatment carried out and possible future developments that could use the work as a starting point, this will be discussed in section 6.2.

6.1 Results Summary & Discussion

Going back to what was explained in section 1.3, the main objective of the thesis work is to lay the foundations for the creation of a tool that implements a design methodology for a multifunctional lander performing Martian ascent and descent, which is divided into a design routine part and a mission analysis routine part, whose mission analysis routine is the subject of interest for this thesis. In chapter 4, the ascent scenario's mission analysis was conducted, aiming at optimizing the scenario both on a sub-routine in MATLAB discussed in section 4.4, and on ASTOS that forms the actual design routine, as discussed in section 4.5. The outputs of these two routines are the input variables for the design routine, such as the total ΔV required to perform the ascent, including gravity and atmospheric drag losses. The losses are the real cornerstone of the analysis as they are the result of how the flight path is modelled and optimised in its dynamics and attitude. The MATLAB sub-routine provides intermediate results results because, as already mentioned in section 4.4 and in section 4.5.2, this model has only 2 degrees of freedom and uses a non-inertial reference system that does not take into account

the increase in velocity given by the rotation of Mars at the departure site given latitude, in addition to using optimization algorithms that are more simplified and less suited to the specific type of mission. All these factors implies that the results obtained from this sub-routine, better exposed in section 4.4.6, are not to be considered definitive, but simply preparatory to the development of the final and more complex model in ASTOS, which instead constitutes the design routine and whose results are exposed in section 4.5.4. The comparison between the results in terms of ΔV and in graphical terms about the flight trajectory are reported in section 4.6. In particular, table 4.7 shows all the output values for the ΔV of both routines, these values do not deviate too much, this is a further factor of reliability of the mission analysis routine, the percentage error between the overall values is about 2% and therefore less than 15% which is the selected threshold. Furthermore, these results are in agreement with the values found in the literature for similar missions towards the Martian orbit, this can be ascertained from the discussions addressed in section 2.3 and in the table 3.1 regarding the statistical analysis, in which it is shown how the ΔV, although very variable depending on the type of mission, can vary between 4000-5000 m/s. Analysing this result another factor must be considered, the trajectory chosen for the ascent is different and less complex than those of the missions discussed in section 2.3 and table 3.1, which have as their target orbits often non-circular orbits, different trajectories and mission architectures involving waiting orbits or more complex manoeuvres for the change of inclination and possibly different atmospheric and aerodynamic models. However, the contribution that this type of work makes is to propose a design routine, albeit approximate, conservative and validated on a type of mission of interest for the challenges that NASA proposes to face from 2030 onwards [1] concerning the realisation of reusable and multifunctional vehicles for the Martian ascent that are also valid for the eventual descent. As far as the descent is concerned, the mission analysis routine plans to output again the ΔV value and the propellant required for the EDL, in order to use them as parameters for a design routine. The model realisation, with the attached theoretical-based estimate of the drag coefficient is reported in chapter 5, the aerodynamic model is discussed in section 5.1 while the implementation in ASTOS in section 5.2. The results obtained here, discussed in section 5.2.5, are not optimized and therefore unreliable for a possible design routine, however, the drag coefficient results obtained and reported in section 5.1.4 at varying altitude represent the application of existing theoretical models to the Martian case by integrating the NASA atmospheric model[18]. It is shown that the influence of altitude has very little effect on the peak, the value of which without considering the shape drag factors due to possible deceleration systems is about 1 per Mach of 1.8. The influence is more incisive for low Mach numbers, which, however, are obtained at low altitudes with effects also on the Reynolds number

which prevent a classical decreasing trend for the coefficient in this range of mach values. This model is certainly a very good result from the point of view of a successful optimisation, as are also the results obtained in ASTOS through simulation alone, reported in section 5.2.5. In fact, in section 5.2.5 it is possible to ascertain that, at least with the level of detail implemented following the literature commented in section 2.2.1 for the definition of the mission and the reference mission, a result in line with expectations for a simple optimization is obtained, with low velocities on arrival but not null, as in particular is found in figure 5.19, and with a value for the descent ΔV required of 751.17 m/s, in line with what is analysed in the literature and reported in section 2.3.3 where, depending on the technology, it is reported as varying between 600 m/s and 800 m/s. What this part of the mission analysis routine brings as a contribution is certainly a further verification that, according to the results of the simulation alone, the theoretical models for aerodynamics can be considered consistent even for manned vehicles of a completely different size and purpose than the small Mars landers used so far, and is therefore a model that can be implemented in a design methodology for a Mars lander with these characteristics. These results shows that an approach such as the one followed, actually brings results at least close to optimization and can potentially be explored further in the perspective of methodology refinement.

6.2 Limits & Future Insights

The results presented in this work in sections 4.4.6, 4.5.4, 5.1.4 and 5.2.5 are obviously limited by the use of a simplifying model. Excluding the limitations of the subroutine in MATLAB just described in section 6.1 due to the use of 2 degrees of freedom and a non-inertial frame, one of the main limitations is dictated by the input law for the thrust angle, a bilinear tangent law for the propelled phases that although representative could be better modelled with more complex, stroke-defined control laws. Although the attitude dynamics and control laws are later better explored in the ASTOS routine, the simplifications implemented here mainly concern the orbit. The limitation of the model is the need to use circular orbits as target orbits, the dynamics modelling becomes much more complex when the target orbits are very eccentric and ASTOS presents many more pitfalls in optimization and the definition of constraints, the software makes debugging complex by not providing much information in the case of unsuccessful optimization. The same problems occur when the inclination of the orbit is very high, which is why the model is simplified by entering an inclination of 20°. As far as descent is concerned, the main limitations stem from the lack of optimization. Without optimization, simulation results alone are unreliable and cannot be used as input parameters for a design routine. Furthermore, the validation is carried out using inflatable

deceleration technology and supersonic parachutes, which, although representative of the most commonly used technologies for this type of mission, does not explore all the alternatives proposed in the literature with slight differences in the flight trajectory and mainly in the masses of the systems for deceleration and TPS. Furthermore, the model proposed here only considers the EDL phases and not any phases of detachment from the Martian transfer module and entry into the low Martian orbit from which to begin the descent. In spite of these limitations, the simulation results reported in section 5.2.5 are nevertheless good when compared with the expectations of the literature and therefore represent a good starting point for possible future developments of the model that may allow optimisation and validation on different technologies.

The main future insights proposed by this work concerns the integration of the mission analysis routine with the lander design routine, which is dealt with in a thesis work conducted in parallel with this one. Having solved the problems relating to the optimization of the descent mission, possibly implementing a subroutine in matlab as well, so as to have a first estimate of the results, the integration of the two routines would lead to the actual development of the design methodology, the two routines could communicate by exchanging their output parameters. Having chosen an initial ΔV from the literature or simply entered as input, the design routine would evaluate and pass to the mission analysis routine the systems and subsystems data mainly concerning dimensions, masses and for the propulsion system, performance and propellant mass. The mission analysis routine, which is currently validated on a single reference vehicle but which may later be validated on slightly different data from other similar vehicles in the literature, would use these parameters provided by the design routine to calculate the ΔV for the two scenarios and so the total mass of the lander. If the difference between the lander mass input to the mission analysis routine and the actual calculated values resulted in a percentage error of less than a threshold, the final design for the lander and the final flight trajectory would be found. In figure 6.1 it is shown how this tool should work, starting from the studies conducted by these thesis already described in figure 1.3.

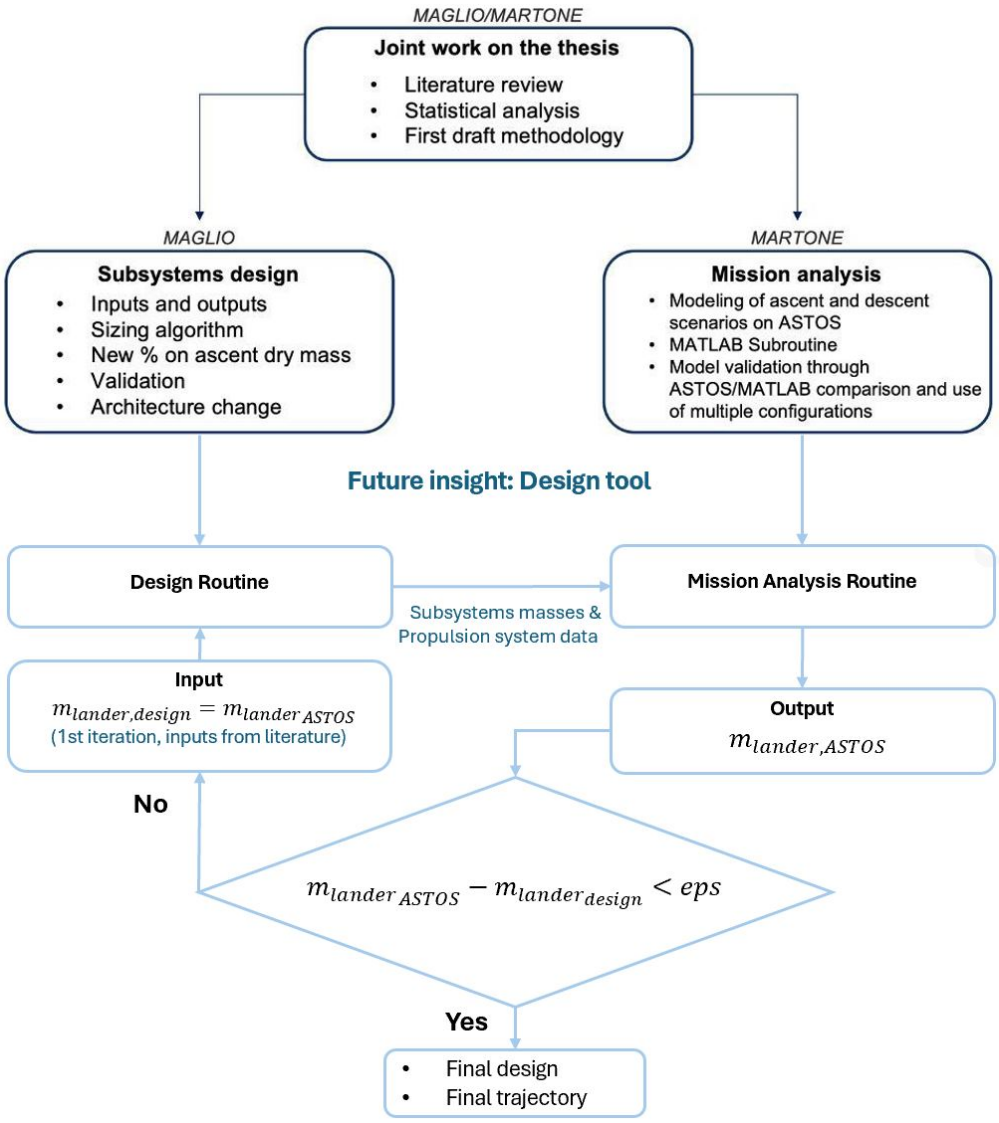

Figure 6.1: Future Insight: Design Tool

Appendix A

MATLAB Ascent Subroutine Code

```
%%%% ASCENT TRAJECTORY %%%
clear all
close all
clc

tic
% CD interpolation

machdata=[0:0.2:0.6 0.7:0.1:1.9 2:0.2:10 11:1:10000];
CD_tot_0=[0.335 0.335 0.330 0.327 0.325 0.324 0.525 0.725 0.865 0.85
    0.825 0.82 0.815 0.8 0.775 0.75 0.725 0.7 0.675 0.63 0.61 0.575
    0.575 0.55 0.525 0.52 0.51 0.49 0.48 0.475 0.465 0.455 0.45 0.445
    0.43 0.427 0.425 0.418 0.413 0.41 0.405 0.4 0.395 0.39 0.388 0.387
     0.38 0.375 0.375 0.375 0.375 0.375 0.373 0.37 0.37 0.368 0.367
    0.365 0.363 0.363*ones(1,9989)];
xx      = 0.1:0.1:10;
yy      = interp1(machdata, CD_tot_0, xx);
CD_int  = yy;
mach_int    = xx;
% INPUT
T_stage1 = 265000; %[N]
T_stage2 = 212000;%159426; %[N]
Isp_1st = 360;  %[s]
Isp_2nd = 360;  %[s]
m0_1st = 60808 %[kg]
m0_2nd = 26566.1 %[kg]
m_fuel_1st = 30808; %[kg]
m_fuel_2nd = 14300; %[kg]
A_1st = 50.27; %[m^2]
A_2nd = 50.27; %[m^2]

```

```
27
28
29 %Number of Phases
30 data.n_stage = 5;
31 %Thrust of each phase
32 data.Thrust = [T_stage1 T_stage1 T_stage2 T_stage2 T_stage2]';
33 %Specific impulse of each stage
34 data.Isp = [Isp_1st Isp_1st Isp_2nd Isp_2nd Isp_2nd]';
35 %Initial mass of the different phases
36 data.m0 = [m0_1st m0_2nd m0_2nd m0_2nd m0_2nd]';
37 %Fuel mass of each phase
38 data.m_fuel = [m_fuel_1st m_fuel_1st m_fuel_2nd m_fuel_2nd m_fuel_2nd
       ]';
39 %Drag coefficient
40 data.cdint = CD_int';
41 %Mach number for estrapolation of drag coefficient
42 data.mach = mach_int';
43 %Cross section for each stage
44 data.Area_list = [A_1st A_1st A_2nd A_2nd A_2nd]';
45 %Target Orbit altitude
46 h_orbit = 390000;
47 %Gravitational parameter
48 G=6.67e-11;
49 M_mars=6.39e23; %Mars Mass
50 global R_mars g0_Earth g0_Mars mu_mars
51 % Mars radius [m]
52 R_mars          = 3389500;
53 % gravitational parameter [m^3/s^2]
54 mu_mars         = G*M_mars;
55 % Gravitational acceleration constant at its sea-level value [m/s^2]
56 g0_Earth               = 9.81;
57 % Gravitational acceleration constant at its sea-level value [m/s^2]
58 g0_Mars               = 3.71;
59 global rho_air_0 %atm_scale_height
60 rho_air_0 = 0.014029863;              % Air density at sea level
61 %atm_scale_height = 8.5*1000;    % Atmosphere scale height
62 % Initial altitude [m]
63 h0 = 0;
64
65 % Target
66 Target = h_orbit + R_mars;
67
68 m_dot_1=data.Thrust(1)/(data.Isp(1)*g0_Earth);
69 data.t_fin1=data.m_fuel(1)/m_dot_1;                    %1st Stage
       Duration
70
71
72 % Pitch function for 1st Stage
```

```
73  data.alpha = @(t, s) atan(((tan(s(2))-(s(5)^s(8))*tan(s(1)))*t/data.
        t_fin1+(s(5)^s(8))*tan(s(1)))/((1-(s(5)^s(8)))*t/data.t_fin1+(s(5)
        ^s(8))));
74
75  % Pitch function for 2nd Stage 1st Burn
76  data.alpha2_1 = @(t, s, tb) atan(((tan(s(4))-(s(8)^s(11))*tan(s(3)))*
        t/tb+(s(8)^s(11))*tan(s(3)))/((1-(s(8)^s(11)))*t/tb+(s(8)^s(11))))
        ;
77
78  % Pitch function for 2nd Stage 2nd Burn
79  data.alpha2_2 = @(t, s, tb) atan(((tan(s(6))-(s(9)^s(12))*tan(s(5)))*
        t/tb+(s(9)^s(12))*tan(s(5)))/((1-(s(9)^s(12)))*t/tb+(s(9)^s(12))))
        ;
80
81  %%%%%%%%%%%%%%%%%%%%%%%%%%%%%%%%%%%%
82  %Pitch function variables to optimize
83  theta_01 = deg2rad(70);
84  theta_f1 = deg2rad(50);
85  theta_02= deg2rad(40);
86  theta_f2 = deg2rad(30);
87  theta_03 = deg2rad(5);
88  theta_f3 = deg2rad(-5);
89  a1 =  100;
90  a2 = 100;
91  a3 = 100;
92  csi1 = -0.5;
93  csi2 = 0.5;
94  csi3 = -0.7;
95  % Initialization control variables
96  eta_min     = 0.01;                                          % Minimum
        throttling (0 not recommended)
97
98  eta_list0   = [0.99 0.99]      % Initial guess of the throttling
99  function_list0 = [theta_01 theta_f1 theta_02 theta_f2 theta_03
        theta_f3 a1 a2 a3 csi1 csi2 csi3];          % Initial guess for
        bilinear tangent control law parameters
100 phase_time_list0 = [44 160 460]
101
102
103 % Initial guess in vector form
104 x0 = [eta_list0(:);function_list0(:);phase_time_list0(:)]
105
106 % Lower and upper boundaries of control variables
107 function_lb = [[-pi/2 -pi/2 -pi/2 -pi/2 -pi/2 -pi/2 60 60 60 -1 -1
        -1]'];
108 function_ub = [[pi/2 pi/2 pi/2 pi/2 pi/2 pi/2 140 140 140 1 1 1]'];
109 time_lb = [1 30 50]';
110 time_ub = [460 350 1550]';
111 lb = [eta_min*ones(2,1);function_lb;time_lb];
```

```
ub = [ones(2,1);function_ub;time_ub];

% Options for the non-linear solver
options = optimoptions('fmincon','Display','iter-detailed', '
    MaxFunctionEvaluations', 2000, 'Algorithm', 'interior-point');

%% OPTIMIZATION TRAJECTORY EVALUATION
% Function to minimize is ((r_a - Target)^2+(r_p - Target)^2);
% During this optimization we use the mean(cd)
[x,fval,exitflag,output,lambda,grad,hessian] = fmincon(@(x)
    objective_fun_circ(x,data, Target),x0,[],[],[],[],lb,ub,@(x) mycon
    (x,data, Target),options)
% Reshape the control variables
eta_list = reshape(x(1:2),[2, 1]);
function_list  = reshape(x(3:end-3),[12,1]);
phase_time_list = reshape(x(end-2:end),[3,1]);
%% Calculate the obtained trajectory
% This trajectory is calculated using the cd(Mach)
[p0,p_total,t_total] = trajectory_optimized(eta_list,function_list,
    phase_time_list, data);

% States
r               = p_total(:, 1);
theta           = p_total(:, 2);
vr              = p_total(:, 3);
vt              = p_total(:, 4);
m               = p_total(:, 5);
drag_loss       = p_total(:, 6);
gravity_loss    = p_total(:, 7);
delta_v         = p_total(:, 8);
% Delta V mission
delta_v_mission = delta_v + gravity_loss + drag_loss;

%% Plot

% Height in function of Time
figure
plot(t_total,(r-R_mars)/1000);
xlabel('Time [s]')
ylabel('Height [km]')
title('Height as a function of time')

% Horizontal distance in function of Time
figure
plot(t_total,R_mars*theta/1000);
xlabel('Time [s]')
ylabel('Horizontal distance [km]')
title('Horizontal range')

```

```
157 % 2D Trajectory
158 figure
159 plot(R_mars*theta/1000,(r-R_mars)/1000);
160 xlabel('Horizontal distance [km]')
161 ylabel('Height [km]')
162 title('Height vs distance')
163
164 % % Trajectory in space
165 % figure
166 % plot(r.*cos(theta+pi/2),r.*sin(theta+pi/2))
167 % hold on
168 % angles = [-180:180]*pi/180;
169 % plot(R_earth*cos(angles),R_earth*sin(angles));
170 % axis equal
171
172
173 % Velocity components in function of time
174 figure
175 plot(t_total,vr)
176 hold on
177 plot(t_total,vt)
178 xlabel('Time [s]')
179 ylabel('Velocity [m/s]')
180 title('Velocity component')
181 legend('Radial velocity', 'Tangent component')
182
183 % Mass in functio of time
184 figure
185 plot(t_total,m)
186 xlabel('Time [s]')
187 ylabel('Mass [kg]')
188 title('Mass')
189
190 % Delta v components in function of time
191 figure
192 plot(t_total,drag_loss)
193 hold on
194 plot(t_total,gravity_loss)
195 plot(t_total,delta_v)
196 xlabel('Time [s]')
197 ylabel('Delta V components [m/s]')
198 title('Delta V components')
199 legend('Drag loss [m/s]', 'Gravity loss [m/s]', 'Delta V orbit [m/s]'
    )
200
201 % Delta v in function of time
202 figure
203 plot(t_total,(delta_v - gravity_loss - drag_loss))
204 xlabel('Time (s)')
```

```
ylabel('Delta V (m/s)')
title('Delta V')

%% DRAG PLOT

cd = data.cdint;
% Area [m^2]
Area = 50.27;
% Mach
mach_int = data.mach;

% Mach number
for i=1:length(vr)
    if (r(i)-R_mars)<7000
        T=-31-0.000998*(r(i)-R_mars);
    else T=-23.4-0.00222*(r(i)-R_mars);
    end
    pressure=(0.699*exp(-0.00009*(r(i)-R_mars)));
    rho=pressure/(0.1921*(T+273.1));
    a0=sqrt(1.29*191.8*(T+273.1));
    pressure=pressure*1000;
    if (r(i)-R_mars)>100000
         pressure=8.6263E-5*1000;
         rho=1.6211E-5;
         T=-246.4;
         a0=sqrt(1.29*191.8*(T+273.1));
     end
Mach    = sqrt(vr(i)^2+vt(i)^2)/a0;
if (r(i)-R_mars) <= 130000
    % Drag coefficient
    if Mach < 0.1
        Cd(i)      = cd(1);
    end
    if Mach >= 0.1 && Mach <= 10
        i_mach  = find(mach_int < Mach +0.1/2 & mach_int > Mach -
           0.1/2);
        i_mach  = min(i_mach);
        Cd(i)      = cd(i_mach);
    end
    if Mach > 10
        Cd(i) = 0.05;
    end
else
    % Out of atmosphere -> No drag
    Cd (i)     = 0;
    rho     = 0;
end


```

```
M(i)=Mach;
ddrag(i)= (0.5*rho*((vt(i)^2+vr(i)^2))*Area*Cd(i))/1000;
end
figure
plot(t_total,ddrag)
xlabel('Time [s]')
ylabel('Drag [kN]')
title('Drag')
%%
toc
```

Bibliography

[1] Greg Williams and Jason Crusan. *Pioneering Space – the Evolvable Mars Campaign*. National Aeronautics and Space Administration (NASA). 2015.

[2] J. N. James. "The Voyage of Mariner IV". In: *Scientific American* 214.3 (1966), pp. 42–53.

[3] Eckart Schmidt, Gerald Brewster, and George Cain. "Mars Lander Retro Propulsion". In: Oct. 1999.

[4] D. C. Gruel. *Testbed Verification of Pathfinder's Martian Entry, Descent and Lnading (EDL)*. Version V2. 1997. DOI: 2014/22949.

[5] Randolph Lillard and Joseph Olejniczak. "Human Mars EDL pathfinder study: Assessment of technology development gaps and mitigations". In: *2017 IEEE Aerospace Conference*. 2017, pp. 1–8. DOI: 10.1109/AERO.2017.7943587.

[6] Richard Welch, Daniel Limonadi, and Robert Manning. "Systems engineering the Curiosity Rover: A retrospective". In: *2013 8th International Conference on System of Systems Engineering*. 2013, pp. 70–75. DOI: 10.1109/SYSoSE.2013.6575245.

[7] Bret G. Drake, Stephen J. Hoffman, and David W. Beaty. "Human exploration of Mars, Design Reference Architecture 5.0". In: *2010 IEEE Aerospace Conference*. 2010, pp. 1–24. DOI: 10.1109/AERO.2010.5446736.

[8] SpaceX. *SpaceX Starship Users Guide*. Revision 1.0. Mar. 2020.

[9] Thomas Zang et al. "Overview of the NASA Entry, Descent and Landing Systems Analysis Stud". In: AIAA SPACE Conference & Exposition, 2010. DOI: 10.2514/6.2010-8649.

[10] Bradley Steinfeldt et al. "High Mass Mars Entry, Descent, and Landing Architecture Assessment". In: AIAA SPACE Conference & Exposition, 2009. DOI: 10.2514/6.2009-6684.

[11] Kartik Naik et al. "Argo Nova: Spacecraft and Mission Design of a Heavy Mars Lander". In: Jan. 2019. DOI: 10.2514/6.2019-0617.

[12] David Lichodziejewski et al. "Design and Testing of the Inflatable Aeroshell for the IRVE-3 Flight Experiment". In: *AIAA 14th Adaptive Structures Conference*. Apr. 2012. DOI: 10.2514/6.2012-1515.

[13] Glen Brown. "Estimating Minimum Inflation Pressure for Inflatable Aerodynamic Decelerators". In: 20th AIAA Aerodynamic Decelerator Systems Technology Conference and Seminar, 2009. DOI: 10.2514/6.2009-2970.

[14] Samareh and J. A. "Estimating mass of inflatable aerodynamic decelerators using dimensionless parameters". In: *8th International Planetary Probe Workshop* (2011).

[15] Bret G. Drake and Kevin D. Watts. *Human Exploration of Mars Design Reference Architecture 5.0 Addendum #2*. Technical Report NASA/SP–2009-566-ADD2. NASA Johnson Space Center, 2009.

[16] Tara P. Polsgrove et al. "Human Mars ascent vehicle configuration and performance sensitivities". In: *2017 IEEE Aerospace Conference*. 2017, pp. 1–15. DOI: 10.1109/AERO.2017.7943583.

[17] Ben B. Donahue. "Crewed Mars Ascent Stages: Propellant Options, Configuration Alternatives and Performance Factors". In: *ASCEND*. 2023. DOI: 10.2514/6.2023-4747.

[18] NASA Glenn Research Center. *Mars Atmosphere Model*. Accessed: 2024-05-08. 2024. URL: https://www.grc.nasa.gov/www/k-12/airplane/atmosmrm.html.

[19] Larissa Balestrero Machado and Markus Wilde. "Parametric Design of a Crew Transfer Vehicle for Earth-Mars Cyclers". In: *Journal of Spacecraft and Rockets* 57.3 (May 2020), pp. 565–579. DOI: 10.2514/1.A34637.

[20] Andrea Paternoster et al. *FEASIBILITY STUDY ON A CREWED MARS LANDER*. Politecnico di Torino - Thales Alenia Space Italia - ISAE Supaero Toulouse, Italy. 2023.

[21] Alexander Seligson et al. *Lightweight Mars Ascent Vehicle*. Paper presented at Cooper Union. 2021.

[22] D. Willson and J. D. A. Clarke. "A Practical Architecture for Exploration-Focused Manned Mars Missions Using Chemical Propulsion, Solar Power Generation and In-Situ Resource Utilisation". In: *Mars Society Australia* (2006).

[23] Scott Alan Geels. "System Design of a Mars Ascent Vehicle". Master's thesis. Massachusetts Institute of Technology, 1990.

[24] Maria Pilar Alliri et al. *Mars Expedition – Project Hugin & Munin: Transfer Vehicles Design*. MSc Project Report. Stockholm, Sweden: KTH, Royal Institute of Technology, 2022.

[25] Humphrey W. Price et al. "A High-Heritage Blunt-Body Entry, Descent, and Landing Concept for Human Mars Exploration". In: *54th AIAA Aerospace Sciences Meeting*. 2016. DOI: 10.2514/6.2016-0219.

[26] Tara Polsgrove et al. "Human Mars lander design for NASA's evolvable mars campaign". In: *2016 IEEE Aerospace Conference*. 2016, pp. 1–15. DOI: 10.1109/AERO.2016.7500778.

[27] Ashley M. Korzun et al. "A concept for the entry, descent, and landing of high-mass payloads at Mars". In: *Acta Astronautica* 66.7 (2010), pp. 1146–1159. DOI: https://doi.org/10.1016/j.actaastro.2009.10.003.

[28] Tara Polsgrove et al. "Human Mars Entry, Descent, and Landing Architecture Study: Deployable Decelerators". In: *2018 AIAA SPACE and Astronautics Forum and Exposition*. 2018. DOI: 10.2514/6.2018-5191.

[29] Tara Polsgrove et al. "Human Mars Entry, Descent, and Landing Architecture Study: Rigid Decelerators". In: *2018 AIAA SPACE and Astronautics Forum and Exposition*. 2018. DOI: 10.2514/6.2018-5192.

[30] Wiley J. Larson and Linda K. Pranke. *Human Space Flight: Mission Analysis and Design*. 1st. McGraw-Hill College, 1999.

[31] Alexandru-Iulian Onel et al. "Drag coefficient modelling in the context of small launcher optimisation". In: *INCAS BULLETIN* 10 (Dec. 2018), pp. 103–116. DOI: 10.13111/2066-8201.2018.10.4.10.

[32] Astos Solutions GmbH. *ASTOS 9 Conventional Launcher Tutorial*. Tutorial Manual. Mar. 2021.

[33] Beauregard Laurent et al. "Multidisciplinary Design Optimization of a Reusable Lunar Vehicle". In: *8th European Conference for Aeronautics and Aerospace Sciences (EUCASS)*. Madrid, Spain, 2019. URL: https://hal.science/hal-03208794.

[34] R. Brusch. "Bilinear tangent yaw guidance". In: *Guidance and Control Conference*. 1979. DOI: 10.2514/6.1979-1730.

[35] Chen Li et al. "Design and Analysis of Low-Gravity Simulation Scheme for Mars Ascent Vehicle". In: *Aerospace* 11.6 (2024). DOI: 10.3390/aerospace11060424.

[36] Charles B. Henderson. "Drag Coefficients of Spheres in Continuum and Rarefied Flows". In: *AIAA Journal* 14.6 (1976), pp. 707–708. DOI: 10.2514/3.61409.

[37] Max Yates. "Stochastic Orbit Prediction Using KAM Tori". In: *Research Gate* (Mar. 2011), p. 217.

[38] Chao Xu et al. "End-to-end Mars entry, descent, and landing modeling and simulations for Tianwen-1 guidance, navigation, and control system". In: *Astrodynamics* 6.1 (Mar. 2022), pp. 53–67. DOI: 10.1007/s42064-021-0115-z.